Summer 8-7-2018

Cellular And Molecular Insight Into Autonomic Function And Dysfunction

Yang Wu
Georgia State University

CELLULAR AND MOLECULAR INSIGHT INTO AUTONOMIC FUNCTION AND DYSFUNCTION

by

YANG WU

Under the Direction of Chun Jiang, PhD

ABSTRACT

The autonomic nervous system (ANS) controls several vital functions of the body, especially the autonomic regulation of respiratory and cardiovascular systems. Dysfunction of either can be life-threatening. Some of cellular and molecular mechanisms underlying the respiratory and cardiovascular dysfunction is more critical and general. The demonstration of such general processes not only may help the understanding of etiology and pathophysiology of the diseases, but also suggests potential therapeutic modalities for the diseases. Severe breathing disorders including high apnea rate and breathing irregularity are found in Rett syndrome (RTT). In a novel rat model of RTT, we compared rat physical condition and behaviors with traditional mouse models of RTT. We found that the novel *Mecp2*$^{-/Y}$ rat model as an alternative RTT model

recapitulated numerous RTT-like symptoms. To uncover the neuronal mechanisms underlying the RTT respiratory disorders, we performed *in vivo* recording from brainstem neurons in ventral respiratory column (VRC). Excessive activity of both inspiratory and expiratory neurons as well as ectopic discharge of phrenic nerve were detected in null rats. Such defects were likely caused by hyperexcitability of respiratory neurons due to inadequate synaptic inhibition necessary for phase switching. Then we took the GABAergic intervention to hyperexcitability of respiratory neurons, and successfully corrected the defects in neuronal firing patterns as well as the RTT breathing phenotypes.

Similarly, change of cellular excitability was also observed in diabetic vascular complications. A critical player for the membrane excitability of vascular smooth muscle cells (VSMCs) is the K_{ATP} channel that is strongly suppressed by methylglyoxal (MGO) known to be overly produced with persistent hyperglycemia. The elevated level of microRNA (miR)-9a-3p contributed to the down-regulation of vascular K_{ATP} channels. miR-9a-3p inhibition using antisense oligonuecleotides corrected the dysfunction of K_{ATP} channels. Since VSMC membrane excitability plays an important role in vascular tone regulation, we generated a new strain of transgenic Tagln-ChR mouse model and demonstrate an alterative to manipulate VSMC membrane excitability and vascular tone using optogenetic approaches. Thus several molecular targets in cardiorespiratory system have been demonstrated underlying membrane excitability and the developments of several disease conditions in this thesis study.

INDEX WORDS: Autonomic nervous system, Respiratory system, Vascular system, Cellular excitation, Rett syndrome, Ventral respiratory column, Diabetic vascular dysfunction, K_{ATP} channels, MGO, MicroRNAs, Optogenetics

CELLULAR AND MOLECULAR INSIGHT INTO AUTONOMIC FUNCTION AND DYSFUNCTION

by

YANG WU

A Dissertation Submitted in Partial Fulfillment of the Requirements for the Degree of

Doctor of Philosophy

in the College of Arts and Sciences

Georgia State University

2018

CELLULAR AND MOLECULAR INSIGHT INTO AUTONOMIC FUNCTION AND DYSFUNCTION

by

YANG WU

Committee Chair: Chun Jiang

Committee: Julia Hilliard

Hang Shi

Electronic Version Approved:

Office of Graduate Studies

College of Arts and Sciences

Georgia State University

August 2018

DEDICATION

To my husband Zhenda Shi, who always support, encourage and take care of me.

To my daughter Yunxi A. Shi, who makes me feel I am the luckiest mom in the world and brings the family so much happiness.

To my mother Liping Yang and my father Yingxue Wu, who love and support me without condition.

To my parents in-law Feng Jiang and Meiquan Shi, both of who are very supportive in my educational pursuits.

To people I love in my hometown and in heaven, I miss you all so much.

ACKNOWLEDGEMENTS

First and foremost, I would like to thank my advisor, Dr. Chun Jiang. He is really a good research advisor and mentor, who has been supporting and pushing me to achieve my Ph.D. degree. Without his guidance and help, I would not be where I am today.

Secondly, I would like to thank my committee members, Dr. Julia Hilliard and Dr. Hang Shi for their invaluable suggestions and advice helping me to perform better research and improved my projects.

I would also like to thank some faculty members at GSU. Dr. Didier Merlin, and Dr. Chung-Dar Lu supplied their valuable advising when I took my qualifying examination. Dr. Brewer and Stephanie offered me the first teaching position and guided my teaching. Dr. Blaustein and Drew helped me be become a qualified teaching assistant by showing me many great teaching skills and providing wonderful teaching guidance. I would like to also thank Dr. Phang Tai and Dr. Yi Pan for their outstanding leadership of our department. Thanks Dr. Vincent Rehder for sharing the important scholarship information.

I would also like to thank the staff at GSU. LaTesha Warren and Tameka Hudson have been so professional in administrative guidance and assistance. Barry Grant for his help with maintenance and repairs. Members from biology core facility, Ping Jiang, Sonja Young, Gemia Cameron, Hyek-Kyu Seoh and Debby Walthall, have been very helpful in completing the related experiments. Tamara Gross, and Karon Mackey-Conyers for their assistance with ordering issues. Department of animal resources staff, especially Joey, Kim, Robert and Courtney, for their assistance and advice for animal handling and maintaining.

I would also like to thank the colleagues and friends I met in GSU, including but not limited to Dr. Ninren Cui, Hao Xin, Dr. Lei Yu, Dr. Shanshan Li, Dr. Xin Jin, Dr. Weiwei

Zhong, Dr. Shuang Zhang, Christopher M. Johnson, Colin Arrowood, Ze li, Dr. Lei (Ray) Zhong, Dr. Yang Yang, Casey Trower, Dr. Max Oginsky, Brian Bondy, Dr. Xiaotao Jin, Dr. Mengru Cao, Dr. Yingji Wang, Ravi T. Pamulapati, Dr. Anuhya S. Konduru and Jyothirmayee S. Tadepalli,

I acknowledge Brain and Behavior (B&B) Fellowship program for their financial support for my study and research.

TABLE OF CONTENTS

LIST OF FIGURES

1 HYPOTHESES AND SPECIFIC AIMS

The autonomic nervous system (ANS) controls involuntary and visceral functions. Two of them are respiration and the cardiovascular system which are essential for survival. Breathing, a perpetual process in life, is controlled by the brainstem as well as higher brain areas. Cardiovascular function relies on the heart, blood vessels and their controlling system. Dysfunction of the respiratory and cardiovascular systems often leads to some of the most challenging diseases and death.

As the intrinsic property of excitable cells, such as neurons and muscle cells, membrane excitability is a critical factor determining the output of a neuron and the performance of smooth muscles in physiological and pathophysiological conditions. Although the understanding of the function of ANS has advanced tremendously over past decades, many questions related to the role of cellular excitability in health and diseases remain open. For instance, how does the ANS dysfunction lead to respiratory and cardiovascular diseases? What cells in the control line of ANS are involved in the respiratory and cardiovascular diseases? Does a change in membrane excitability of these cells play a major role? What are molecules critical for the change in membrane excitability? Can these molecules be targeted to manipulate cellular excitability for therapeutic purposes? To address these questions, we performed these studies using a multidisciplinary approach with RNA interference, optogenetics, transgenic animal models, *in-vitro* organ, tissue and cellular physiology, *in vivo* electrophysiology and behavioral studies. My **hypothesis** is that several receptors and ion channels controlling membrane excitability in the ANS not only are involved in the development of certain pathological conditions when they are defective, but also provide specific accesses to the diseases for therapeutic purposes.

Specific Aim 1: The novel *Mecp2*$^{-/y}$ rat model recapitulates numerous RTT-like symptoms.

Respiratory system as a part of ANS is critical for lives and can become abnormal in certain genetic diseases such as Rett syndrome (RTT). RTT is a neurodevelopmental disease caused mostly by mutations of Methyl CpG binding protein 2 (*MECP2*) gene. With the mutations patients usually suffer from life-threatening breathing disorders. Although there are mouse models of the disease currently, the body size of mice limits the understanding of cellular physiologic approaches for mechanistic studies. A novel rat model of RTT was generated recently, which is ideal for the studies of cellular mechanisms for the breathing disorders. We thus performed studies in the rats focusing on several representative RTT phenotypes, including motor dysfunction, defects in social behaviors, breathing abnormalities and brainstem neuronal excitability.

Specific Aim 2: Hyperexcitability of medullary respiratory neurons is responsible for breathing abnormalities in *Mecp2* disrupted rats.

Breathing abnormalities are contributing to the high incidence (26%) of sudden death in RTT patients, while the underlying neurobiological mechanisms are still unknown. Using the rat model of RTT, we recorded directly from brainstem respiratory neurons *in vivo*, and showed how the *Mecp2* disruption affected neuronal excitabilities, discharge patterns, as well as cellular grouping, how these changes were closely associated with abnormal phrenic nerve discharges, and how the abnormal respiratory neuronal activity together with breathing disorders responded to pharmacologic agents.

Specific Aim 3: miRNA as a genetic mechanism targets the SUR2B subunit of rat vascular K_{ATP} channel.

Cardiovascular diseases are the major causes of deaths world-wide. Excitability of vascular smooth muscle cells (VSMCs) determines the vascular tone, blood pressure and

regional blood flow, while a critical regulator of VSMC excitability, the ATP-sensitive K^+ (K_{ATP}) channel, is known to be disrupted in diabetic conditions. Thus, we screened the expression levels of potential microRNAs (miRNAs) targeting on the K_{ATP} channel in rat VSMCs treated with diabetic metabolites, and investigated the functional consequences.

Specific Aim 4: Optogenetic intervention manipulates the vascular smooth muscle excitability and the consequent vasoconstriction.

Currently, studies of the cardiovascular system heavily rely on pharmacological strategies. The emerging optogenetics technique provides an alternative approach to the cardiovascular system. By expressing exogenous rhodopsin genes, cells can be selectively inhibited or excited with lights. Therefore, we generated a novel mouse strain allowing real-time manipulation of membrane excitability of VSMCs, and studied vascular tones by optical activation in a temporally and spatially specific manner.

2 INTRODUCTION

2.1 Cellular and molecular basis of autonomic function

Autonomic nervous system (ANS) controls involuntary and visceral functions and systems such as respiration, cardiovascular system, gastrointestinal (GI) tract, genitourinary system, pupillary response, sweating and certain reflex actions such as swallowing, vomiting, coughing and sneezing. It is also called vegetative nervous system. The control center of ANS is located in the hypothalamus and the brainstem, which act as integrators of sensory inputs and higher levels of central nerve system (CNS). Neurons from these areas project to motoneurons located in the brainstem and spinal cord. The motor outputs can be involuntary and voluntary (see Section 2.2). Involuntary functions are carried out by the conventional ANS consisting of the sympathetic nervous system, the parasympathetic nervous system and the enteric nervous system (also called metasympathetic system) [1]. The sympathetic nervous system with central nervous connections in the thoracic and lumbar segments (T1 to L2-3) of the spinal cord is often called the "fight or flight" system which is a physiological reaction that responses to a sudden event. The parasympathetic nervous system with the cranial connections and connections in the sacral segments (S2-S4) is considered as the "rest and digest" or "feed and breed" system which responses to stimulate activities related to digestion, salivation, urination, lacrimation and sexual arousal. The enteric nervous system is the intrinsic nervous system in the GI system.

The major divisions of the ANS include sympathetic and parasympathetic nervous systems which have a complementary functions to each other. In many cases, the sympathetic and parasympathetic nervous systems work in opposition to each other, even though they sometimes complement each other. Many of the tissues are innervated by both systems. The activation of sympathetic nervous system dilates the bronchioles of the lung for better oxygen

exchange, triggers vasoconstriction tract to divert blood flow away from skin and GI tract (non-essential organs) to skeletal muscles and lungs, increases heart rate and the contractility of cardiomyocytes, relaxes the ciliary muscle to dilate the pupils, provides vasodilation in coronary vessels and inhibits peristalsis. These changes make body able to take the "fight or flight" responses. In contrast, the activation of parasympathetic system constricts the bronchioles to diminish the oxygen exchange, dilates blood vessels in GI tract to help digestion, reduces heart rate, contracts the ciliary muscles to constrict the pupils, accelerates peristalsis and stimulates saliva secretion. Generally, one system prepares the body for emergency situations, and another controls body processes during ordinary situations. The functions of the ANS in effector organs rely on the anatomic distribution of the sympathetic and parasympathetic nervous systems, the types of the ganglionic fibers and the expression of the neurotransmission receptors in target organs.

Both sympathetic and parasympathetic efferent pathways have two neurons before reaching the target tissues and organs. The preganglionic neurons form synapse onto the ganglionic neurons. Sympathetic ganglia are located adjacent to the spinal cord, then the ganglionic fibers run from the ganglia to the effector organs. The preganglionic fibers in the parasympathetic system exiting from brain and sacral spinal cord exchange neurons in the ganglia located within the effector organs. The preganglionic nerves of both systems release acetylcholine (ACh) activating nicotinic ACh receptors on the postsynaptic ganglionic cells. The ganglionic cells release norepinephrine (NE) to target organs acting on adrenergic receptors in sympathetic system, while ACh is the neurotransmitter released from ganglionic cells to internal organs acting on muscarinic receptors in parasympathetic system.

There are exceptions in neurotransmission of sympathetic system. The adrenal medulla is directly stimulated by ACh released from preganglionic neurons of sympathetic division, acting on nicotinic ACh receptors. Working as the principal site to release catecholamines, stimulation of adrenal medulla secretes NE and epinephrine (EPI) directly into the bloodstream, which quickly triggers a widespread sympathetic activity [2]. Sweat secretion controlled by the ANS is another exception. Efferent innervation to sweat glands is from preganglionic sympathetic neurons of which ACh mediates the sweat gland secretion. On the other hand, sweating is also mediated by the release of catecholamines, NE and EPI, from the adrenal medulla [3]. In addition, renal blood vessels are mediated by dopamine released in the kidney from sympathetic nerve terminals [4].

In the effector organs, NE released from sympathetic ganglionic cells and other catecholamines, such as EPI and dopamine, acts on adrenoceptors, a class of G protein-coupled receptors (FPCRs). There are two major groups of adrenoceptors, α and β. Each of them has several subtypes. Activation of α_1 receptor coupling to $G_{\alpha q}$ protein results in increase of intracellular Ca^{2+} though phospholipase C (PLC) pathway. The activation of α_2 receptor coupling to $G_{\alpha i}$ protein has an inhibitory effect on adenylate cyclase (AC) from generating cyclic adenosine monophosphate (cAMP) from cytosolic adenosine triphosphate (ATP), then inhibiting the downstream protein kinase A (PKA) signals. The β receptor has three subtypes, β_1, β_2 and β_3, which are linked to G_s proteins with AC pathway. The β_2 receptor also couples to G_i proteins [5].

These receptors play different roles in different organs and tissues. The main function of α receptors that are broadly expressed on most cells is vasoconstriction [6]. The α_1 receptors are expressed in most of the organs, including heart, blood vessels, brain, liver, prostate, kidney and spleen, in which they function in regulation of the cardiac inotropy and chronotropy,

vasoconstriction, neurotransmission and metabolism [7]. The α_2 receptors also mediate responses to their ligands in central nervous system and peripheral tissues, such as heart, blood vessels, pancreas, adipose tissues and platelets [8,9]. Besides the general functions of the α receptors, the α_2 receptors have a negative feedback effect on mediation of synaptic transmitter, inhibiting insulin-release and inducing glucagon release from pancreas, inhibiting lipolysis in fat cells and promoting thrombocyte aggregation [10]. The β_1 receptors are majorly expressed in heart, whose activation has positive chronotropic and inotropic effects. Their activation increases the secretion of renin in kidney and ghrelin in stomach as well [11]. The activation of β_2 receptors has minor cardiac effect compared to β_1 receptors. In addition, their activation promotes vascular and nonvascular smooth muscle relaxation, dilation of bronchiole, lipolysis in fat tissue, insulin release, glycogenolysis and gluconeogenesis and renin secretion in kidney. The β_3 receptors mainly exist in adipose tissues, in which their activation enhances the lipolysis [12].

The release of ACh from parasympathetic ganglionic fibers triggers the activation of the muscarinic (M) cholinergic receptors in effector organs. There are five subtypes of M receptors whose activation is through binding to G proteins [13]. M_1, M_3 and M_5 activate the PLC pathway through G_q. M_1 receptor is common in CNS and exocrine glands, whose activation facilitates the transmitter or hormone release. It is predominantly bound to G_q proteins upregulating PLC and consequent increasing intracellular Ca^{2+}. In certain tissues, activation of M_1 receptors can also activate G_i and G_s pathway. The M_3 receptors coupled to G_q proteins are expressed in many tissues and organs, such as smooth muscles in lung, endothelial cells in vessels and the endocrine and exocrine glands, in which their activation leads to bronchoconstriction, vasodilation, and gland secretion respectively. M_3 and M_5 are also found in the brain, but in low abundance. The inhibitory M_2 and M_4 receptors act via G_i proteins. They modulate several types of ion channels,

thus regulating the activities of the neurons in CNS [14]. In addition, the M_2 receptors act to slow down the heart rate and reduce the contractile forces of cardiomyocyte as well as the conduction velocity of atrioventricular (AV) node. The M_4 receptors are one of the predominant muscarinic ACh receptors expressed in the CNS [14]. Activation of M_4 inhibits the ACh released in brain.

In summary, the ANS regulates many critical body processes, such as blood pressure, heart contraction and breathing. Disorders of this system can lead to severe health problems affecting many body parts due to its wide range of coverage. Some can be acute and life-threatening, others are progressive and reversible. This thesis will focus on the autonomic functions and dysfunctions in cardiovascular and respiratory systems, top two systems that are closely linked to our health.

2.2 Autonomic regulation of respiration

Breathing is a special automatic function as its activity can be voluntary and involuntary. An adult human breathes about 20 times per minutes, while the breathing rate in an adult mouse can be up to 200/min. Breathing allows inhalation of O_2 and exhalation of the CO_2. In addition, the respiratory system plays a role in speaking, singing, eating, drinking, body postures，defecation, childbirth, body temperature regulation, pH regulation, etc.

2.2.1 Respiratory rhythm generation and modulation

2.2.1.1 Respiratory centers

Breathing is a complex motor act, the control of which engages widespread parts of the central nervous system. The breathing controlling centers are located in brainstem, specifically medulla oblongata and pons. There are two medullary respiratory centers, dorsal respiratory group (DRG) and ventral respiratory group (VRG), and two pontine respiratory centers, apneustic center and pneumotaxic center. All the respiratory centers are located bilaterally in the

brainstem. These respiratory groups function in an integrated manner, precisely controlling the breathing rate and ventilation depth to accommodate the sufficient oxygen supply to the body.

In the medulla, the DRG contains mainly inspiratory neurons, whereas the VRG contains both expiratory and inspiratory neurons. The DRG is located in the nucleus tractus solitarius (NTS) within periaqueductal gray (PG), sending signals to the motor neurons of external intercostal muscles and diaphragm. In addition, the DRG receive sensory impulses through vagus and glossopharyngeal nerves from upper and lower airways, peripheral chemoreceptors and joint proprioceptors [15,16]. Neurons in DRG are stimulated by the impulse from the apneustic center, and are inhibited by the signal from the pneumotaxic center. The VRG is located around nucleus ambiguus (NA) in rostral retrofacial nucleus area (expiratory Bötzinger complex (BötC), pre-Bötzinger complex (preBötC) (inspiratory), nucleus paraambiguus area (inspiratory rostral VRG (rVRG) and nucleus retroambiguus area (expiratory caudal VRG (cVRG) [17-20]. The VRG is considered as one ventral respiratory column (VRC) in some cases. The inspiratory VRG neurons transmit impulses to the laryngeal and pharyngeal muscles through vagus nerve and to diaphragm and external intercostal muscles through their motor nerves. Whereas, the expiratory impulses from cVRG are sent to abdominal and internal intercostal muscles. The most rostral group of the VRG, BötC, also fires an expiratory pattern, which is mainly thought as an inhibitory nucleus sending signals to inhibit VRG and DRG impulses [21-23].

The pontine respiratory groups are involved in controlling the rhythmic breathing pattern as well. The pneumotaxic centers are identified in the dorsolateral pons, caudal to the inferior colliculus in most of species, while the apneustic center is thought in central area of the lower pons without anatomical certainty. The names of “apneustic” and “pneumotaxic” are inspired by the transection experiments observing the breathing patterns [24,25]. The absence of the rostral pons

(cut both vagus nerves and pneumotaxic center) produces the prolonged inspiratory gasps interrupted by occasional expirations (apneusis). Transections at the pontomedullary junction result in gasping and irregular breathing. The pneumotaxic centers contain medial parabrachial nucleus (mPB) and Kolliker-Fuse nucleus (K-F) [26]. They play an important role in rhythmic generation, respiratory phase switch and modulation of respiratory reflex. There are inspiratory and expiratory cells as well as phase-spanning cells in pneumotaxic centers. Although the interactions between the pneumotaxic and apneustic centers are still poorly understood, the pneumotaxic centers are considered to limit the inspiration and increase the respiratory rate via sending inhibitory impulses to medullary inspiratory neurons, acting as an antagonist to the apneustic center [27]. In contrast, apneustic center causes switch-off failure of DRG inspiratory neurons and consequent larger tidal volumes if pneumotaxic signals are severed. The existence and the function of the apneustic center can only be demonstrated only if its connection to pneumotaxic centers are interrupted and the vagus nerves are cut.

Therefore, the general function of the medullary respiratory centers is to produce the basic inspiration and expiration, while the pontine respiratory centers are in charge of modulating the breathing pattern.

2.2.1.2 Respiratory phases

The eupneic respiration can be commonly divided into three phases: inspiration (I), post-inspiration (post-I) or "passive" stage 1 expiration (E_1) and "active" stage 2 expiration (E_2) [28,29]. Some studies further divided inspiratory phase into three subtypes [30]. The inspiratory premotor neurons start a sudden onset and increases gradually at the end of the expiration probably due to a retreat of inhibitory signals on them, leading to a progressive contraction of inspiratory muscles. This ramp pattern makes the inflation of the lungs smooth. As the inspiratory ramp

signal strengthens, the off-switch mechanisms are recruited and finally strong enough to switch off inspiratory signals. The subsequent termination of inspiration is followed by post-I or E_1 stage during which some inspiratory muscles are being activated again while the expiratory motor activity is not facilitated yet [31]. The post-I activity exhibits an initial maximum and a gradual decline in inspiratory promotor activity. Expiratory motor activity is recruited only in E_2 phase when the ventilation needs are increased, especially during exercise[31]. During exercise, when the quick and frequent gas exchange is required, various peripheral reflexes and receptors are involved to influence the medullary respiratory neurons, steepening the inspiratory ramp signal and making inhalation faster.

2.2.1.3 Central pattern generators (CPG) of respiration

The exact origin of the breathing rhythm and the interplay of the inspiratory and expiratory neurons in respiratory centers still need to be unveiled in neuroscience. Currently, there are two predominant theories of respiratory rhythm generation. One classical theory suggests that the rhythmic breathing is the results of reciprocal inhibition between the pools of inspiratory and expiratory neurons in medulla [32]. However, this theory seams untenable with cumulated evidence [28,30,33,34]. The rhythmogenesis theory is the dominant concept currently. This theory proposes that certain medullary neurons have intrinsic pacemaker properties. And rhythmic breathing is the consequence of the neuronal interactions between independent oscillatory neuronal networks. The three basic respiratory phases are generated by anatomically distinct rhythm-generating networks. The preBötC is the undisputed generator of inspiration (I) [18,35,36]. The retrotrapezoid nucleus/parafacial nucleus (RTN/pFRG) is the widely accepted site for the generation of active expiration (E_2). Recently, a special excitatory group of cell around BötC, the post inspiratory complex (PiCo), has been described responsible for post-I (E_1).

The preBötC is considered both sufficient and necessary for the generation of inspiratory motor output. No matter in *in vivo* rat brain stem transection preparation [37], in *in-situ* heart-brainstem preparation [36], or in *in-vitro* rodent slice preparations [18], the preBötC has been confirmed able to generate rhythmic inspiratory breathing patterns. There are about 5-25% of the preBötC inspiratory cells exhibit bursting pacemaker properties. In addition, targeting lesioning of the preBötC neurons by neurotoxin in intact adult rats leads to the disturbed breathing with ataxic breathing and even apneas [38,39]. Its "pacemaker" bursts is associated with the persistent Na^+ current (I_{NaP}) and the Ca^{2+}-activated nonspecific cation current (I_{CAN}) in the preBötC [36,40,41]. But these currents are not unique in preBötC neurons. One view believes that the preBötC starts the timing signals which are broadcast to the rest of the network transforming these timing signals into appropriate motor patterns [33]. Breathing rhythm may be initiated by special group of glutamatergic pacemaker neurons within the preBötC without requirement of conventional postsynaptic inhibition on phase transitions [42-44]. But this does not appear to be the case, because of the existence of the distinct oscillatory populations for both inspiration and expiration. Therefore, how the rhythm is originated in preBötC is still elusive. Rhythmicity may need bursting pacemaker neurons, and reciprocal inhibition and excitatory synaptic transmission.

RTN/pFRG as the likely location of the central pattern generation for active expiration is proposed recently. The pFRG overlaps with RTN anatomically, whose activation is observed prior to the onset of inspiration [45]. RTN is a site for central chemoreception for H^+ and CO_2 [46,47]. These two groups are usually referred to as the RTN/pFRG located ventral to the facial nucleus and rostral to the BötC. The non-chemosensitive function of the RTN/pFRG is identified through transection of the brainstem just caudal to it, after which the active expiration is abolished without much effect on inspiratory phase [37]. In addition, the brainstem-spinal cord preparation

containing the RTN/pFRG but conditionally muting the rhythm of the preBötC with opioid inhibition adds another piece of evidence for the RTN/pFRG as a conditional oscillator of active expiration [48]. Furthermore, the stimulation of the RTN/pFRG transforms a resting breathing pattern without active expiration into an active expiration pattern with tonic activity of abdominal muscles in E_2 phase [49]. Therefore, the RTN/pFRG is defined as an independent but conditional oscillator of active expiration.

There is still debate on the generator controlling the post-I phase of breathing. The glutamatergic PiCo located dorsal and caudal to the facial nucleus is recently identified as the putative site for post-I generation [50]. It is believed that its oscillatory activity is independent of inspiratory activity, but receives dominate GABAergic modulation over the concurrent glutamatergic excitation from the preBötC. Post-I activity may have mutually inhibitory relationship with inspiratory activity. In addition, the PiCo rhythm could be modulated by cholinergic mechanisms as well. Other researchers suggest that the site gating post-I activity is located in the pons instead of the medulla [36]. Pontomedullary transection at various levels of the facial nucleus in rat transforms the normal three-phase respiratory pattern to a two-phase pattern making post-I activity missing in respiratory cells in VRG area. In pons, the K-F in the pneumotaxic centers is the nucleus hypothesized gating post-I phase [51]. It seems like the post-I may not be generated by a single oscillatory network. Because the post-I activity in crural diaphragm can be abolished via stimulation of the midbrain PG [52].

2.2.1.4 Respiratory neuronal circuits

The underlying neural machinery is an integration of the physiology and the behavior, and a quite complicated process. Current view about the brainstem circuits of respiratory

generation and control is that the respiratory neurons in VRC interact within VRC as well as interconnected with several pontine nuclei.

Even though original concept of the respiratory circuits that the inspiration-expiration cycle is generated by the reciprocal inhibition of two groups of interneurons is not rigorously tested, the role of inhibitory neurons in the respiratory circuits cannot be underestimated. It is believed that the BötC and preBötC are the major components of the VRC generating respiratory patterns in rhythmogenic circuits. BötC is the population proposed playing important inhibitory role. In BötC, over 50% neurons are inhibitory, mostly glycinergic, some GABAergic [53]. A hypothesis proposes an "inhibitory ring" model taking preBötC as the center of timing signals with reciprocal inhibition between the preBötC and other respiratory centers, such as BötC, producing the three-phase breathing pattern [54]. In this model, the kernel reciprocal inhibitory connectivities include direct inhibitory connection or connection through inhibitory interneurons between early-inspiratory (early-I) neurons in preBötC and post-I neurons in BötC, and the inhibitory connection between these inhibitory neurons and the neurons such as pre-inspiratory/inspiratory (pre-I/I) excitatory neurons in preBötC and augmenting expiratory (E_2) neurons in BötC. The latter connection allows the coordination of I and post-I activities. In some studies, the kernel reciprocal "inhibitory ring" is composed of early-I, post-I and E_2 neurons [55].

The excitatory neuronal circuits between respiratory components are not very clear. Neurons within the compartments in VRC, including BötC, pre-BötC, rVRG and cVRG, are proposed to receive drives from the pontine respiratory groups, medullary DRG and other respiratory related medullary nuclei. It is believed that most of these drives are tonic, phasic or rhythmic excitatory inputs [55]. Furthermore, the two neuron groups in rVRG and cVRG are mainly premotor neurons. The excitatory kernel of the respiratory network, the pre-I/I neurons in

pre-BötC, projects to different cranial premotor neurons (the promotor neurons of vagus and hypoglossal motor neurons) and to excitatory inspiratory premotor neurons in rVRG (the promotor neurons of phrenic motor neurons). The projection to abdominal and thoracic expiratory motor neurons in spinal cord is from excitatory expiratory premotor neurons in cVRG. Spinal cord contains the interneuronal circuits controlling respiratory motor activities as well.

Although the work of understanding how respiration is generated is far from complete, there have some evidences suggesting the interaction between the main rhythmic generators. Some progress has been made. There are some evidence supporting the interaction between the preBötC and the RTN/pFRG. In postnatal stage, animal experiments suggest the RTN/pFRG provide only excitatory drive to the preBötC, while the preBötC provides both expiratory and inhibitory influences on RTN/pFRG neurons [34,56]. As mentioned above, the RTN/pFRG is conditionally activated to generate active expiratory activity. Thus the preBötC is probably as the source of excitation simultaneously required for the activation of E_2 network. In addition, the interaction between the preBötC and the potential post-I generator, PiCo, is proposed recently [50]. When $GABA_A$ receptor antagonist is applied to the horizontal slice retaining the connection between the preBötC and PiCo, their firing discharges are progressively synchronize in I phase. This suggests that inhibitory connection between the preBötC and PiCo helps in coordinating the phasing and timing of the breathing rhythms. A concurrent excitatory input of preBötC onto PiCo could be unmasked after blocking the inhibitory influence from the preBötC onto PiCo. Together, under normal conditions, inhibitory input dominants over the excitatory input from the preBötC onto PiCo. Even though the great progress has been achieved on the studies of the neuronal control of respiration, our understanding of the underlying mechanisms is still limited.

Further studies are imperative to fully elucidate the mechanisms of respiratory rhythmogenesis and the oscillatory networks.

2.2.1.5 Modulation of neuronal excitability

The medullary respiratory centers, especially VRG, contain both excitatory and inhibitory respiratory neurons. The dominant excitatory neurons in the ventrolateral medulla are glutamatergic, and the inhibitory neurons are mostly glycinergic [33]. Glutamate is the essential excitatory neurotransmitter for rhythmogenesis in preBötC, while the role of glycine is in shaping the respirator pattern instead [57]. Excitatory preBötC pacemaker neurons are necessary for rhythmogenesis, and the inhibitory pacemaker neurons also exist. It should be mentioned that not all pacemaker neurons are obligatory for rhythmogenesis [58-60]. Instead, they could play a modulatory or stabilizing role in rhythm generation. In the preBötC, about half of the neurons are glycinergic, of which one quarter are with inspiratory pacemaker properties [61]. The GABAergic neurons are also identified in this area, and some of them are also with inspiratory pattern [62]. These inhibitory neurotransmissions within preBötC area, possible including BötC, slow down the rhythm without inducing apnea [57], suggesting the postsynaptic inhibition in this area is not essential for the respiratory pattern generation, but is important for the respiratory rhythmic modulation. The rVRG and cVRG also use glycine as the primary neurotransmitter for the phasic inhibition of the respiratory network [63].

Many pain-relieving drugs, such as opioids, barbiturates and benzodiazepines, can lead to suppressing of breathing via effecting on neurons in the preBötC [64,65]. The use of opioid analgesic drugs can cause a reduction in sympathetic nervous system tone, respiratory depression and analgesia. By local manipulation, the neurokinin-1 receptor-expressing preBötC is reported most sensitive to opioids and fully responsible for respiratory depression even fatal apnea in rats

[64]. This opioid-induced respiratory depression is likely through μ-opioid receptors on NK1R-expressing preBötC neurons, and can be reversed by serotonin agonists without loose of analgesia effect [65-67]. The averting effect against opioid-induced breathing cessation is possible via serotonin receptors in glycinergic preBötC neurons [67].

CNS depressant drugs, such as ethanol, benzodiazepines, barbiturates, γ-hydroxybutyric acid, and other sedatives also produce respiratory depression when they are overdosed or used in combination. A lot of them work as agonists on the GABA receptors in the mammalian brain. For example, benzodiazepines controls the excitability of neurons by binding to the $GABA_A$ receptor. And barbiturates are relatively nonselective ligands binding to many ligand-gated ion channels, including $GABA_A$ receptor, glycine receptor, $5\text{-}HT_3$ receptor and nicotinic ACh receptor. γ-hydroxybutyric acid could have weak agonist effect on the $GABA_A$ receptor when reaching high concentration in brain. Acting by enhancing the activities of the inhibitory neurotransmitters in respiratory networks may be the mechanisms of breathing depression. Therefore, it is necessary to consider the possible respiratory depression for safe medication.

2.2.2 Rett syndrome

Because of breathing abnormalities, researchers who are interested in the central respiratory function and dysfunction are trying to understand the neuronal mechanisms that affect breathing in Rett syndrome (RTT). Although transgenic animal models benefit the studies, it remains unclear how the respiratory disturbances occur.

2.2.2.1 Overview

RTT is a neurodevelopmental disorder caused mainly by single gene mutations in the *MECP2* gene on X chromosome encoding the transcription factor methy-CpG-binding protein 2 (MeCP2) [68]. It predominantly affect baby girls with ~ 0.01% morbidity rate worldwide. In the

rare case, boys inherit mutations in *MECP2*. Although MeCP2 is expressed in most tissues, its disruption results primarily in neurological symptoms. Normally, the patients develop symptoms starting from 6 months of age, and gradually deteriorate the conditions. The symptoms of RTT including mental and growth retardation, loss of acquired purposeful hand skills and spoken language, autism-like behaviors, walking or gait abnormalities, repetitive stereotypic hand movements, and severe breathing disturbances. The severe breathing disorders of RTT usually end up with the high incidence of sudden infant death syndrome (SIDS) which kills about 6 in 1,000 infants younger than 1 year old [58]. Unfortunately, there is no cure for RTT at present.

2.2.2.2 Symptoms of RTT

RTT is found almost exclusively in girls who are normally heterozygous carrying a mutation in *MECP2* gene. The lack of extra X chromosome copy makes the boys with mutant *MECP2* often die before or shortly after birth. The disease is featured by the random X-chromosome inactivation (XCI), which means half of the cells have inactivated the mutated X chromosome bearing the mutant *MECP2* allele. The RTT patients are chimeras for both mutant and wide-type cells. As a neurodevelopmental disease, RTT is predominantly affect the brain because MeCP2 is mainly expressed in differentiated neurons with highest expression level in the more mature neurons [69].

RTT symptoms progress in four stages [70]. The early onset period usually begins when the patient is 6 to 18 months old. During this stage, the symptoms are slight and may not be noticeable. They could only have delayed skills, such as speaking, sitting and crawling, and loss of attention and interest in things. The stereotypic movement and deceleration of the head growth appear at this stage. Stage II happens between 1 to 4 years old. Patients exhibit the rapid regression of development, losing expressive language and acquired hand skills. Microcephaly is

noticeable at this stage. Breathing irregularities, such as episodes of apnea and hyperventilation, may occur. Some girls also display abnormal motor and autism-like behaviors. These behavior abnormalities become severe at stage III which begins between 2 to 10 years old and last for years. Seizures and apraxia often occur during this stage. The last stage may last for years even decades. Patients usually suffer from motor and social dysfunctions, anxiety, seizures and life-threatening breathing disorders. Their phenotype varies among individuals, and some RTT girls have shorter lifespan.

Breathing disturbances are the major problem in RTT. The patients exhibit alternation of hypoventilation and irregular hyperventilation [71]. The periods of forced breathing, shallow breathing, Valsalva's maneuvers, Biot's breathing, air swallowing, breath holding and central and obstructive apnea [72,73], as well as abnormalities of cardiorespiratory integration [74], are observed on RTT patients. These breathing disturbances are reported more apparent during day time, but also occurs during sleep [71,73].

2.2.2.3 RTT mice and rat models

MeCP2 as a transcriptional repressor binds to methylated DNA and interacts with repressor complexes, eventually reducing the target gene transcription. The mutation of gene *MECP2* is the main cause of RTT clinically. The transgenic mouse and rat models were established as tools for studies of RTT. The mouse models of RTT display many of the RTT-like symptoms. They are viable and appear relatively healthy at birth and gradually gain featured characteristics, such as malocclusion, hindlimb clasping, small body size, and behavior disorders.

A variety of mouse models were used in the RTT study, in which functional deletion of exon 3 and/or 4 in *Mecp2* gene is the main strategy of the generation of the RTT models [75-77]. Other RTT murine models include the ones with site-specific mutations [78-80]. Although the

genetic background of mouse RTT models varies, these autonomic phenotypes of cardiorespiratory dysregulation are also observed in mice with *Mecp2* disruption [81-84]. On *Mecp2* defect mice, high breathing variation and apnea rate are usually seen starting at ~3 weeks and deteriorate with time. The long lasting breath holding often occur when the animal is dying. Hyperventilation is also common in mouse models. Since *Mecp2*$^{-/-}$ female animals cannot be produced as the *Mecp2*$^{-/Y}$ males are infertile, the studies of RTT are performed with *Mecp2*$^{-/+}$ female and *Mecp2*$^{-/Y}$ male animals. The hemizygous null male mice begin to display RTT-like phenotypes, including autism-like behaviors and motor dysfunction, at postnatal 4 weeks with an average survival age of ~8 weeks [75,77]. The severe breathing problem is observed as early as postnatal 3 weeks. The studies on heterozygous *Mecp2*$^{-/+}$ female mice are necessary. XCI makes the incidence relatively low in females, because half of the cells have inactivated the X chromosome carrying mutant *Mecp2* allele. The Skewed XCI which favors the expression of the intact wide-type X chromosome makes the symptomized female animals even less with heterozygous *Mecp2*$^{-/+}$ background [85,86]. The female *Mecp2*$^{-/+}$ mice have a late symptom onset at ~4 to 6 months old. Some of the phenotypes can be detected earlier, such as apneic breathing difficulties [87]. The severity of the symptoms is not as much as null male mice because of the potential phenotypic variability. This can also be explained by mosaic expression of the *Mecp2* mutation due to XCI.

Since multiple animal models are required for RTT studies. Recently, a novel MeCP2 knockout rat model has been developed by Sage Labs [84,88,89]. The *Mecp2*-null rat has 71 bp deletion on exon 4 in the *Mecp2* leading to complete elimination of the MeCP2 protein in male rats. The null male rats show RTT-like symptoms as early as ~4 weeks of age, which are comparable to that in the mouse models. Whereas the *Mecp2*$^{-/+}$ female rats display motor

behavior and breathing abnormalities later in development. More detailed phenotypes of this rat model will be described in the results section. The large body size and the rich behaviors of rats provides profound advantages in the studies of disease mechanisms of RTT and towards the development of potential therapeutics.

2.2.2.4 Dysfunction in neurotransmitter and neuromodulator systems of Mecp2-null mice

The studies on mouse models of RTT as good tools to uncover the underlying neurologic mechanism of the ANS dysregulation. It is reported that the neurologic defects resulting from abnormal patterns of neurotransmitter and neuromodulator expression throughout the brainstem respiratory network are contribute to respiratory dysfunctions in *Mecp2* disrupted mice. The defects in neurochemical signaling include brain-derived neurotrophic factor (BDNF), biogenic amine, glutamate and GABA.

BDNF is a member of the neurotrophin family of growth factors, involved in neuronal survival, differentiation, maturation and synapse plasticity. MeCP2 is reported acting as transcriptional repressor of BDNF. BDNF signaling is impaired leading to disturbed Ca^{2+} transients in *Mecp2*-null neurons within preBötC [90], which is an important process during neuronal remodeling during development. Therefore, the disturbance of Ca^{2+} homeostasis caused by inhibited BDNF signaling in RTT mouse models possibly facilitates the morphology changes responsible for breathing irregularities in *Mecp2*-null mice. Other respiratory controlling centers, such as K-F, BötC and nucleus NTS may be modulated by abnormal BDNF signaling as well [91-93], if the *Mecp2* is disrupted.

Serotonin system is reported disturbed by *Mecp2* mutation, and median survival rate increased by augmenting this inhibitory system using serotonin 1a agonist [94]. Serotonin reuptake inhibitor treatment helpes improve CO_2 chemosensitivity in *Mecp2* knockout mice as well [95]. NE

involves in modulating the activity of the preBötC, which is significantly reduced in CNS [96-98]. About 90% of the NE is release from locus coeruleus (LC) in CNS. And hyperexcitability of LC neurons as a compensatory mechanism of making up the defect of certain neurotransmitter is reported in *Mecp2* defect mice [98]. Enhancing the NE content by desipramine, an NE reuptake blocker, alleviates the respiratory disorders in *Mecp2*-null mice [99,100].

Dysfunction in glutamatergic and GABAergic systems is identified in many brain regions of *Mecp2* KO mice [83,101-103]. Studies conducted in both RTT patients and animal models suggest increased expression of N-methyl-D-aspartate receptors (NMDARs), and the synaptic hyperexcitability can be reversed by NMDA receptor antagonist or conditional deletion of NMDAR subunit [104,105]. Genetic deletion of the NMDAR subunit, GluN2A, is able to prevent some RTT phenotypes, such as regression of vision [105]. On another hand, a decrease of the inhibitory neurotransmitter GABA is found in many brain regions including hippocampus, substantia nigra, cerebellum, and ventrolateral medulla [101,103]. Additionally, decreased GABAergic inputs is identified in LC whose malfunction could lead to the autonomic deficits including breathing disorders [96,106]. Deficiency of GABAergic synaptic inhibition within K-F area also contributes to respiratory rhythm irregularity in a mouse model of RTT [107]. Furthermore, conditional knockout *Mecp2* from forebrain GABA-releasing neurons reduces the inhibitory GABA neurotransmission and recapitulates many RTT-like behaviors in mice including severe respiratory irregularity [108]. To sum, defect of MeCP2 protein seems to be associated with inhibitory and excitatory imbalance. Experimental evidences support that the imbalanced excitation and inhibition in CNS plays an important role attributing to RTT-like symptom including breathing abnormality [101,109,110].

2.2.2.5 Dysfunction in central respiratory network of Mecp2-null mice

Besides synaptic signaling imbalance, mice studies of RTT also suggest the responses to hypercapnia are impaired by Mecp2 disruption [111]. *Mecp2*-null mice lose sensitivity to mild hypercapnia (1-3% CO_2), while the one to high CO_2 level (6-9% CO_2) is intact. This affected chemosensibility is contributed by the overexpression of the Kir4.1 subunit of the neuronal pH-sensitive potassium channels leading to the reduction of the pH sensitivity of the Kir4.1-Kir5.1 channels. This does not allow CO_2 to be detected by the chemosensitive site in CNS until hypercapnia becomes really severe, contributing to alternation of hyperventilation and hypoventilation in *Mecp2*-null mice. Furthermore, the restoration of MeCP2 in medulla containing preBötC, the I phase generator, restores a normal hypoxic respiratory response [82].

Some studies attributed the respiratory disorders such as apneas, air swallowing and periodic breathing to obvious prolonged and enhanced post-inspiratory (post-I) which may due to hyperexcitation of the pontine post-I oscillator, K-F nucleus [94,110]. The dysregulation of post-I activity may contribute to the central apneas caused by failed inspiration initiation in *Mecp2*-null mice. Additional evidences support this ideal. At ~2 postnatal months, the deteriorated breathing disorders found on *Mecp2*-null mice are characterized by reduced breathing frequency [112] which is highly possible due to elongated expiration phase or apnea, because the inspiratory phase is not reported elongated obviously [73,110]. Dysfunction of K-F in mutants may also contribute to obstructive apnea due to a poor coordination of glottal closure during swallowing which is a common feature of RTT [94]. Therefore, the impaired expiratory activity raises the possibility that the apneas and upper airway problems in RTT may be caused by increased excitatory input to expiratory neurons and/or decreased excitatory input to inspiratory neurons.

2.2.2.6 Potential therapeutical strategies

The inhibitory and excitatory imbalance might be a common feature of RTT. Accumulating evidences supports this. Some RTT patients are suffering from recurrent seizures [113-116], which may due to the defect of GABAergic transmission [117]. Additionally, Stereotypic hand wringing observed in RTT patients [118], and tremor or striking myoclonic jerk on forelimbs and paws observed in mice with truncated MeCP2 protein [119] suggest hyperactivity of the cortical neurons. These behavior abnormalities as well as the breathing disruptions mentioned above suggest the in RTT patients may due to insufficient inhibitory inputs to the certain brain regions. Therefore, one important treatment strategy is targeting on rebalancing the neuronal excitation and inhibition by augmentation of the GABAergic system or suppression of the glutamatergic system. The GABA reuptake blockers, such as NNC-711 [94,107], the extrasynaptic GABA receptor agonists, such as THIP [120-122], and the synaptic GABA receptor agonist, such as diazepam and L-838,417 [94], have been used in the mice studies as the treatment strategies for RTT. These treatments can decrease the apnea rate, correct the breathing irregularity, prolong survival and alleviate other symptoms. Besides, modulation of glutamate transmission is considered as another efficient way to treat RTT. The glutamate NMDA receptor antagonists, katamine [105] and memantine [123], also have therapeutic potential to improve the key RTT-like phenotypes. These methods targeting on rebalance inhibition and excitation in CNS can shed insight into the treatment of RTT.

In addition, the serotonin 1a receptor agonists, 8-OH-DPAT and F15599 [94,124], decreasing expiratory neuron activity also reduce apnea and correct irregular breathing pattern. The selective serotonin re-uptake blockers which are shown to increase the expression of MeCP2 proteins could also be a potential therapy [125]. Other pharmaceutical intervention includes the

interventions to increase the biogenic amine that is also reported decreased with *Mecp2* disruption in RTT mouse models. For instance, an NE reuptake blocker, desipramine, is able to alleviate the breathing problems and extend the lifespan in RTT mouse model [99,100]. These achievements from mouse model build the cornerstone in RTT treatment.

The clinic or pre-clinic treatments of RTT are difficult. Some clinical trials have been conducted but only with minor improvements and questionable side effects. Currently, a preclinical trial is started on the study of the insulin-like growth factor 1 (IGF-1) which shares similar signaling pathways with BDNF. IGF-1 is widespread in CNS just like BDNF, but has the capability to penetrate the blood-brain barrier (BBB). It is U.S. Food and Drug Administration (FDA) approved and currently under clinical trial to test the side effects and the disease improvement in RTT [125]. Mice Studies show the beneficial effects of IGF-1 to partially reverse the RTT-like symptoms [125,126]. Similarly, boosting the level of endogenous BNDF by an ampakine drug improves the respiratory frequency in RTT mouse model [127]. The exogenous BNDF application may also benefit the RTT treatment, if the problem of short-life and low BBB permeability could be fixed.

Beside the pharmaceutical intervention mentioned above, genetic strategies are challenging but potentially exciting to treat RTT. The cause of RTT is the mutation of MeCP2. Working as a transcription factor, MeCP2 activates and represses a large number of target genes. The *MECP2* mutations shorten the half-life of the MeCP2 proteins. Therefore, a promising way to control this disease could be through genetic methods. Two potential therapies are mentioned by Chpleau et. al. [125]. One way is through stabilizing the expression level of normal MeCP2, such as using selective serotonin re-uptake blockers mentioned above to increase MeCP2 expression thus maintaining the sufficient level of MeCP2 protein. Another potential treatment

approach is through taking advantage of XCI. If the mutate allele of *MECP2* is turned off and the normal one is turned on at the early stage of development, it could markedly reduce the severity of the RTT symptoms.

2.3 Autonomic regulation of cardiovascular system

2.3.1 Overview

The cardiovascular system is another critical system controlled by ANS. It is composed of the heart, vessels and blood, and controls the blood circulation and transportation of oxygen, nutrients, hormones and cellular waste products to target cells in different organs of the body. The cardiovascular system plays three major function: homeostasis regulation of the body, cargo transportation and protection against pathogens.

Heart is a hard-working organ of the body. It pumps approximately 5 liters/h of circulatory blood throughout the body. The cardiac muscle tissue is known as myocardium which is composed of individual cardiomyocytes. These involuntary striated muscles are stimulated by the Ca^{2+} which is stored in the sarcoplasmic reticulum and normally released by stimulation of action potentials from cardiac pacemaker cells in the sinoatrial (SA) node. Once one cardiomyocyte depolarized, a chain reaction is triggered, in which the electricity flows from one cell to another cell via gap junctions of intercalated discs. Intercalated discs secure the synchronized contraction of myocardium. The SA node is regulated by the ANS. In general, the sympathetic nervous system is attributable to the increased heart rate during exercise, while the activation of the parasympathetic nervous system lowers the heart rate.

Blood vessels allow blood to flow between heart and different regions of the body. There are three main types of vessels: arteries, capillaries and veins. All blood vessels are lined with a layer of endothelium in the inner layer. The capillary as the smallest blood vessel is only formed

by a single layer of endothelium cell. The middle layer consists of elastic fiber, connective tissue and vascular smooth muscle, which varies in number depending on the size of the vessels. The outer layer is made of connective tissue. In the larger blood vessels, this layer also contains innervated nerves and nutrient capillaries.

An adult human have ~7-liter blood, 5 liters of which is used in circulation, also known as the effective circulating volume. It transports numerous substances through the body and helps to maintain the homeostasis of gases, water, nutrients, electrolytes and hormones. The contents in blood include red blood cells, immune cells platelets and liquid plasma.

The control of cardiovascular system depends on both local and central mechanisms. Blood flow is determined by the integration of the local control via metabolic stimuli, pressure changes and tissue resistance, and the central control via the ANS. The heart receives innervations from both divisions of ANS. Sympathetic stimulation increases myocardial contractility and heart rate as well as induces blood vessel constriction. In contrast, the simulation of parasympathetic nervous system decreases heart rate [128].

2.3.2 Regulation of vascular tone

Vascular tone which refers to the degree of vasoconstriction and determines the resistance of the circulation varies among organs and is determined by a number of dilator and constrictor substances and ANS. It is the major determinant of blood flow resistance through the circulation. Organs with large vasodilatory capacity usually have high vascular tone, such as skeletal muscle, skin, myocardium and splanchnic system [129]. Some organs, such as brain and kidney, with relatively low vasodilatory capacity in their circulation systems have low vascular tone. The neurohumoral factors are primary mechanisms to regulate the blood pressure via altering the systemic vascular resistance.

Vascular smooth muscle in the middle layer of arteries and veins controls the caliber of the vessel, and is innervated primarily by the sympathetic nervous system. The arteriole as the major contributor to the peripheral resistance is critical to the regulation of systemic blood pressure due to the sympathetic control, while the veins containing less vascular smooth muscle receive limited inputs from sympathetic nerves. In contrast, the small vein and capillary lack of vascular smooth muscle are not directly innervated by sympathetic nerves.

2.3.2.1 Regulation by sympathetic nervous system

The sympathetic nervous system regulated the vascular tone by different stimuli. For example, temperature drop, emotional stimuli, exercise activity, hypoglycemia and stimulation of baroreceptors can increase sympathetic outflow. In general, the sympathetic nervous system regulates the contraction of VSM through adrenergic receptors. And the main endogenous agonist for these receptors is NE which is released from the sympathetic vasoconstrictor fiber and activates on α_1, α_2 and β_2 adrenergic receptors [130]. Since the distribution of α_1 receptors is greater in the arteries, the activation of sympathetic nervous system leads to the integrated vasoconstriction and increases the blood pressure. β_2 receptors which show higher affinity for EPI can be activated by low level of EPI and leading to vasodilation in vessels [131].

In vasculature, dopamine can act on dopamine receptors and inhibit the release of NE as a vasodilator [132]. Its production in the blood stream may be from sympathetic nervous system [4]. Other neurotransmitters contribute to modulate the vascular tone includes neuropeptide Y (NPY) or ATP released from the vascular sympathetic nerve endings [133]. These co-transmitters are able to increase the intracellular Ca^{2+} and produce vasoconstrictive effect via NPY Y_1 receptors and purinergic P_2X receptors respectively [133].

Besides, the renin-angiotensin-aldosterone system (RAAS) is believed having a crosstalk with sympathetic nervous system. This system is one of the most important regulators of blood pressure. The adrenal medulla in RAAS receives sympathetic preganglionic innervation and release catecholamines in turn increasing sympathetic tone. Renin can be released from renal juxtaglomerular cells into circulation by sympathetic stimulation, and carries out the conversion of angiotensinogen released from liver to angiotensin I which is a substance of angiotensin-converting enzyme (ACE) found in lungs. ACE converts angiotensin I to angiotensin II acting as a potent vasoconstrictor that causing blood vessels to narrow [134]. Angiotensin II also activates the secretion of aldosterone from adrenal gland promoting the reabsorption of Na^+ and water and excretion of K^+. In addition, angiotensin II may act as an endogenous neurotransmitter inside the sympathetic coeliac ganglia [135].

2.3.2.2 K^+ channels action in vascular tone regulation

K^+ channels in VSMC play an important role in setting resting membrane potential and regulating vascular tones. For example, Ca^{2+}-activated K^+ (BK) channels are abundantly expressed in VSMCs [136]. They are characterized by their large conductance for K^+ ions. BK channels play important role in vascular tone regulation, in which their activation leads to hyperpolarization of cell membrane by a raised intracellular Ca^{2+} from intracellular stores and extracellular influx [137]. Micromolar Ca^{2+} sparks can activate BK channels in rat cerebral artery smooth muscle [138]. Thus, they regulate vascular tone and function to buffer vasoconstriction. In disease conditions, such as diabetes and hypertension, the function of BK channels can be impaired [139,140].

ATP-sensitive potassium (K_{ATP}) channels widely distributed in the vascular system are also critical in regulating the membrane excitability of VSMC [141]. The K_{ATP} channels are

inhibited by increase of intracellular ratio of ATP and ADP, causing membrane depolarization and consequent vasoconstriction. K_{ATP} channels can be targeted by multiple vasoconstrictors and vasodilators, such as α-adrenoceptor agonists and β-adrenoceptor agonists respectively. A subtype of K_{ATP} channels, Kir6.1/SUR2B channel, can be targeted by many reactive oxygen species (ROS), leading to post-translational modification which alters the channel activity [142]. Furthermore, in some disease conditions, such as septic shock, an upregulation of Kir6.1/SUR2B expression is observed, represented by raised blood pressure through increasing systemic vascular resistance [143,144].

2.3.2.3 Role of endothelium in vascular tone regulation

The endothelium also contributes to local blood flow regulation by releasing endothelium-derived contracting factors, such as thromboxane A_2 (TXA2) and endothelin, and endothelium-derived relaxing factors, such as nitric oxide (NO), prostacyclin (PFI_2) and endothelium-derived hyperpolarizing factors (EDHFs) [145,146]. The release of these factors varies in different vessels [147]. For example, NO released in a vessel size-dependent manner is the major vasodilator in conduit arteries. And small resistance vessels have more contents belonging to EDHFs. Epoxyeicosatrienoic acids (EETs), hydrogen peroxide (H_2O_2) and endothelium-derived K^+ ions are considered as EDHFs. Besides, endothelium can communicate with VSMCs through gap junction, which is involved in endothelium-dependent hyperpolarization [146]. These mechanisms driven by endothelium ensure the proper maintenance of vascular tone under physiological and pathophysiological conditions.

2.3.3 Diabetes mellitus and Vascular lesions

Diabetes mellitus is a group of diseases in which the blood glucose level is too high over a prolonged period. There are two main types of diabetes. Type I diabetes results from the failure

of sufficient insulin production. Type II diabetes relates to unhealthy lifestyle, and is caused by insulin resistance with obesity and insufficient exercise. Cardiovascular diseases are the principal cause of morbidity and mortality in patients with diabetes. Hyperglycemia is a major contributor of the development of micro- and macro-vascular complications in diabetes through different mechanisms [148,149]. The microvascular complications in the retina is one major cause leading to blindness and visual disability in diabetes. While, atherosclerosis and medial calcification are the common macrovascular diseases in diabetes. High blood sugar level in diabetes generates oxidative stress, accelerate inflammation, activate protein kinase C (PKC) pathway and increase formation of advanced glycation end products (AGEs) contributing to the damages of the vasculature.

2.3.3.1 Oxidative stress in diabetic vascular lesion

Oxidative stress refers to an elevated intracellular level of reactive oxygen species (ROS), such as hydrogen peroxide (H_2O_2), hydroxyl radical ($OH^{\bullet}$), superoxide anion ($O_2^{\bullet -}$), and hypochlorous acid (HOCl) [150-152]. ROS are generated as byproduct of cellular metabolism. There is considerable evidences indicating that hyperglycemia-induced endoplasmic reticulum stress and mitochondrial dysfunction promote the accumulation of ROS. ROS can also be generated by endothelial NAD(P)H oxidase, a membrane-associated enzyme catalyzing the production of superoxide, and endothelial uncoupled eNOS, a mechanism leading to excessive superoxide [153-155]. Without appropriate compensation by the antioxidant defense network, excessive ROS contributes to the development and progression of cardiovascular disorders in diabetes. Hyperglycemia-caused oxidative stress induces dysfunction of the vascular endothelium, the primary defense against thrombosis and other vascular injury. The overproduced ROS results in reduced endothelial production of NO and irreversible post-translational modification of K_{ATP}

channel on the membrane of VSMCs, thus leading to impairment of vasodilation [156,157]. Oxidative stress may also promote the expression of pro-coagulant and pro-inflammatory factors as well as induce cell apoptosis [155]. Besides, it also potentially involve in atherosclerotic instability and subsequent rupture through promoting both VSMC apoptosis and its proliferation [158,159].

2.3.3.2 Inflammatory status in diabetes vascular lesion

Accumulating evidence suggests that hyperglycemia is associated with inflammatory state characterized by increased level of pro-inflammatory cytokines and markers which raise the risks of diabetic cardiovascular disorders [160]. For example, atherosclerotic cardiovascular disease is one of the most common inflammatory diseases in diabetes. Evidence indicates that hyperglycemia may play a role in atherosclerosis by promoting pro-inflammatory responses of myeloid cells, such as monocytes, macrophages and T lymphocytes, which are rapidly accumulated at the site of inflammation in vessel [161-163]. In addition, the differentiation and maturation of dendritic cells from type II diabetic patients are impaired with high glucose exposure [164]. The hypoglycemic stress caused by overdose insulin, excessive exercise or fasting in diabetes patients also contributes to elevation of the pro-inflammatory leukocytosis and cytokines [165].

Oxidative stress and inflammation state usually interact with each other. ROS whose production is enhanced in diabetes by increased dysfunctional mitochondrial can act as a mediator of inflammation, aggravating the tissue injury thus progressing the inflammatory disorders [166]. Activated polymorphonuclear neutrophils at the inflammatory site, in turn, increase the generation of ROS [167].

2.3.3.3 Activation of PKC pathway in diabetic vascular lesion

PKC pathway can be stimulated by hyperglycemia, having a big impact on ROS and NO generation. PKC activated by glucose may be implicated in the activation of NAD(P)H oxidase and the consequent production of superoxide. Indeed, increased activity of this enzyme is found in internal mammary arteries and saphenous veins of diabetes patients [168]. In addition, activation of PKC inhibits the activity of the phosphatidylinositol 3 kinase (PI3K) pathway, an important pathway to generate vasodilator NO in endothelium in response to insulin stimulation in order to maintain glucose homeostasis [169]. Inhibition of PKC pathway can restore the abnormal endothelium-dependent relaxation of animal aorta caused by hyperglycemia [170]. In addition, hyperglycemia activated PKC signaling may contribute to the hypercoagulable state and the formation of thrombus as well, by activation of platelets and clotting factors and impairing fibrinolytic capacity [171,172].

2.3.3.4 Advanced glycation end products (AGEs) in diabetic vascular lesion

AGEs are glycated proteins or lipids as a result of exposure to glucose [173]. AGEs, such as glyoxal, 3-deoxyglucosone and MGO, can be generated from many processes [174]. Mitochondrial superoxide also increases the production of AGEs [175]. Increased AGEs induced by hyperglycemia is found in diabetic retinal vessels and renal glomeruli [176,177]. AGEs can induce crosslinking of collagen fibers in the artery walls, leading to vascular stiffening and entrapment of low-density lipoprotein particles (LDL). Both of these events are associated with arterial complications, such as arteriosclerosis [178]. AGEs can also lead to the glycation of LDL which promotes its oxidation as one of the major contributors in development of atherosclerosis [179]. Furthermore, AGEs adversely affect cellular function by activation of the AGEs receptors (RAGE), inducing pathological changes in gene expression and increase endothelial permeability

to macromolecules [173,180]. AGEs also contribute to production of ROS and diminished NO activity [173]. Oxidative stress caused by hyperglycemia in patients with diabetes facilitates the formation of AGEs. In sum, AGEs affect many of molecules and cells, and interact with other hyperglycemia-induced mechanisms of vessel lesion.

2.3.4 Intervention to cardiovascular system

The study of the cardiovascular system has attracted considerable attention due to the large prevalence and the high fatality of cardiovascular diseases. The world health organization reports that the death roll of cardiovascular diseases in 2008 is about 17.3 million people, and this number is going to increase to over 23 million in 2030 [181]. Therefore, both the clinic assessments and the laboratory interventions to cardiovascular functionality are important in diagnosis and treatment of these diseases. The clinic assessments, such as electrocardiogram (ECG), heart rate monitoring, invasive and noninvasive blood pressure measurements and cardiovascular imaging technology, help the doctors to diagnose the function of the cardiovascular system. The laboratory intervention allows researchers to reveal the underlying mechanisms of the cardiovascular functions and dysfunctions for potential treatment methods.

2.3.4.1 In vitro experimental strategies for cardiovascular investigation

In order to better understand the mechanisms of cardiovascular function and dysfunction, novel experimental approaches to the vessel and heart are needed. Under *in vivo* conditions, the cardiovascular system responses to current pharmacological approach may depend on complicated events such as different cell types, hormones in blood, neuronal regulators, metabolic products from surrounding tissues, shear stress, transmural pressure and certain reflex responses. The complexity of the system limits the mechanistic insight. Therefore, the discovery

of alternative experimental approaches such as the emerging optogenetics may be helpful (see below).

Multiple cultured cell lines including endothelial cells lines, VSMC lines and cardiomyocyte cell lines are used as *in vitro* model systems for various physiological and pathological researches. Parameters such as temperature, osmotic pressure, O_2, CO_2, nutrition and pH can be easily controlled through the culture medium. The obvious advantages of using the cultured cell lines include fast growth, minimal care, simplicity of circumstances species specificity and instant response to reagents. They are very good tools to study the signaling pathways. The disadvantages is also obvious: the change of phenotype over time and no crosstalk between cell species.

Isolated and perfused blood vessels are a useful approach for the studies of functional blood vessels. This technique allows us to exam vessel rings with diameter ranging from 20 μm to several millimeters. The isolated vessels segments can consist of the intact endothelial cells in the tunica intima and VSMCs in the tunica media as well as fibroblasts, fat cells and even nerve end in the tunica adventitia. Endothelial cells can be removed in the denuded vessel segments according to demands [182]. The tunica adventitia can be selectively removed as well. Two methods to prepare cylindrical vessel segments are developed. The ring vessel segments are prepared by threading vessels segments onto two metal hooks or wires [183,184]. In most of the recording, vessel rings are prepared under isometric conditions in which the initial loading force is given and changes of vascular tone is recorded by a force transducer connected to one of the hooks or wires. Another method is cannulated vessel segments which are prepared by fixing the vessel segment on two pipettes between which the vessel segment is perfused by applying a flow at a desired rate [185]. This preparation is considered to be closer to *in vivo* conditions. These

methods help in understanding the mechanisms of vascular regulatory processes in health and diseases. However, current technique only allow experiment to be conducted on relatively large vessels. The application of this technique is restricted when handling the arterioles, capillaries and vessels embedded in the organ and entangled with connective tissues, such as coronary artery.

Isolated and perfused heart (Langendorff isolated heart perfusion system) is a valuable approach for study of cardiovascular function and dysfunction since its introduction by Oskar Langendorff at the late 19th century. This heart preparation method is still being used even after 100 years. It can be applied on both large animal models, such as pig, dog, cat and rabbit, and small animal models, such as frog, rat and mouse. In the Langendorff preparation, the heart is removed from the body and perfused in a reverse direction through aorta root [186-188]. The retrograde flow closes the aortic valve and force the oxygenated solution into the coronary artery. The less-oxygenated solution is collected in the right atrium through coronary sinus, and finally drains through vena cava. The Langendorff isolated heart system has led to a number of fundamental discoveries in cardiac physiology and pathology. A variety of parameters including the condition of the myocardium and the coronary vessels can be measured through this system with great pharmacological value, high reproducibility and relatively low cost. Although a few shortcomings exist, including the difficulty to maintain the high coronary flow especially in larger animal models, and the absence of the neuronal regulation and normal humoral influences, it has brought many valuable achievements in studies of ischemia-reperfusion injury, coronary occlusion, arrhythmias and heart preservation for transplantation [189].

2.3.4.2 Optogenetics in cardiovascular studies

Optogenetics is a new technique which combines genetic and optical technologies for studies of specific biological processes. It has been rapidly progressing since Dr. Boris Zemelman and Dr. Miesenböck developed a method to stimulate the genetically designed neurons optically in 2002 [190]. The restricted control of the neuronal activity expends the knowledge of the neural remote control, the function of specific types of neurons, and the neural circuit mapping through activation of rhodopsin transgenic mice optically. The high temporal and spatial resolution makes optogenetics an excellent tool in the neural studies [191,192].

The optogenetic methods are also useful in cardiovascular field [193,194]. The spatiotemporal precision and noninvasive control are the major advantages which have been disgusted in some of the prior studies. The optoregulatory method is considered to be an ideal alternative to control the heart rhythm by conditionally expressing opsins in cardiomyocytes or transplanting a group of engineered non-excitable cells with optical excitability into the heart [193,195]. The former can be achieved by directly delivering opsins to normal myocytes using viral vectors, while the latter method can take advantage of the formation of gap junctions between the donor cells and the host myocytes [195]. The optogenetic technique has a potential to be applied to the cardiac arrhythmias termination and the cardiac pacing therapy [196-200]. Despite its highly promising potentials, whether the optogenetics can be used in in cardiovascular research remains to be demonstrated. Thus, we applied optogenetics to the vascular tone manipulation, aimed at controlling the vasoconstriction in various tissues and organs.

3 SIGNIFICANCE

The ANS regulates many important body processes in health and diseases, such as the rate of breathing and the blood pressure. These two processes are so critical that the disorders of any of them can cause severe health problems and even threaten lives.

RTT is a progressive neurological disorder, predominantly affecting female children worldwide with an incidence of 1: 10,000 female births. Children with RTT develop normally in the earlier age. By the age of 18 months, most of the RTT patients start to display developmental regression. The most serious disorder among the core RTT symptoms is respiratory disturbances, such as hyperventilation, apnea, hyperpnoea, breath holding and etc. Mental and growth retardations are also observed accompanying with autistic syndromes. The severe breathing disorders of RTT usually end up with the high incidence of sudden death and contribute the abnormality of the brain during development. Because of lack of understanding of the disease, effective therapies are still unavailable. Therefore, it is necessary and significant to reveal the mechanisms of RTT.

Nevertheless, the genetic basis of RTT is known. Mutations of *MECP2* gene result in more than 90% of RTT pathology. MeCP2 is a transcriptional factor. Its defect or deficiency can cause disruptions and dysfunction in the CNS, whereas the neurobiological mechanisms of the RTT and the causal relationship between defect of *MECP2* and RTT are still poorly understood. Animal models have been developed and used in the study of RTT for more than a decade, including *Mecp2*$^{-/Y}$ (*Mecp2*-null) males and *Mecp2*$^{-/+}$ females mouse models. However, the mouse models have some limitations. Firstly, the small body size of the mouse models limits the feasibility of *in vivo* neuronal studies under physiological condition, such as *in vivo* electrophysiological recordings from central neurons. Secondly, the timely blood gas analysis

cannot be achieved due to the small quantity of blood. Thirdly, information obtained from the mouse models in the studies of RTT needs to be validated on another RTT animal models. Also, studies in multiple animal models of RTT are highly necessary for drug development to increase the translatability. Therefore, we take the advantage of the novel *Mecp2*–null rat model and performed a number of studies that cannot be done in the mouse models.

Breathing abnormalities are major challenge in RTT patients. More than half of the RTT patients show hypoventilation alternating with irregular breathing or hyperventilation (central and obstructive apneas, apneustic breathing, breath holding, periodic breathing, Valsalva's maneuvers and Biot's breathing). The "skipped breathing" usually leads to the retardation of CO_2 and the severe reduction of O_2 in the vasculature and organs. The mouse models show similar phenotypes as human, displaying apneic and irregular breathing patterns that progressively worsen until death [81,112], which facilitate the discovery of the RTT mechanisms. However, the mechanism underlying the periodic alternation of hypo- and hyperventilation of RTT is still elusive, especially the activity aspects of the neurons involved in respiration. Additionally, due to the size limit and fragileness of mice, *in vitro* electrophysiology, *in situ* arterially perfused brainstem-spinal cord and *in vivo* plethysmography are the major strategies used before, but not *in vivo* electrophysiological study which provide the straightforward views of the cells in the physiological condition. By using the newly available RTT rat model, we are able to perform *in vivo* electrophysiological studies on the respiratory neurons in the ventral respiratory group. The new RTT animal model will help us to confirm the truth of the previous findings and open the new avenue to the study of RTT. Our studies on rat model of RTT may open up the field of research into new treatments for respiratory-control disorders in humans.

Cardiovascular regulation is another critical process controlled by ANS. Cardiovascular diseases are the number one challenge to medical sciences globally: more people die annually from these diseases than from any other diseases. According to WHO in 2015, about 17.7 million people dies from cardiovascular diseases, which count almost one third of the global deaths [201]. A considerable part of these deaths are due to diabetic cardiovascular complications and hypertension. Diabetes is the leading health challenge, especially in developing and developed countries. This metabolic disorder can have both acute and chronic complications such as diabetic ketoacidosis, cardiovascular disease and stroke, in which cardiovascular lesions were caused by accumulation of various intermediary metabolites. MGO as one of the intermediary metabolites is a highly reactive carbonyl species (RCS) [202,203]. It is known that MGO can impair structure and function of the vascular wall, which contributes to diabetes-related vascular disorders including hypertension [204,205]. But what it targets to cause the damage of the vascular tone is still unclear. An isoform of the K_{ATP} channels in vascular smooth muscles which is critical in vascular tone regulation is recently found to be a target of MGO [206]. Via certain unknown mechanisms, MGO acts on the mRNA of this channel reducing its expression leading to augmented vasoconstriction [206]. Therefore, we studied how MGO down-regulates K_{ATP} channel mRNAs.

For a long period, the accessibility to the vasculature heavily relies on pharmacological agents. The advantage is systemic effect of these agents, but the obvious disadvantage is also little spatial resolution. Thus, alternative accesses to the cardiovascular system are needed. The advance in optogenetics opens a new avenue to access the cardiovascular system. However, this promising technology has not been extended to vascular system. Therefore, we generated a novel mouse strain with expression of ChR2 in VSMCs, and tested the expression and excitability of

ChR2 in VSMCs of multiple organs. Our studies indicate that the application of optogenetics in vasculature could be a potent tool to produce reproducible and light intensity-dependent vasoconstriction with high spatiotemporal specificity.

4 MATERIAL AND METHODS

4.1 Animal

All animal experiments were conducted in accordance with the National Institutes of Health (NIH) *Guide for the Care and Use of Laboratory Animals* and were approved by the Georgia State University Institutional Animal Care and Use Committee.

4.1.1 Rat

The experiments were performed on male *Mecp2*$^{-/Y}$ rats. To breed these males, the female heterozygous *Mecp2*$^{+/-}$ rat ((SD-*Mecp2*^{tm1sage}, strain code: TGRA6090) from the supplier company Horizon Discovery Group (Boyertown, PA) were crossbred with the male Sprague-Dawley wild-type rat (WT). The genotyping protocol from Sage Labs in Horizon Discovery Group was used to identify WT, heterozygous, and homozygous animals based on a 71bp deletion in the *Mecp2* (Primer F: GCAGCATCAGAAGGTGTTCA, Primer R: GACCTCAATGCTGACGGTTT). Animals used in the electrophysiological experiments were 1.5-2.5 month male rats. Humane endpoints of all null rats were determined independently by staff members in our school animal facility.

4.1.2 Mice

Female heterozygous mice (Genotype: *Mecp2*$^{+/-}$; Strain name: B6.129P2(C)-*Mecp2*tm1.1Bird/J; Stock number 003890) from Jackson Lab were crossbred with male C57BL/6 mice to produce the *Mecp2*$^{-/Y}$ mice.

For the generation of Tagln-ChR Mice, two stains of mice were used to generate mice with ChR2 expression in VSM cells: 1. Tagln-cre mice (Jackson Laboratories, West Grove, PA; 004746, STOCK Tg(Tagln-cre)1Her/J) expressing Cre recombinase under the control of *Tagln* promoter, and 2. ChR-LoxP mice (Jackson Laboratories; 012569, B6; 129S-

Gt(ROSA)26Sor$^{tm32(CAG-COP4*H134R/EYFP)Hze}$/J) expressing the channelrhodopsin2 (H134R)/eYFP fusion protein following a LoxP-flanked STOP cassette. The male homozygous Tagln-cre mice were crossed with the female heterozygous ChR-loxP mice. Their offspring were found to be ChR2$^{+/-}$-Tagln-cre$^{+/-}$ (Tagln-ChR) or ChR2$^{-/-}$-Tagln-cre$^{+/-}$ (Tagln-cre). Genotypes were determined by using the primers provided by the Jackson Laboratories. Tagln-ChR and Tagln-cre mice were used in the present study as the test and control groups respectively. Genotyping of these mice was shown (Fig. 8.1). Crossing heterozygous ChR-loxP mice with the homozygous Tagln-cre mice led to the removal of the STOP signal before ChR2-eYFP (Fig. 8.1A). The offspring Tagln-ChR contained both ChR-loxP and Tagln-cre genes, while ChR-loxP was missing in Tagln-cre mice (Fig. 8.1B).

4.2 Animal behavior tests

4.2.1 Body Weight and In-cage Conditions

Body weight of animals was measured and recorded every week starting from postnatal day 7 (P 1w) till death. Tooth growth, food and water intake, movements and other body condition were regularly checked as well. Overly grown incisors that affected the food intake were monitored and trimmed by the veterinarian weekly.

4.2.2 Grip Strength

During the experiment, an animal was lifted by the tail, and their forelimbs were allowed to grasp the metal mesh fixed to a force-electricity transducer (CB Sciences, Inc., Milford, MA). The animal was then gently pulled upward while it grasped the mesh (10mm x 10mm) with both forelimbs. The maximal force reached immediately before it released the mesh was taken as the grip strength. Signals were amplified, collected with the Clampex 9 software and stored in a computer. Comparison between rats and mice was done in animals aged 5~6 weeks.

4.2.3 Spontaneous Locomotion Test

Locomotion activity of male rats aged 4~5 weeks was tested in a test chamber made of white plexiglass boards (80 cm × 80 cm × 30 cm). The arenas were divided into 10 cm × 10 cm squares (n=64) by drawing thin black lines on the floor. The locomotion apparatus for male mice aged 5-6 weeks was constructed with the same material in size 50 cm × 50 cm × 30 cm with 10 cm × 10 cm square lines. Animals were carried to the test room in their home cages and habituated for 30 min before the locomotion test. Each tested animal was placed in a center of the box and observed for 5 min. Each trail was recorded with a video camera. Measures of square crosses (all four paws cross) were obtained from the video record. After the test, the apparatus was thoroughly cleaned using 70% ethanol and then H_2O to eliminate potential residual odors and contaminants.

4.2.4 Three-chamber Test

WT and *Mecp2*$^{-/Y}$ male rats, aged 4~5 weeks, were tested in a three-chambered apparatus (90 cm × 60 cm × 30 cm), where three chambers (30 cm × 60 cm × 30 cm each) were separated by two transparent plexiglass walls with an opening in each wall. Two buckets (12 cm in diameter × 20 cm in height) made of 1 cm × 1cm metal mesh were placed in the center of the two side chambers. Similarly, mice aged 6-7 weeks were tested in an apparatus with three 20 cm × 30 cm × 40 cm chambers. The buckets and the metal mesh were 1/3 smaller in mice than in rats. On the test day, animals were allowed for 30 min habituation to its environment. A three-step procedure was performed. First, the tested animal was placed in the center chamber, and allowed to freely move over all three chambers for 10 min. The time spent in each chamber was recorded with a video camera. Second, sociability was tested, in which a male intruder (Animal 1) in one mesh bucket was introduced to one of the side chambers randomly, while the other

bucket was kept empty. The test animal was allowed to explore both the chambers for 10 min with the total time spent in the chamber measured. The intruder was randomly assigned in one of the side chambers to avoid the side bias. Lastly, the social novelty was tested by switching the familiar intruder into the other chamber and introducing a novel male intruder (Animal 2) to the chamber. The tested animal was monitored for 10 min as well. The time spent in each side chamber was measured. The apparatus was thoroughly cleaned between trails using 70% ethanol and H_2O. All behavior tests were performed during the light cycle (from 10 am to 7 pm).

4.2.5 Plethysmograph Recording

Breathing activities of awake animal were recorded with a plethysmograph chamber. The individual animal was kept in the plethysmograph chamber with air ventilation at a rate of ~1000 ml/min. After at least 20 min adaptation, breathing activity was recorded continuously for 20 min as the barometrical changes between the plethysmograph chamber and the reference chamber with a force-electricity transducer (Emka, Oxford, UK). The signal was amplified and recorded with AxoScope 10.3 software in a computer. The data was analyzed with Clampfit 10.3 software. Apnea rate and respiratory frequency variation were measured. Apnea was considered only if the inspiration interval was twice longer than the previous breathing. Breathing frequency variation was defined as the standard deviation (SD) of the breathing frequency divided by their arithmetic mean. The SD and arithmetic mean were measured from ~200 successive breathing events.

4.3 Lifespan

WT and *Mecp2*$^{-/Y}$ animals were randomly selected from litters. Their lifespan were monitored. Death date of each group was recorded. Both in-cage death and the cases reach humane endpoint determined by the animal facility at Georgia State University were counted. One outlier at each end was removed from the data analysis to minimize the data variation.

4.4 Electrophysiology

4.4.1 In vitro Electrophysiology

Experimental rats or mice were decapitated after deep anesthesia with inhalation of saturated isoflurane. The brainstem was obtained and immediately placed in an ice-cold and sucrose-rich cutting (in mM) solution containing 220 sucrose, 33 $NaHCO_3$, 1.9 KCl, 6 $MgCl_2$, 1.2 NaH_2PO_4, 0.5 $CaCl_2$ and 10 D-glucose. The solution was bubbled with 95% O_2 - 5% CO_2 (pH 7. 40). Transverse pontine sections (150~300 μm) containing the LC were obtained by using a vibratome sectioning system and then recovered at 33 °C for 60 min in normal artificial cerebrospinal fluid (aCSF) (in mM) solution containing 124 NaCl, 26 $NaHCO_3$, 3 KCl, 2 $MgCl_2$, 1.3 NaH_2PO_4, 2 $CaCl_2$ and 10 D-glucose. The brain slices were kept at room temperature before usage. At recording, the slices were perfused with oxygenated aCSF at a rate of 2 ml/min and maintained at 34 °C in a recording chamber by a dual automatic temperature control (Warner Instruments).

Whole-cell current clamp was performed on LC neurons in the brain slices. Patch pipettes with a resistance of 3~5 MΩ were prepared with Sutter pipette puller (Model P-97, Novato, CA). Only were the neurons with membrane potential less than -40 mV and action potential larger than 65 mV accepted for further experiments. The pipette solution (in mM) contained 130 K gluconate, 10 KCl, 10 HEPES, 2 Mg-ATP, 0.4 EGTA and 0.3 Na-GTP (pH 7. 3). The bath solution was normal aCSF bubbled with 95% O_2 balanced with 5% CO_2 (pH 7. 40). Recorded signals were amplified with an amplifier Axopatch 200B (Molecular Devices, Union City, CA), digitized at 10 kHz, filtered at 2 kHz, and collected with the Clampex 8.2 data acquisition software (Molecular Devices).

The single-cell voltage clamp was used to record whole cell K_{ATP} currents in cells transfected with different agents. Patch-clamp protocols were performed as previously described [206]. Briefly, the patch pipettes were made with 1.2 mm borosilicate glass capillaries (with resistance of 2~5 MΩ). Current records were filtered with low pass (2 kHz, Bessel 4-pole filter, -3 dB), digitized (20 kHz, 16-bit resolution), and analyzed with Clampfit 9 software (Axon Instruments, Union City, CA) The bath solution contained (in mM) 10 KCl, 135 potassium gluconate, 5 EGTA, 5 glucose, and 10 HEPES (pH 7.4). The pipette solution contained (in mM) 133.0 K^+ gluconate, 10.0 KCl, 5.0 EGTA, 5.0 glucose, 1 K_2ATP, 0.5 NaADP, and 10.0 HEPES (pH 7.4). The final Mg^{2+} concentration was adjusted to 1 mM. The membrane potential was held at 0 mV and stepped to -80 mV every 3~4 s.

The whole-cell voltage clamp and current patch clamp were used to demonstrate optostimulation of isolated aortic VSM cells. Recorded signals were amplified with an Axopatch 200B amplifier (Molecular Devices, Union City, CA), digitized at 10 kHz, filtered at 2 kHz, and collected with the Clampex 10 data acquisition software (Molecular Devices, Union City, CA). The patch pipettes with resistance of 4~6 MΩ were made with 1.2 mm borosilicate glass capillaries. All recordings were performed at room temperature. The optostimulation was performed by using a xenon arc lamp with high speed switcher Lambda DG-4 system (Sutter Instruments, Novato, CA). The light source was connected to the incident-light illuminator port of the microscope, and passed through a 470 nm bandpass filter (~20 mW/mm^2). Light pulse trains were generated with the Digitimer D4030 pulse generator (Digitimer Ltd, Letchworth Garden City, UK). The solution applied to the bath contained (in mM) 130.0 NaCl, 10.0 KCl, 1.0 $MgCl_2$, 1.5 $CaCl_2$, 10.0 glucose, 10.0 HEPES and 3.0 NaOH (pH 7.4). The internal (pipette) solution contained (in mM) 10.0 KCl, 133.0 K^+ gluconate, 5.0 EGTA, 5.0 glucose, 1.0 K_2-ATP,

0.5 Na-ADP, and 10.0 HEPES (pH 7.4), and the final Mg^{2+} concentration was adjusted to 1 mM using a [Ca^{2+}]/[Mg^{2+}] calculation software.

4.4.2 In vivo Electrophysiology

Rats were anaesthetized with the urethane (1.5 g/kg, i.p.) followed by intercollicular decerebration in a stereotactic device. The animals were allowed to breathe spontaneously. Phrenic nerve was exposed at cervical cord C3-C6 level from the dorsal side, and its activity was recorded with bipolar silver hook electrodes. Mineral oil was applied to prevent the dryness of the nerve during recording. Phrenic signal was amplified and filtered (300 Hz to 5 kHz) with an A-M systems (Model 1700 Differential AC Amplifier, A-M SYSTEMS^{TM}). Phrenic discharge was recorded with Clampex 8.2 software and analyzed with Clampfit 10.3 software. Integrated phrenic signal was obtain through a Paynter filter (50 ms time constant, BAK Electronics Inc., Rockville, MD.).

Partial cerebellum was removed using vacuum suction to expose the brainstem. Single neuronal activity was recorded with tungsten microelectrodes covered with glass. The signals were amplified (Instrumentation Amplifier, Model 210 A, Brownlee BP precision) (Axoclamp-2B Current and Voltage Clamp Amplifier, Axon Instruments. Inc.), digitized (Digidata 1322A, Axon Instruments. Inc.), recorded (Clampex 8.2 software, Molecular Devices) and off-line analyzed (Clampfit 10.3 software, Molecular Devices). After completion of the surgery, rats were stabilized for 20-30 min. The obex on the dorsal surface of the medulla was used as the land marker to locate the recording sites. Body temperature and heart rate were closely monitored during surgical and recording procedures. Lost fluid was supplied with warm saline through i.p. injection.

Stimulation bipolar electrode was inserted controlaterally into the lateral or ventrolateral funiculi) of the C2 to stimulate the axons of the inspiratory premotor neurons. The depth of the stimulation site was determined by giving the maximum orthodromic monosynaptic response in the phrenic recording (~2 mm from the dorsal surface of spinal cord). Single pulse (1 Hz, 0.1 ms duration, 3-20 volts) was delivered through a stimulus isolation unit (Model SIU5C, Grass Instrument Co., Quincy, MA). Neurons were identified as bulbospinal neurons by collision tests. Stimulus intensity was set at the threshold for antidromic activation of bulbospinal neurons.

4.5 Cell culture and transfection

HEK293 cells (CRL-1573; American Type Culture Collection, Manassas, VA) and rat VSM cells (A10 cell line, CRL-1476; American Type Culture Collection) were cultured in complete DMEM (10% FBS) in a 5% CO2 atmosphere at 37°C. Two to four generations were used for experiments. After growth arrest, the cells were transfected using lipofectamine. Subsequently, the cells were switched to complete DMEM (10% FBS) and cultured in a 5% CO2 atmosphere at 37°C for another 24~48 h.

4.6 microRNAs intervention

4.6.1 Bioinformatics prediction of miR targets

To identify the candidate miRs that potentially targeted rat Kir6.1 (*Kcnj8*), we used the miRWalk database (https://www.umm.uni-heidelberg.de/apps/zmf/ mirwalk/index.html) that is supported by eight miRNA prediction programs on 3'-UTRs of all known genes of the human, mouse, and rat. A probability distribution of random matches of a subsequence (miR 5'-end sequence) in the given sequence was calculated by using Poisson distribution, where a low probability implies a significant hit [207,208]. The default *P* value (0.05), the mirSVR score ≤ 0 [209], plus at least six complementarity seeds were used for miR/*Kcnj8* alignment. A number of miRs

potentially target Kir6.1 3'-UTR. To limit the number we used the following criteria: *1*) their high conservation across a wide range of mammals and *2*) their potential involvement in diabetes in existing literature. On the basis of these criteria, three potential Kir6.1-targeting miRs were selected for further screening. Similarly, six potential miRs for SUR2B CDS targeting were predicted using the same database. The targeting site conservation was examined among rats, mice, and humans by comparing NCBI BLAST alignment as the similar searches with human KCNJ8/ABCC9 showing no miRs matches in the same 3'-UTR/coding region.

4.6.2 Synthesis of miR-9a-3p and anti-miR-9a-3p

Chemically synthesized and optimized double-strand nucleotides (m-9) were designed to mimic endogenous mature miR-9a-3p in VSM and scrambled RNAs (scmiR) was synthesized as negative control (Qiagen, Sample & Assay Technologies, Valencia, CA). Single-strand antisense oligonucleotides (anti-9) complementary to the mature miR-9a-3p were synthesized to specifically target and knock down endogenous miR-9a-3p in VSM (Sigma-Aldrich).

4.7 K_{ATP} channel expression

4.7.1 Construction of Kir6.1 and SUR2B mRNA expression vectors

The cDNAs encoding rat Kir6.1 mRNA (GenBank no. D42145.1) and mouse SUR2B mRNA isoform (GenBank no. D86038, mRNA isoform NM_011511) were cloned and inserted into pcDNA3.1 (an eukaryotic expression vector), respectively, as previously described [206], which were named with Kir and SUR, respectively.

The mutated pcDNA3.1 construct of the SUR2B (M-SUR) was obtained using the Stratagene QuikChange mutagenesis (New England BioLabs, Ipswich, MA) and used for real-time quantitative PCR (qPCR) and patch studies. The mutagenic oligonucleotide primer pair was designed according to the desired mutation in its seed match sequences. Briefly, the M-SUR was

cloned with the primer pair (forward: CCCTAAATTACTTTTGGCCTTATTCCTGTACTGG; reverse: CCAGTACAGGAATAAGGCCAAAAGTAATTTAGGG), containing two site mutations in position 622 and 625 of SUR2B mRNA (Fig. 8.1*B*).

4.7.2 Heterologous expression of K_{ATP} channel

K_{ATP} channels were heterologously expressed in HEK293 cells as previously described [206]. Briefly, the constructions of Kir6.1 and SUR2B mRNA expression vectors were cotransfected to the HEK293 cells (ratio of 1:3), and the pEGFP-N2 (Clontech, Palo Alto, CA) was transfected together to identify the positively transfected cells. One day after transfection, the cells were again transfected with synthesized m-9 or anti-9. After another day in culture, the cells were used for electrophysiological studies and luciferase analysis.

4.8 Real-time quantitative PCR

The qPCR analysis was performed with high-capacity cDNA Reverse Transcription Kit and Fast SYBR Green Master Mix (Applied Biosystems, Life Technologies, New York, NY) following the manufacturer's instructions. Primers specific for Kir6.1, SUR2B, miRs, RNU6B, and GAPDH were synthesized from Sigma Genesis (Sigma). The qPCR was performed with a Fast Real-time PCR system (Applied Biosystems 7500) for 40 cycles. The fold increase relative to control samples was determined by the $2^{-2\Delta\Delta CT}$ method. Expression levels of target mRNAs were determined using total RNA from A10 or HEK cells. GAPDH was used as internal control for SUR2B mRNA expression. RNU6 was used for normalization of miR-9a-3p expression.

4.9 Histology

Mice at the age 2 to 3 months were euthanized by deep anesthesia followed by thoracotomy. The heart, kidney, mesentery, small intestine, uterus and skeletal muscle tissues were collected from the mice. After four hours fixation in 1% Paraformaldehyde (PFA) at room

temperature, the tissues were treated overnight with 30% sucrose in Phosphate Buffered Saline (PBS) buffer at 4°C. The tissues were embedded in the Tissue-Tek^{TM} CRYO-OCT Compound (Andwin Scientific, Torrance, CA, 4583), and cut into 8 μm slices by using the Microm HM 550 Cryostats system (Thermo Scientific, PA, 22-050-337). YFP fluorescence was detected with 514/527 nm (excitation/emission wavelength) filters under the microscope (Carl Zeiss, Gottingen, Germany, Axiovert 200). Images were analyzed with the ImageJ 1.48 (NIH, Bethesda, MD).

4.10 Organ and cell preparation

4.10.1 Acute dissociation of VSM cells

Thoracic aorta was dissected free in the dissection solution containing (mM): 140.0 NaCl, 5.4 KCl, 1.0 $MgCl_2$, 0.1 $CaCl_2$, 10.0 glucose, 10.0 HEPES (pH was adjusted to 7.4), cut into 1-2 mm segments, and incubated in 0.1 ml dissection solution containing 20 unit/ml papain (Worthington, Lakewood, NJ, LK003176) and 1.25 mg/ml DTT for 15 min at 37℃. The tissue segments were further digested with 440 unit/ml collagenase type IA (Sigma, St. Louis, MO, C0130) for 2-3 min at 37℃, followed by three washes and gentle trituration with a fire polished glass Pasteur pipettes. The solution containing individual VSM cells was dropped in a Petri dish coated with poly-L-lysine (Sigma, P8920) and prepared for patch clamp and contractile studies. The cell suspension was stored at 4℃ and used within 4 hrs.

4.10.2 Contractile assessment of individual VSM cells

Zeiss Axiovert 200 system was used to observe cell shape changes with optical stimulation. The T-Cube LED Driver (Thorlabs, Newton, NJ, LEDD1B) and Blue (470 nm) Fiber-Coupled High-Power LED (Thorlabs, Newton, NJ, M470F1) were used to generate optostimulation (~24 mW/mm^2) with optical fiber (Thorlabs, Newton, NJ, FT400EMT). Cell

images were recorded continuously with a 20 s interval. Additional cell contraction was achieved with a 5 min exposure to 20 mM KCl. Data were accepted for further analysis if the features of VSM cells were seen with YFP signal and KCl response. Cell shortening was measured along its longitudinal axis by the ImageJ 1.48 software.

4.10.3 Arterial rings

The vascular rings were prepared by the technique stated in our previous studies [210]. Briefly, mouse mesenteric arteries were dissected free, placed in the Krebs solution containing (in mM/L) 118.0 NaCl, 3.6 KCl, 1.2 $MgSO_4$, 2.5 $CaCl_2$, 1.2 KH_2PO_4, 11.0 glucose, 25.0 $NaHCO_3$ (pH 7.4). The arteries were cut into 2 mm ring segments in which a stainless steel triangle wire was inserted. The prepared rings were placed in the 37℃ tissue bath filled with Krebs solution bubbled with 95% O_2 and 5% CO_2. Changes of the contractile force were measured with a force-electricity transducer. Signals were amplified, collected with the Clampex 9 software (Molecular Devices), and stored in a PC computer. Blue light was generated by T-Cube LED Driver and Blue Fiber-Coupled High-Power LED (Thorlabs). Intensity of six levels with equal interval (from 10 to 24 mW/mm^2) was given to the rings in light-intensity test. Other optical contractile force was generated with ~24 mW/mm^2 light intensity.

4.10.4 Langendorff heart

After the mouse was euthanized, the heart was rapidly removed and placed in the ice-cold Krebs-Henseleit (KH) solution composed of (in mM): 119 NaCl, 4.7 KCl, 2.5 $MgSO_4$, 2.5 $CaCl_2$, 10 glucose, 0.5 disodium EDTA, 25 $NaHCO_3$ bubbled with 95% O_2 and 5% CO_2 (pH 7.4). The left ventricle was intubated, the aorta was tightened, and vena cava was cut open. The isolated heart was then placed in a moisture air chamber with the temperature maintained at 35℃, and perfused with a syringe pump (Syringe Pump, Farmingdale, NY, NE-300, NE4000) at

constant flow speed to produce 80 cm H_2O ventricular pressure at baseline. The force-electricity transducer (Model eTH-400, CB Sciences) was used to monitor the perfusion resistance and heart rate. Only hearts that had heart beat >200 times per min with a clear vasodilation response to 10 μM isoproterenol were accepted for further studies. The Lambda DG-4 Plus system (Sutter Instruments, Novato, CA) with a 470 nm filter (fiber diameter 3 mm) was used to generate the blue light. The data was recorded with Clampex 8 (Molecular Devices), and analyzed with Clampfit 9 (Molecular Devices). Recording started after 30 min equilibration when the perfusion resistance and heart rate were stable.

4.10.5 Isolated kidney preparation

Kidneys from both Tagln-ChR and control mice were prepared in ice-cold KH solution. The kidney was intubated through one end of the abdominal aorta with the other end tightened. The rest of experimental procedure was similar to that for the isolated and perfused heart.

4.11 Data analysis

Neuronal activities and phrenic activity were measured with at least 40 consequent bursts of eupnea.

For western blot analysis, proteins extracted from A10 and HEK cells were detected using a standard Western blot protocol. GAPDH was used as an internal control.

Data analyzed with Student's *t* test and Two-way ANOVA were presented as means ± SE. Comparisons of data were accomplished by one-way ANOVA followed by student's t-test for parametric data. Kruskal-Wallis and Mann-Whitney (U) tests were used for non-parametric data. Data analyzed with either Student's *t* test, Two-way ANOVA or $\chi 2$ test were considered with significant difference when $P<0.05$.

5 RESULT 1: CHARACTERIZATION OF RETT SYNDROME-LIKE PHENOTYPES IN MECP2-KNOCKOUT RATS

Published as "**Yang Wu**, Weiwei Zhong, Ningren Cui, Christopher M. Johnson, Hao Xing, Shuang Zhang and Chun Jiang. Optogenetic approach for functional assays of the cardiovascular system by light activation of the vascular smooth muscle. ***J Neurodev Disord.*** 2016 Jun 16;8:23."

5.1 Acknowledgements

This work was supported by NIH grant R01-NS-073875 and International Rett Syndrome Foundation.

5.2 Abstract

Rett Syndrome (RTT) is a neurodevelopmental disease caused by the disruption of the *MECP2* gene. Several mouse models of RTT have been developed with *Mecp2* disruptions. Although the mouse models are widely used in RTT research, results obtained need to be validated in other species. Therefore, we performed these studies to characterize phenotypes of a novel *Mecp2*$^{-/Y}$ rat model and compared them with the *Mecp2*$^{tm1.1Bird}$ mouse model of RTT. RTT-like phenotypes were systematically studied and compared between *Mecp2*$^{-/Y}$ rats and *Mecp2*$^{-/Y}$ mice. In-cage conditions of the rats were monitored. Grip strength and spontaneous locomotion were used to evaluate the motor function. Three-chamber test was performed to show autism-type behaviors. Breathing activity was recorded with the plethysmograph. Individual neurons in the locus coeruleus (LC) were studied in the whole-cell current clamp. The lifespan of the rats was determined with their survival time. *Mecp2*$^{-/Y}$ rats displayed growth retardation, malocclusion and lack of movements, while hindlimb clasping was not seen. They had weaker

forelimb grip strength and a lower rate of locomotion than the WT littermates. Defects in social interaction with other rats were obvious. Breathing frequency variation and apnea in the null rats were significantly higher than in the WT. LC neurons in the null rats showed excessive firing activity. A half of the null rats died in two months. Most of the RTT-like symptoms were comparable to those seen in *Mecp2*$^{-/Y}$ mice, while some appeared more or less severe. The findings that most RTT-like symptoms exist in the rat model with moderate variations and differences from the mouse models support the usefulness of both *Mecp2*$^{-/Y}$ rodent models. The novel *Mecp2*$^{-/Y}$ rat model recapitulated numerous RTT-like symptoms as *Mecp2*$^{-/Y}$ mouse models did, which makes it a valuable alternative model in the RTT studies when the body size matters.

5.3 Introduction

Rett syndrome (RTT), a progressive neurodevelopmental disorder, affects predominantly female children worldwide with an incidence of 1: 10,000 female births. People with RTT display a developmental regression which is characterized by a loss of acquired functions such as speech and hand skills, and development of stereotypic hand movements, gait apraxia, ataxia and seizures [211-213]. Breathing disorders are common including hyperventilation, apnea, hyperpnoea, breath holding, etc [74,114,214,215], which contribute to the high incidence of sudden death.

Defects in the X-linked gene *MECP2* encoding the methyl CpG binding protein 2 (MeCP2) known as a transcriptional regulator, are identified in more than 90% RTT patients. Mutations or altered expression of *Mecp2* in mice result in a spectrum of RTT-like neurodevelopmental disorders. Thus, several mouse models of RTT have been developed and used in RTT studies over the past years [76,216]. For example, *Mecp2*$^{tm1.1Bird}$, *Mecp*^{2Jae} and *Mecp2*^{neoTam} mouse models with exon 3 and/or 4 deletions in the *Mecp2* are widely used in the

etiologic and therapeutic studies [75-77]. Other mouse models with site-specific mutations, such as *Mecp2*$^{T158A/y}$, *Mecp2*^{R168X} and *Mecp2e1*$^{-/Y}$, were developed in recent years [78-80]. By using these mouse models, considerable progress has been made in the studies of the neurobiological mechanisms underlying or associated with RTT [83,104,108,217,218]. *Mecp2*$^{tm1.1Bird}$ mice, the most widely used mouse model of RTT, show several phenotypes similar to human patients with RTT, such as early death, motor problems and autistic behaviors, which progressively worsen until death [81,112]. Autonomic dysfunction is another characteristic manifestation including breathing disorders, cardiac arrhythmias and constipation [74,111,219]. Brainstem monoamine modulatory systems are involved. Electrophysiological and molecular biological studies in the *Mecp2*$^{tm1.1Bird}$ mouse model suggest that neurons in the locus coeruleus (LC) are defective, showing impaired neuronal activity, abnormal CO_2 chemosensitivity and reduced expression of enzymes for NE biosynthesis [83,98,106,111].

Although the mouse models are widely used in RTT research, results obtained need to be validated in other species, which is particularly important when therapeutic modalities are aimed to develop. Thus, studies on multiple animal models of RTT are necessary and highly significant. A novel *Mecp2*-knockout rat model, SD-*Mecp2*^{tm1sage} rat. The null rats had a deletion of exon 4 in the *Mecp2* leading to complete elimination of the MeCP2 protein. Since the rat model may provide useful information on RTT mechanisms and treatments, we performed systematic studies of the RTT-like symptoms identified previously in *Mecp2*$^{-/Y}$ mouse models, and compared these RTT-like phenotypes with those found in the male mouse model of RTT.

5.4 Results

5.4.1 General RTT Features

Mutation of the *Mecp2* gene in rats caused several developmental abnormalities. Some of the abnormalities have previously been identified in *Mecp2*$^{-/Y}$ mice, and others seemed more or less obvious in rats than in mice. The body weight of *Mecp2*$^{-/Y}$ rats was monitored every week starting from postnatal day 7 (P7) till death. In comparison to their WT littermates, *Mecp2*$^{-/Y}$ rats had a much smaller body size and lower body weight. When the body weight was compared between *Mecp2*$^{-/Y}$ and WT rats, significant difference was observed in week 4 (75.6 ± 16.6 g in 18 *Mecp2*$^{-/Y}$ rats vs 90.3 ± 14.8 g in 20 WT; $P = 0.004$, df = 41, t = -3.057), and the difference increased with growth (Fig. 5.1A,B). In addition, adult *Mecp2*$^{-/Y}$ rats showed prolapsed penis (Fig. 5.1C) and severe malocclusion (overgrowth of incisor teeth and misplaced midline) (Fig. 5.1D). Hindlimb grasping, a typical phonotype of *Mecp2*$^{-/Y}$ mice, was absent in *Mecp2*$^{-/Y}$ rats (Fig. 5.1E). The *Mecp2*$^{-/Y}$ rats were also occasionally observed with porphyrin (red tear), which was not seen the WT littermates, and usually indicated sickness and stress.

5.4.2 Muscle Strength and Locomotion

People with RTT have defects in motor functions, some of which have been found in *Mecp2*$^{-/Y}$ mice. Similarly, *Mecp2*$^{-/Y}$ rats showed fewer movements than their WT littermates. Hence, we examined the motor function with grip strength test and the observation of spontaneous locomotion. Grip strength of the forelimbs was monitored weekly in 14 *Mecp2*$^{-/Y}$ rats and 19 WT rats. The *Mecp2*$^{-/Y}$ rats showed a significant decrease in muscle strength starting in 4 weeks after birth (P4w), and remained significantly lower thereafter than that of the WT (Fig. 5.2A). The maximum grip strength was reached in P7w in null rats. In comparison, the grip strength of WT rats continued to increase with growth.

When the grip strength was compared in P6w, the muscle strength of both *Mecp2*$^{-/Y}$ rats and mice was significantly lower than that of their WT littermates (Fig. 5.2B). Because of the body size, rats were much stronger than mice. We thus normalized the grip strength to the WT in each group. After normalization, similar reductions in the muscle strength were observed in both *Mecp2*$^{-/Y}$ rats (by 29% of the WT value) and *Mecp2*$^{-/Y}$ mice (by 34%) with no statistical difference found between species (Fig. 5.2C).

The spontaneous movement was measured with traveling distance to indicate locomotor activity. A rat was placed in the center of an enclosure and allowed to explore around for 10 min. The number of the squares crossed by the rat was counted and recorded as locomotion activity (squares crossed per min). The less square traveling, the lower locomotor activity. The locomotion activity of both *Mecp2*$^{-/Y}$ strains were significantly lower than the WT littermates (35.4 ± 3.1 squares/min in 9 WT mice vs 26.2 ± 2.4 squares/min in 9 *Mecp2*$^{-/Y}$ mice, $P = 0.031$, df = 17, t = 2.367; 28.3 ± 3.3 squares/min in 12 WT rats vs 16.2 ± 3.3 squares/min in 11 *Mecp2*$^{-/Y}$ rats; $P = 0.016$, df = 21, t = 2.609) (Fig. 5.2D). After normalization to the WT level, *Mecp2*$^{-/Y}$ rats showed 43% reduction in locomotor activity, while *Mecp2*$^{-/Y}$ mice had 26% reduction (Fig. 5.2E). The low locomotion activity of *Mecp2*$^{-/Y}$ rats suggests that the *Mecp2* disruption causes motor dysfunction in both rats and mice with similar severity.

5.4.3 Autism-like Behavior

Another clinic manifestation of RTT is the autism-like behavior that also occurs in *Mecp2*$^{-/Y}$ mice. Using the three-chamber test, therefore, we studied the autism-like behavior in *Mecp2*$^{-/Y}$ rats. During the tests, a rat was placed in the middle chamber of the three-compartmental box with an opening to each of the side chambers. During the first 10 min habituation period, rat preference to either side chamber was recorded as the time spent in each

chamber (Fig. 5.3A,B). Only the animals showing no preference to either side of chambers in the habituation time were used for further tests.

Then, sociability was tested in a three-chamber apparatus with two identical mental-mesh buckets introduced to each side chamber. An intruder animal was randomly placed in one of the buckets, and the other was kept empty. The mesh bucket allowed the animal to have visual, olfactory and auditory contact and exploration. During this 2nd 10 min tests, WT rodents spent more time with their kinds than the empty chamber (259.8 ± 24.5 sec vs 183.1 ± 21.3 sec in 10 WT mice, $P = 0.045$, df = 19, t = 2.156; 346.4 ± 41.9 sec vs 142.4 ± 24.2 sec in 10 WT rats, $P < 0.001$, df = 19, t = -4.217) (Fig. 5.3C,D), consistent with previous reports [220-222]. Such a preference was not seen in both *Mecp2*$^{-/Y}$ rodents. *Mecp2*$^{-/Y}$ rats spent less time in the intruder chamber than in the empty one (99.2 ± 48.8 sec with Animal 1 vs 169.5 ± 74.5 sec in empty; n = 11, $P = 0.439$, df = 21, t = 0.789), similar to *Mecp2*$^{-/Y}$ mice (214.5 ± 50.4 sec with Animal 1 vs 224.4 ± 53.0 sec in empty; n = 8, $P = 0.895$, df = 15, t = -0.135) (Fig. 5.3C,D). The results suggest that the defect of sociability was comparable between *Mecp2*$^{-/Y}$ rats and mice.

The social novelty was tested during the last 10 min when a novel stranger (Animal 2) in addition to the first intruder (Animal 1 or familiar) was introduced to the previously empty bucket. The time spent in either side chambers was measured. Consistent with previous reports [221,222], the WT animals showed a clear tendency of social novelty by spending a longer time with the stranger animal than with the familiar one (363.4 ± 34.5 sec with Animal 2 vs 140.4 ± 27.5 sec with Animal 1 vs in WT mice, $P < 0.001$, df = 19, t = 5.052; 395.4 ± 56.3 sec with Animal 2 vs 101.8 ± 28.1 sec with Animal 1 in WT rats, $P = 0.002$, df = 19, t = -4.666) (Fig. 5.3E,F). Such a preference disappeared in *Mecp2*$^{-/Y}$ animals (227.7 ± 63.1 sec with Animal 1 vs 256.7 ± 55.3 sec with Animal 2 in *Mecp2*$^{-/Y}$ mice, $P = 0.422$, df = 15, t = 0.828; 250.1 ± 76.0 sec with

Animal 1 vs 171.8 ± 68.1 sec with Animal 2 in *Mecp2*$^{-/Y}$ rats, $P = 0.452$, df = 21, t = 0.767) (Fig. 5.3E,F). Therefore, the results suggest that the *Mecp2*$^{-/Y}$ rats show the autism-like social defects similarly to *Mecp2*$^{-/Y}$ mice.

5.4.4 Breathing Abnormality

People with RTT as well as the mouse models of RTT show breathing abnormalities [74,114,214,215]. Thus, we measured the breathing activity using the plethysmography in conscious animals. Two most reliable breathing phenotypes, apneas and breathing frequency variations, were analyzed as shown in several previous studies [94,111]. High apnea rate and breathing frequency variations were seen in *Mecp2*$^{-/Y}$ rats. They started showing a significant difference from those in the WT rats in P4w, and deteriorated with growth (Fig. 5.4A-D). By P7w, the apnea rate was raised to 49.3 ± 2.9 hr^{-1} of *Mecp2*$^{-/Y}$ rats in comparison to 26.5 ± 2.7 hr^{-1} of WT (Fig. 5.4C), and the breathing variation increased to 0.21 ± 0.02 in 15 *Mecp2*$^{-/Y}$ rats comparing to 0.09 ± 0.01 in 8 WT (Fig. 5.4D). The breathing abnormalities of *Mecp2*$^{-/Y}$ rats were compared with those in the *Mecp2*$^{-/Y}$ mice at the same age group (5-7 weeks). Both *Mecp2*$^{-/Y}$ strains had severe breathing problems in comparison to their WT littermates with a higher apnea rate (22.8 ± 6.5 hr^{-1} in 12 WT mice vs 107.0 ± 7.4 hr^{-1} in 24 *Mecp2*$^{-/Y}$ mice, $P < 0.001$, df = 35, t = -7.335; 19.7 ± 1.8 hr^{-1} in 11 WT rats vs 44.8 ± 2.7 hr^{-1} in 27 *Mecp2*$^{-/Y}$ rats, $P < 0.001$, df = 37, t = -5.784) (Fig. 5.4E) and a higher respiratory frequency variation (0.12 ± 0.02 in 14 WT mice vs 0.26 ± 0.02 in 25 *Mecp2*$^{-/Y}$ mice, $P < 0.001$, df = 38, t = -6.184; 0.08 ± 0.01 in 11 WT rats vs 0.18 ± 0.02 in 27 *Mecp2*$^{-/Y}$ rats, $P < 0.001$, df = 37, t = -4.454) (Fig. 5.4F). However, the apnea rate was significantly lower in *Mecp2*$^{-/Y}$ rats than in the *Mecp2*$^{-/Y}$ mice ($P < 0.001$, ANOVA and Student's *t*-test) (Fig. 5.4E,G), while the frequency variation had no significant difference

between species (Fig. 5.4F,H). These results suggest that the breathing abnormalities seem less severe in *Mecp2*$^{-/Y}$ rats than in *Mecp2*$^{-/Y}$ mice.

5.4.5 Hyperexcitability of LC Neurons

Several groups of brainstem neurons are involved in breathing controls including those in the LC. Previous studies indicate that the *Mecp2* disruption in mice causes hyperexcitability in LC neurons [83,97]. To test whether there is a change in LC neuronal excitability in *Mecp2*$^{-/Y}$ rats, we studied the cells in brain slices. In whole-cell current clamp, LC neurons in *Mecp2*$^{-/Y}$ rats (P4w-P6w) showed spontaneous firing rate 3.0 ± 0.3 Hz, which was significantly higher than the WT 1.9 ± 0.2 Hz (Fig. 5.5A-C. $P = 0.006$, df = 34, t = -2.921 Student's *t*-test). The firing rate of LC neurons in *Mecp2*$^{-/Y}$ rats was increased by 54.0 ± 14.6 % over the WT level (Fig. 5.5C). Similar results were found in *Mecp2*$^{-/Y}$ mouse model in the same age range as well (Fig. 5.5D). There were no differences in the membrane potential, input resistance and action potential amplitude between *Mecp2*$^{-/Y}$ and WT rats (Fig. 5.5E-G), neither between rats and mice. In *Mecp2*$^{-/Y}$ rats, the threshold of action potential was shifted to significantly more hyperpolarizing potentials from -34.4 ± 1.2 mV to -37.2 ± 0.8 mV (Fig. 5.5H), which appeared to contribute to the increased firing activity of LC neurons.

5.4.6 Lifespan

These RTT-like symptoms may affect the lifespan of rats. Therefore, we examined the survival time in the novel *Mecp2*$^{-/Y}$ rat model of RTT. The death was determined by either in-cage death or the humane endpoint determined by our school veterinarian. A total of 18 WT males and 18 *Mecp2*$^{-/Y}$ rats were used in the studies, and two outliers (the longest and shortest survivors) were removed. Figure 5.6A shows that *Mecp2*$^{-/Y}$ rats died as early as at P45, and all died by P82. Only 2 out of 16 tested rats survived beyond 80 days. Similar results were found in

mice (not shown). In comparison, 50% of the *Mecp2*$^{-/Y}$ rats died at P63, while 50% of the *Mecp2*$^{-/Y}$ mice died at P52 (Fig. 5.6C). To compare these two groups of animals, we performed the χ^2 test, and did not find any statistical difference in the ratio of survival vs death between these rats and mice at P52, neither at P63 (Fig. 5.6D,E).

5.5 Discussion

RTT is a progressive neurodevelopmental disorder caused mostly by different mutations in the *MECP2* gene. The disease affects females mainly. Male infants rarely survive with pathogenic *MECP2* variations, because knockout of *MECP2* gene causes lethal miscarriages and early death in males [223,224]. However, the male mice with *Mecp2* disruption survive, and show reliable and consistent RTT-like symptoms. This leads to wide uses of these mice in RTT studies. Experimental approaches to the female mouse models have limitations because of the X-chromosome inactivation and the large symptomatic variation among individuals. With the same consideration, our experiments were performed on the *Mecp2*$^{-/Y}$ male rats as well. This novel RTT rat model has a 71-bp deletion in exon 4 at 53900-53970 of the *Mecp2* gene by Zinc Finger Nuclease technology. This results in a fragment deletion as well as a shift of the open reading frame leading to a complete knockout of MeCP2 [225]. Consistently, our studies demonstrate that the male *Mecp2*-null rats experience severe RTT-like symptoms.

5.5.1 Recapitulation of RTT-like Phenotypes in Mecp2^{-ec} *Rats*

Many general RTT-like features have been recapitulated in the rat model of RTT, including growth retardation, malocclusion, lack of movement and early death. The *Mecp2*$^{-/Y}$ rats show weaker forelimb grip strength and less locomotion activity than the WT littermates, which are similar to those observed in their mouse counterparts. Defects in sociability and social novelty were seen in these *Mecp2*$^{-/Y}$ rats. Breathing abnormalities of the *Mecp2*$^{-/Y}$ rats including

irregular respiratory rhythm and high apnea rate resemble closely respiratory dysfunction in RTT patients and mouse models. Besides, LC neurons of *Mecp2*$^{-/Y}$ rats show excessive firing activity, which has also been observed in the mouse models before. A half of the *Mecp2*$^{-/Y}$ rats died in two months. These RTT-like symptoms observed in *Mecp2*$^{-/Y}$ rats thus are comparable to those seen in *Mecp2*$^{-/Y}$ mice [94,111,220]. Consistently, a recent study has demonstrated that the *Mecp2*$^{-/+}$ rats had similarly impaired auditory responses as *Mecp2* heterozygous female mice [225,226], which is seen in RTT patients as well [227]. Therefore, *Mecp2*$^{-/Y}$ rats recapitulated most of the RTT-like symptoms, making them a quality RTT model.

5.5.2 Onset Time of RTT-like Symptoms in Mecp2^{-ns} Rats

RTT is characterized by relatively normal development at the earlier stage of life. The asymptomatic time window is usually from birth to 6 months in humans with RTT [228]. In mouse models, the onset time and the disease progression vary depending on the nature of *Mecp2* variants and genetic background of mice. Most studies agree that *Mecp2*$^{-/Y}$ mice have no overt RTT symptoms within the first 3 weeks of life. After that, the null mice show rapid development and progression of RTT-like symptoms. Growth retardation can be observed in P4w [112,229,230]. Locomotor problems appear in P3w-P4w in mouse models [75,231]. Social defects are observed as early as 4 weeks after birth in mice [232]. Breathing disturbances occur in null mice at P3w-P4w [112]. In *Mecp2*$^{-/Y}$ rats, these RTT-like symptoms also take place as early as 3 weeks, and become obvious at P4w. Thus, the onset time of the RTT-like phenotypes in the *Mecp2*$^{-/Y}$ rats is comparable to that in *Mecp2*$^{-/Y}$ mice.

5.5.3 Defects of Neuronal Activity in Mecp2^{-ef} Rats

LC neurons are the predominant source of noradrenergic modulation in the CNS [233,234]. They project to various regions in the brain, including forebrain, diencephalon, brainstem,

cerebellum and even spinal cord [233,234]. Defects of LC neurons lead to dysfunction of autonomic nervous system, consistent with the characteristic RTT-like symptoms. In *Mecp2*$^{-/Y}$ mice, the LC neurons show electrophysiological defects as increased neuronal firing activity, which is likely to be a result of the impaired intrinsic membrane properties and the deficiency in GABA-ergic inhibition [98,106,235]. Similar hyperexcitability of LC neurons is found in *Mecp2*$^{-/Y}$ rats, suggesting that the *Mecp2*$^{-/Y}$ rats may develop similar neuronal defects as *Mecp2*$^{-/Y}$ mice. In addition to LC neurons, neuronal hyperexcitability is seen in neurons in the hippocampus, neocortex and other brainstem areas in *Mecp2*$^{-/Y}$ mice, which contributes to the defects in motor function, cognition, sleep and other autistic features [102,104,117]. These, though still unclear, may occur in other neurons of the *Mecp2*$^{-/Y}$ rats.

5.5.4 Symptomatic Difference between Mecp2^{-ym} Rats and Mice

Although the *Mecp2*$^{-/Y}$ rat model has many similarities to the *Mecp2*$^{-/Y}$ mouse models, our studies suggest that the former is not a complete replica of the latter. Indeed, some RTT-like phenotypes are quite different between rat and mouse models. All *Mecp2*$^{-/Y}$ rats displayed malocclusion that appears more severe than null mice. The incisor teeth overly grow which may be due to the reduction of the central command of chewing activity, sick jaw muscles and/or abnormal propriosensation in the transgenic rats. Besides, the *Mecp2*$^{-/Y}$ rats had a proportional reduction in body size compared to their WT littermates, which seems more obvious than that seen in *Mecp2*$^{-/Y}$ mice. Another difference found in over a half of *Mecp2*$^{-/Y}$ rats is the penile prolapse. This symptom has been reported in transgenic mice with neurodegeneration [236] but not in *Mecp2*$^{-/Y}$ mice. This often hinders the penis from retraction even with the lubrication treatment, which contributes to the humane endpoint of the rats. *Mecp2*$^{-/Y}$ rats did not show the typical hindlimb grasping as *Mecp2*$^{-/Y}$ mice did [237]. In the three-chamber test, old (P7w)

Mecp2$^{-/Y}$ rats barely switched between each chamber due to the poor locomotor activity, which has caused rejection of them from social behavioral tests. In contrast, mice do not show such age-dependent deterioration in locomotor activity as defects in social behaviors are reported at various ages from P4w to P12w in different mouse models [112,238]. Furthermore, breathing abnormalities appear less severe in *Mecp2*$^{-/Y}$ rats than in *Mecp2*$^{-/Y}$ mice. This may be related to the low breathing frequency of the rats. In general, these symptomatic differences between *Mecp2*$^{-/Y}$ mice and *Mecp2*$^{-/Y}$ rats are rather moderate and quantitative rather than qualitative.

5.5.5 Advantages and the Applications of the RTT Rat Model

The rat model has several potentials in RTT studies. The understanding of the link between RTT phenotypes and the neuronal cellular and network mechanisms relies on *in vivo* approaches that are still difficult to be fulfilled in mice. The larger body size of rats may satisfy the requirement for the *in vivo* studies. The larger body size may benefit certain tests that need repetitive and timely samplings, such as measurement of blood gases, electrolytes and hormonal levels in circulation blood and cerebrospinal fluid, monitoring of systemic physiological parameters and EEG recordings. The richness of the social and communication repertoire of rats may also benefit the behavior studies, such as cognitive processes, anxiety, social acoustic memory, cooperative behaviors and auditory responses [239]. Most importantly, studies on multiple animal models can benefit RTT research, especially when therapeutic agents are to be developed.

Our studies indicate that the novel *Mecp2*$^{-/Y}$ rats recapitulate numerous RTT-like symptoms as the *Mecp2*$^{-/Y}$ mouse model do. The RTT rat model, as a valuable model in the studies of RTT, may provide a useful alternative in RTT studies when body size is considered to be a critical factor.

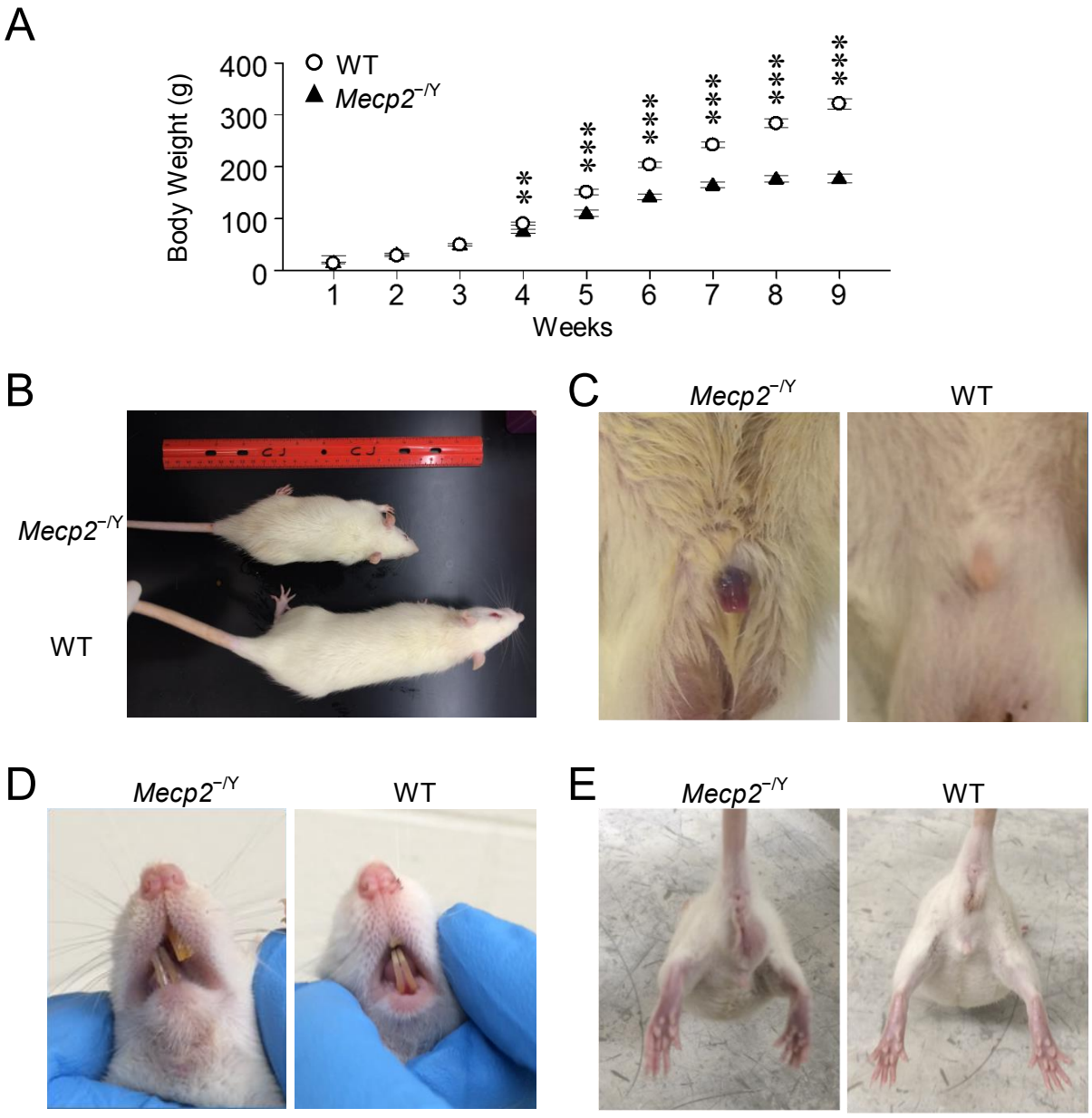

Figure 5.1 General abnormalities of* Mecp2$^{-/Y}$ *rats.

(A) Body weight of *Mecp2*$^{-/Y}$ rats was significantly lower than that of WT littermates at P4w, and the difference became larger with growth (*** $P < 0.001$, ** $P < 0.01$; Student's *t*-test). *Mecp2*$^{-/Y}$ rats also showed growth retardation **(B)**, prolapsed penis **(C)**, and malocclusion **(D)**. **(E)** Typical hindlimb grasping seen in *Mecp2*$^{-/Y}$ mice was not observed in *Mecp2*$^{-/Y}$ rats.

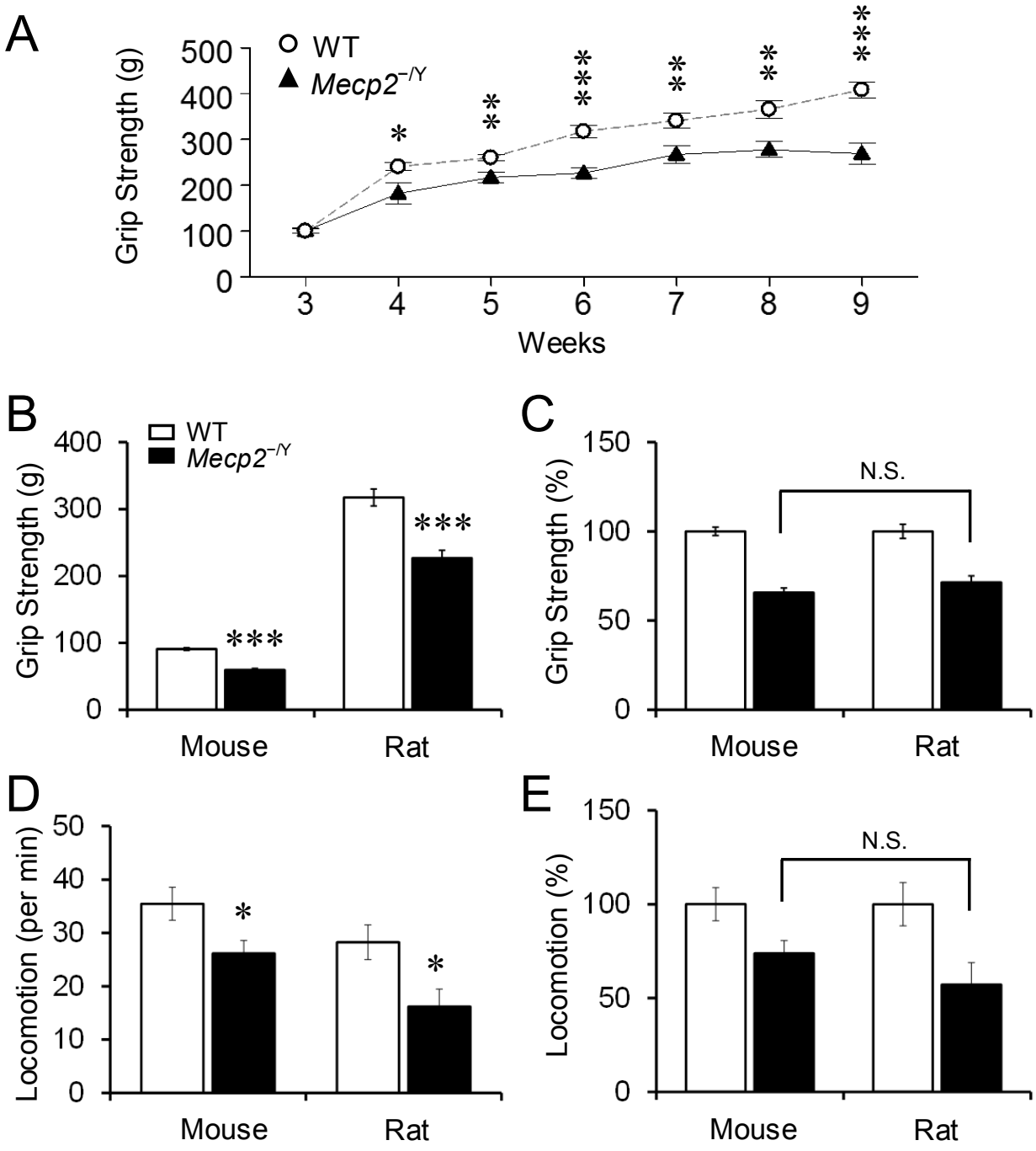

Figure 5.2 Reduced muscle strength and locomotor activity.
(A) *Mecp2*$^{-/Y}$ rats exhibited decreased forelimb grip strength compared to WT (*** $P < 0.001$, ** $P < 0.01$, * $P < 0.05$; Student's *t*-test). **(B)** In comparison to the WT, both *Mecp2*$^{-/Y}$ rats and mice showed a significant decrease in grip strength (Student's *t*-test). **(C)** No statistical significance in the grip strength differences was found between species after normalization to the WT levels. **(D,E)** Locomotor activity was also significantly reduced in *Mecp2*$^{-/Y}$ rodents. No statistical significance was found between species either although the null rats appeared to move less (Student's *t*-test).

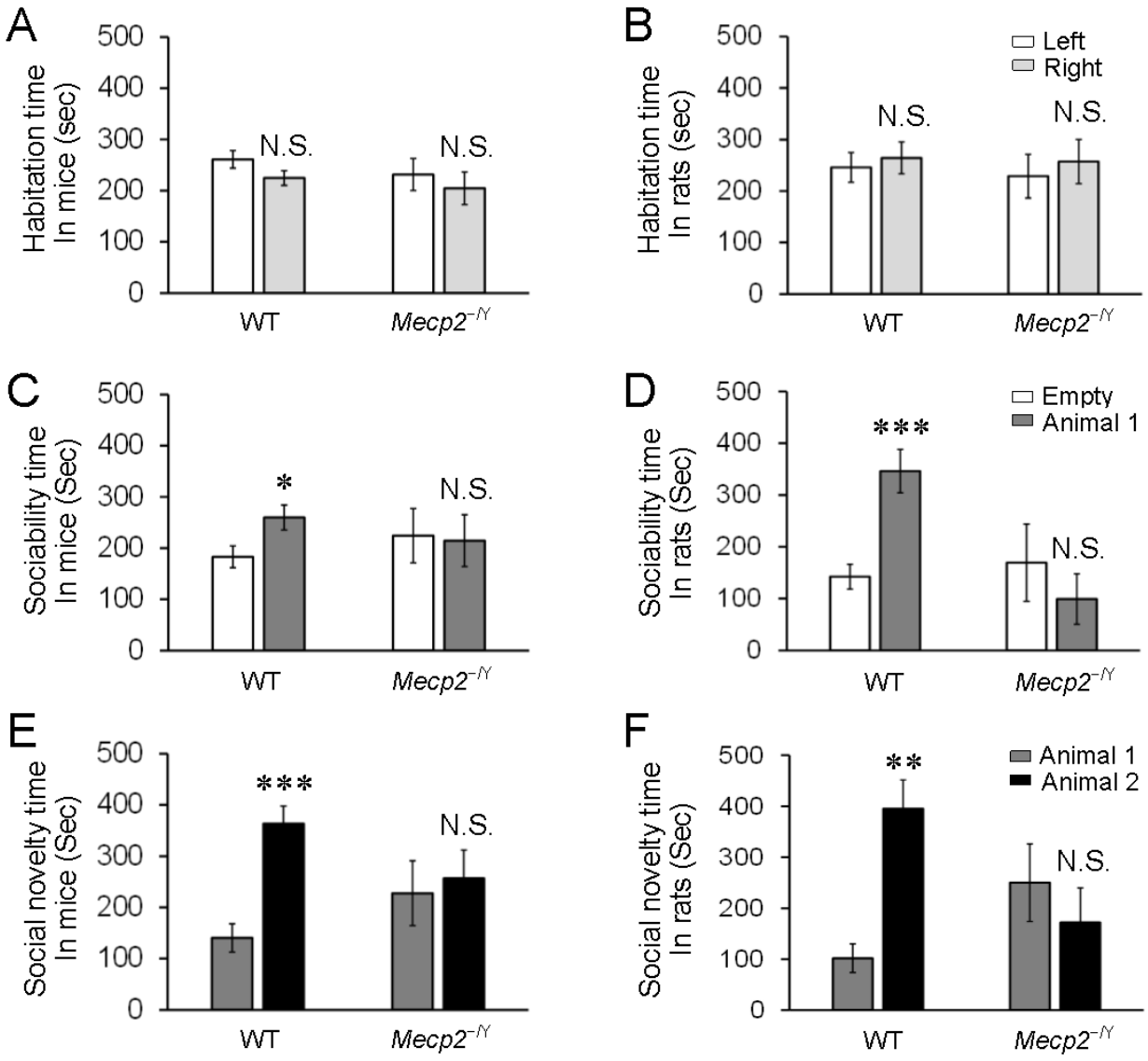

Figure 5.3 Social behavior defects of* Mecp2$^{-/Y}$ *rats.

(A,B) The habituation time in side chambers had no significant difference in *Mecp2*$^{-/Y}$ animals and WT littermates. **(C,D)** The time spending of both *Mecp2*$^{-/Y}$ animals in the intruder chamber (Animal 1) was more than in the empty bucket chamber (Empty). **(E,F)** The animal preference disappeared in both *Mecp2*$^{-/Y}$ animals. Familiar animal is indicated as Animal 1, and unfamiliar animal is labeled as Animal 2. (*** $P < 0.001$, ** $P < 0.01$, * $P < 0.05$; Student's *t*-test)

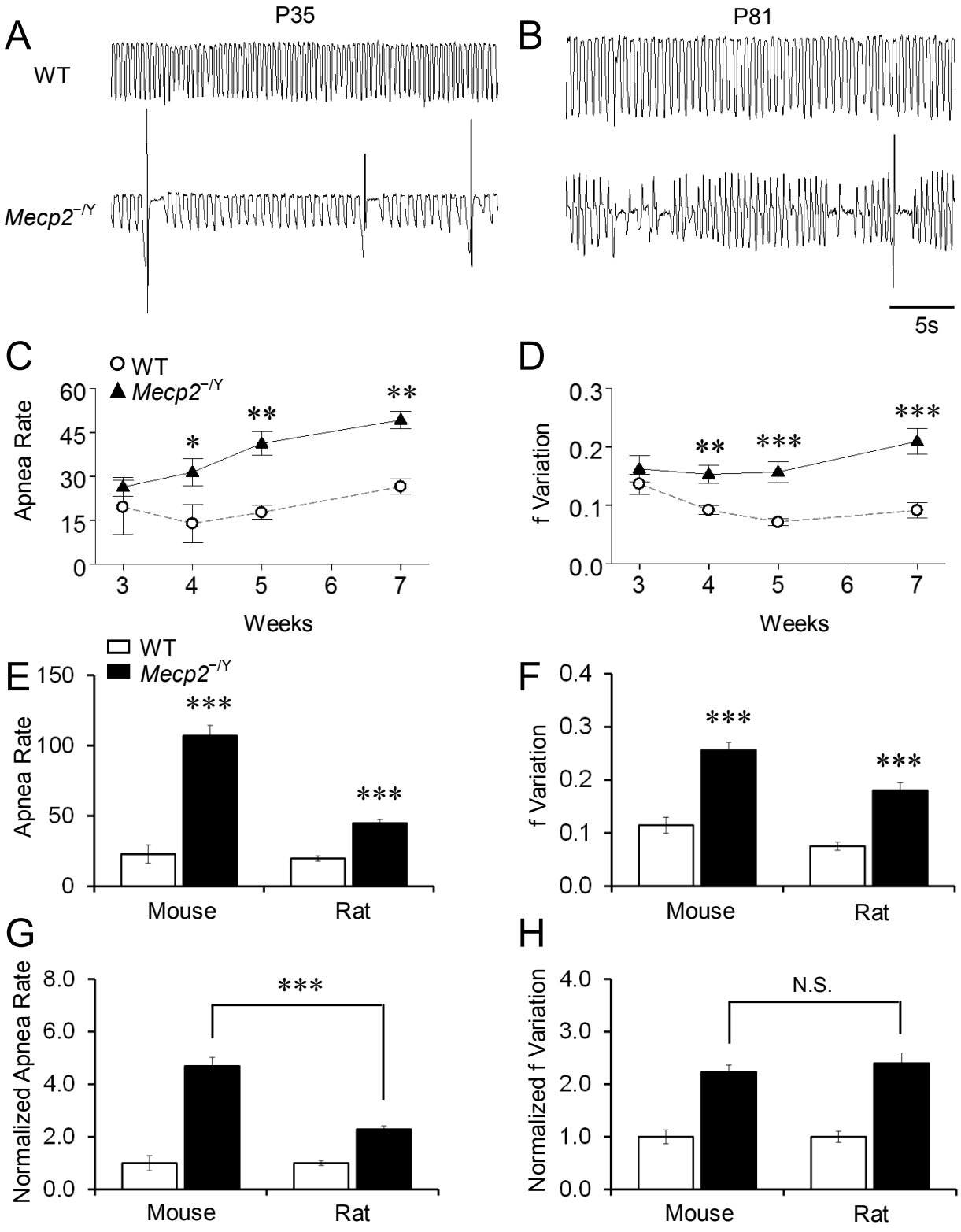

Figure 5.4 Breathing abnormalities.
(A,B) Abnormal breathing activity including apnea and irregular breathing were observed in *Mecp2*$^{-/Y}$ rats at P35 and P81. (**C,D**) Apnea rate and respiratory frequency variation were

significantly more in *Mecp2*$^{-/Y}$ rats than in the WT (*** $P < 0.001$, ** $P < 0.01$, * $P < 0.05$; Student's *t*-test). **(E-H)** the breathing abnormalities were compared between mouse and rat (*** $P < 0.001$; Student's *t*-test). **(G)** The apnea rate of *Mecp2*$^{-/Y}$ rats was significantly lower than the *Mecp2*$^{-/Y}$ mice after data normalization to the WT levels. **(H)** The severity of breathing frequency variation was not significantly different between rats and mice.

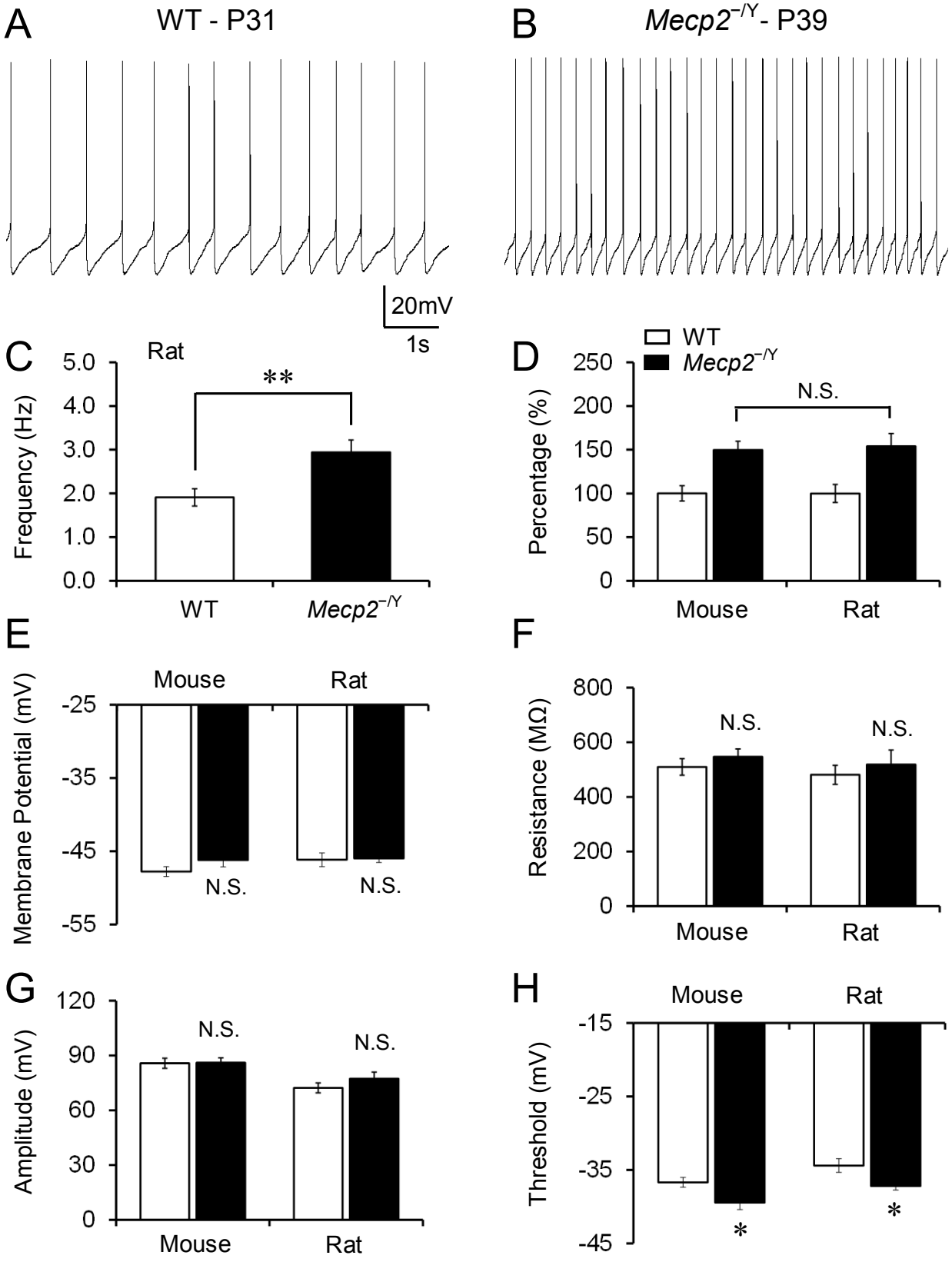

Figure 5.5 Increased excitability of LC neurons.

(A,B) Typical recordings of spontaneous firing activity in WT and *Mecp2*$^{-/Y}$ rat LC neurons. **(C)** In *Mecp2*$^{-/Y}$ rats, LC neurons showed a significant increase in firing frequency in comparison to the WT. **(D)** The ratio of increased spontaneous firing rate, however, was similar between rats and mice. **(E,F)** No significant differences were found in membrane potential and resistance between WT and *Mecp2*$^{-/Y}$ rats, which was similar as in the mouse model. **(G,H)** In comparison to the WT, *Mecp2*$^{-/Y}$ rats showed more hyperpolarized threshold of the action potential in LC neurons, whereas the amplitude was not altered. Similar results were found in the mouse model (** $P < 0.01$,* $P < 0.05$; Student's *t*-test).

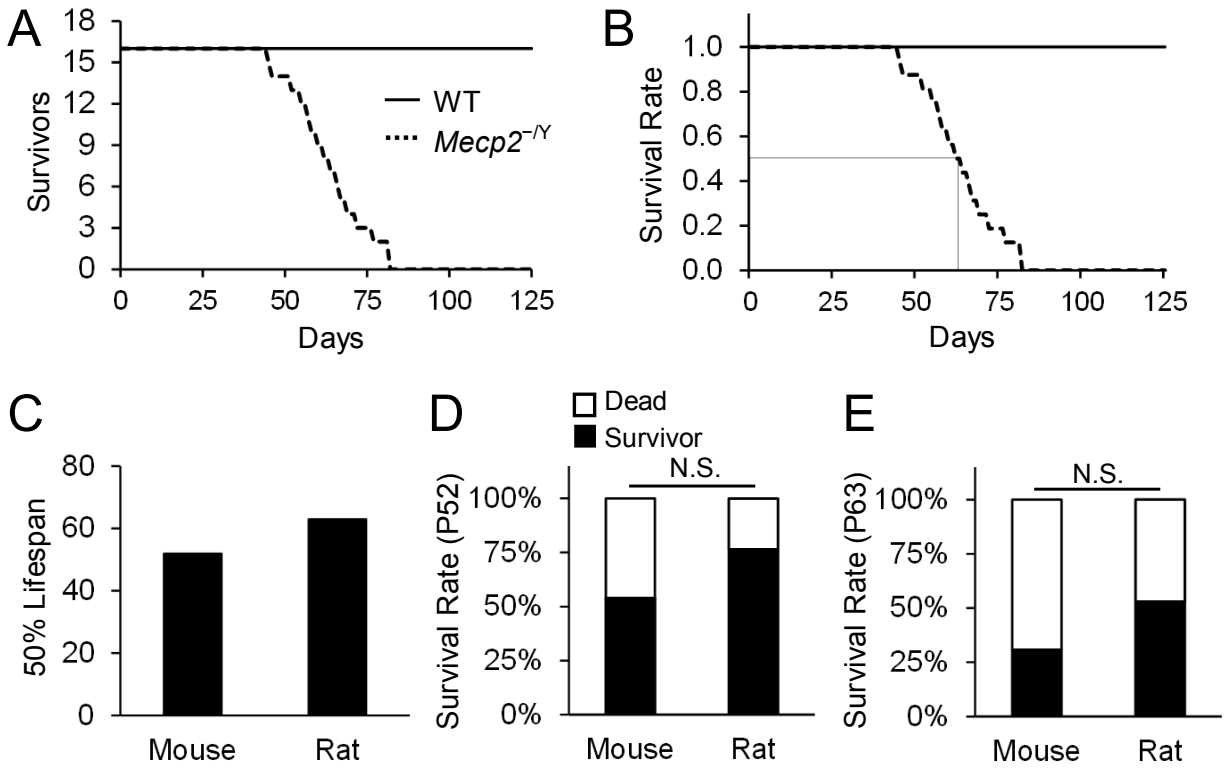

Figure 5.6 Survival rate.

(A) The survival time of *Mecp2*$^{-/Y}$ rats was plotted in comparison to WT littermates (n = 16). **(B)** The 50% lethality was shown after normalization of the initial rate to 1. **(C)** A half of *Mecp2*$^{-/Y}$ rats died at P63, while 50% *Mecp2*$^{-/Y}$ mice dies at P52. **(D)** At P52 when 50 % mice were survived, while about 3/4 rats were still alive. **(E)** At P63 or the half survival age of *Mecp2*$^{-/Y}$ rats, only about one third of the mice were still alive. Despite these, no statistical significance was found between rats and mice (D,E).

6 RESULT 2: *MECP2*-DISRUPTION IN RATS CAUSES BREATHING DISORDERS BY RESHAPING MEDULLARY RESPIRATORY NEURONAL FIRING PATTERNS

Manuscript is submitted for publication

Authors: **Yang Wu**, Ningren Cui, Hao Xing, Weiwei Zhong, Colin Arrowood, Christopher M. Johnson, and Chun Jiang

6.1 Acknowledgements

This work was supported by NIH grant R01-NS-073875 and IRSF grant CON006087.

6.2 Abstract

Brainstem mechanisms underlying respiratory disorders of Rett Syndrome (RTT) are still unknown. Here we show a cellular mechanism for the respiratory disorders. In comparison to their wild-type counterparts, both inspiratory and expiratory neurons in *Mecp2*-null rats extended firing duration and fired more action potentials during each burst *in vivo*. Most inspiratory neurons changed their firing pattern to phase-spanning type, and kept firing during expiration and even apneas. Excessive activity of the inspiratory neurons raised bulbospinal drive to motoneurons, producing ectopic phrenic discharges during expiration. The firing patterns suggest inadequate synaptic inhibition necessary for phase switching. Testing this hypothesis, we found that the abnormalities in respiratory neuronal firing, phrenic discharge and breathing all can be rescued by augmenting GABAergic inhibition. Thus, the respiratory disorders in *Mecp2*-null rats appear to result from prolonged firing of the respiratory neurons, likely due to insufficient synaptic inhibition for phase switching.

6.3 Introduction

Rett Syndrome (RTT) is a neurodevelopmental disease caused mainly by mutations in the *MECP2* gene [240]. People with RTT show breathing disorders, especially hypoventilation. The

hypoventilation including hypopnea, gasping and apnea occurs as more severe state of the disease and is contributting to a high incidence of sudden death and developmental illnesses of the central nervous system [72,241-243]. The underling mechanisms for the hypoventilation are unclear, while dysfunction in brainstem respiratory neuronal activity seems critical. The hypoventilation in RTT is believed to result from insufficient central inspiratory activity and/or deficient inspiratory premotor output. To prove that this scenario is correct, following events should occur: 1) Brainstem inspiratory neurons including bulbospinal cells switch to a firing pattern with shorter burst and lower overall activity; 2) phrenic nerve stop activity during expiration (E2 phase); 3) during central apnea that manifests itself as cessation of inspiratory motor neuronal activity, the inspiratory neurons suspend their activity, and phrenic discharges pause completely. In the rat model of RTT that shows frequent hypoventilation [84], we found that all these were surprisingly opposite. Both inspiratory and expiratory neurons reshaped their firing patterns with extended firing duration, fired more action potentials in each burst, kept firing even during apneas, and produced ectopic phrenic discharges during expiration. These firing pattern changes suggest inadequate synaptic inhibition for phase switching. By enhancing GABAergic inhibition, we found that the abnormalities in respiratory neuronal firing, phrenic discharge and breathing all can be rescued.

6.4 Results

6.4.1 Activity and grouping

Experiments were performed in WT and *Mecp2*-null (*Mecp2*$^{-/Y}$) rats that underwent intercollicular decerebration following initial anesthesia. Phrenic nerve discharges of null rats showed breathing rhythmic abnormalities consistent with previous plethysmograph recordings (Fig. 6.1) [84,88]. In the rats, we performed *in vivo* recordings from neurons in the ventral respiratory column which resembled the ventral respiratory group (VRG) and the Bötzinger Complex (BötC) in cats [244-246]. Because of this, we adopted the same terminologies as used in cats for each subgroup. Expiratory (E) neurons were mostly recorded in the caudal and far rostral

parts of the ventral respiratory column, corresponding to the cVRG and BötC in cats, respectively. Inspiratory (I) neurons were found in between, or the rostral VRG (rVRG), although there were overlaps (Fig. 6.2). Such cell-type grouping did not show evident difference between *Mecp2*-null and WT rats.

6.4.2 Firing patterns of E and I neurons

Although respiratory neurons were still retained in three major subgroups, their firing patterns were clearly altered in *Mecp2*-null rats (Fig. 6.3A-C). In comparison to the WT, averaged firing frequency of rVRG and cVRG neurons in null rats was significantly reduced, while no difference was found in BötC neurons (Fig. 6.3D). However, the peak frequency of all three groups of neurons remained the same to their WT counterparts (Fig. 6.3E). One obvious and consistent change in null rats was the extension of burst duration of all three types of neurons (Fig. 6.3F). Such a change seems to lead to underestimation of neuronal firing activity as the burst duration is the denominator for calculation of the averaged frequency of all neurons. Thus, we analyzed the overall neuronal firing activity as spikes number per burst, as well as frequency (in Hz) multiplied by duration (in sec). Both I and E neurons in the ventral column showed a higher overall firing activity in *Mecp2*-null rats than in the WT (Fig. 6.3G,H).

6.4.3 E-I phase-spanning neurons

Strikingly, we found that most neurons in the rVRG of null rats showed E-I phase-spanning firing pattern (Fig. 6.4A-D), which accounted for two thirds of all cells (85 out of 120 cells), in comparison to 18% (18 out of 100 phase-spanning neurons) in WT rats ($P<0.001$, $\chi 2$ test) (Fig. 6.4C). Like other respiratory neurons in null rats, the burst duration of the phase-spanning neurons was much longer than that of the WT phase-spanning cells (Fig. 6.4D). Because the phase-spanning neurons can be converted to I type by enhancing GABA inhibition (see below), the presence of a large number of these cells also indicates the extended firing of I neurons in *Mecp2*-null rats.

6.4.4 Post-I neurons

A group of neurons fired action potentials in the post-inspiratory (Post-I) phase of the phrenic discharge [247,248]. These post-I neurons have previously been shown to exist in the BötC area. We found 49 Post-I neurons in 105 BötC cells in the WT, but only 15 of 101 BötC neurons in *Mecp2*-null rats ($P<0.001$, χ^2 test) (Fig. 6.4E,F; Fig. 6.5). The reduction in Post-I cell number was likely to be a result of the extension of the burst length of the cells, making them merge in other E neurons in null rats.

6.4.5 Changes in phrenic discharge patterns

As previously reported, only 50% *Mecp2*-null rats survive up to two months of postnatal age [84,88,89]. At the age their breathing was much slower than that of the WT (Fig. 6.4G,H). Analysis of the eupneic phrenic activity revealed that the inspiration time (T_I) had no significant difference between null and WT animals (Fig. 6.4I), while the expiration time (T_E) of *Mecp2*-null rats was significantly elongated (Fig. 6.4J). The elongated T_E was consistent with increased burst length of medullary E neurons (above) and the increased excitability of E neurons.

With the changes in T_I vs T_E, their ratio was significantly reduced in null rats, leading to slow breathing (Fig. 6.4K). In contrast, the frequency per burst of phrenic discharges was increased in null rats, which measured as the amplitude of integrated phrenic activity twice as high as the WT (Fig. 6.4L). A similar phenomenon was observed in plethysmograph breathing recording in conscious rats. This suggests that the *Mecp2*-null rats seem to switch their phrenic output to a slow and deep respiratory pattern that may allow decent blood gas levels despite the low breathing frequency.

6.4.6 Neuronal activity during apnea

Apnea is considered when the bursting phrenic activity escaped at least one regular breathing cycle, which was believed to be a result of suspension of central I activity. Studying activity of I and phase-spanning neurons in the rVRG during apneas, we found that most of them did not pause their activity during apnea, although their firing became irregular (Fig. 6.6A,B). In

the meantime, E neurons in the BötC and cVRG maintained their firing frequency as during eupneic expiration (Fig. 6.6C,D). Statistical analysis indicated that firing frequency of these I and phase-spanning neurons was significantly higher during apnea than during eupneic expiration, while E neurons in BötC and cVRG did not change firing rate (Fig. 6.6E,F). These results indicate that apneas in the null rats may not result from suspension of central I activity.

6.4.7 Ectopic phrenic activity

Although phrenic activity is exclusively inspiratory with brief post-I activity in mammals, expiratory phrenic activity was found in *Mecp2*-null rats (Fig. 6.6A-C, Fig. 6.7). Such expiratory phrenic activity was produced by discharges of a small number of motor neurons (Fig. 6.7A), which occurred in middle or late expiration in some null rats (Fig. 6.7A), or throughout the entire expiration phase in others (Fig. 6.7B). Such ectopic phrenic activity remained during apneas (Figs. 6.6A-C, 6.7A). The ectopic phrenic activity was seen in ~ one third (8 of 22) of null animals (Fig. 6.7C), and appeared to be related to rat physical conditions. Seven out of the 8 animals had reached humane endpoints at the time of experiments (Fig. 6.7D). The association of the ectopic phrenic activity with the health status as well as its potentially adverse effects on ventilation suggests that such unexpected motor neuronal excitation may be one of the terminal events of lives in null rats.

Antidromic stimulation of the contralateral bulbospinal pathway in the cervical cord showed that some of the E-I phase-spanning neurons projected to the spinal cord (Fig. 6.6G-I), suggesting that the ectopic phrenic activity is likely produced by the phase-spanning drive from the brainstem.

6.4.8 Effects of GABA inhibition

The excessive firing activity of medullary respiratory neurons may be due to the insufficient GABAergic inhibition in *Mecp2*-null mice [96,101,103,106,108]. If so, augmentation of GABAergic synaptic inhibition should diminish the abnormalities in the respiratory neuronal firing. With this reasoning, we applied NNC-711, a GABA uptake transporter blocker, to the

rats. The NNC-711 treatment (10mg/kg, i.p.) reduced the difference of neuronal firing activity between null and WT rats, even eliminated the difference in some cell types (Fig. 6.8A-F, Fig. 6.9), which appeared to be more potent on rVRG and cVRG neurons, whereas BötC neuronal activity of null rats was only modestly reduced by the GABA uptake blocker. The extrasynaptic GABA receptor agonist THIP had similar effects (Fig. 6.8A-F, Fig. 6.9).

A single dose of NNC-711 started to have an evident effect ~20 min after injection. The ratio of phase-spanning neurons in the rVRG of *Mecp2*-null rats was reduced to ~49% and ~57% after NNC-711 and THIP treatment respectively (Fig. 6.8G), in comparison to ~71% in null rats with saline injection. Both changes were statistically significant. The same treatments had no significant effects on WT neurons. Moreover, the difference of burst duration of phase-spanning neurons between *Mecp2*-null and WT rats was reduced after drug treatments (Fig. 6.8H,I).

A long period of recordings was made, including two phase-spanning neurons before and during NNC-711 exposure (Fig. 6.10). The acute NNC-711 treatment converted the firing pattern of both cells from phase-spanning to I type (Fig. 6.10A,B), while in control rats with saline injection, phase-spanning neurons did not change their firing pattern (Fig. 6.11). Meanwhile, the acute NNC-711 treatment reduced the firing frequency of these cells and shortened their discharge duration (Fig. 6.10C,D). The ectopic activity of phrenic nerve was drastically reduced with the NNC-711 treatment, accompanied by reduction of breathing rhythmic variation (Fig. 6.10B,E). Acute THIP treatment had robust effects in some null rats as well, in which the breathing rhythmic variation was suppressed, the rhythmic breathing rate was increased, the amplitude of integrated phrenic discharges was reduced, and the ectopic phrenic activity was totally eliminated (Fig. 6.12A). As a result, the breathing pattern of null rats appeared to be rescued to the WT pattern. Such a rescue effect of THIP was also seen in awake rats tested in plethysmograph (Fig. 6.12B-D). Of 5 null rats that had reached humane endpoints with severe apnea and dyspnea, one dose of THIP injection (20mg/kg, i.p.) made the breathing patterns of all rats resemble the WT. Oral THIP administration in the drinking water (10mg/kg/day) was given

to four of these rats 48 h later for 7 consecutive days. Three of them extended their lifespan longer than 2 weeks with no obvious apnea and dyspnea during the period (Fig. 6.12E).

6.5 Discussion

This is the first demonstration of central respiratory neuronal activity in RTT models *in vivo*. Using the decerebrate preparation with spontaneous breathing, known to have no evident side-effects on respiratory neuronal activity, we have systematically studied all major types of respiratory neurons in the ventral respiratory column of the medulla oblongata. A number of findings has been made, many of which were unknown and unexpected.

Our results have shown that the high incidence of hypopnea, gasping and apnea in the RTT model is not due to insufficient central I activity. Instead, I neurons, as well as the E neurons, show excessive firing activity with extended firing duration. The extended firing duration of these neurons can cause destabilization of the rhythmic respiratory oscillation that depends on coordinated synaptic interactions of the E and I neurons. A critical step in the events is the transition from E phase to I phase. Such a phase transition may rely on synaptic inhibition where GABA seems to play a role, while GABA is known to be deficient in *Mecp2*-null mice [96,101,103,106,108,249]. With the GABAergic defect, presynaptic neurons need to fire more action potentials for sufficient GABA release, while postsynaptic neurons need a longer time to become silent. Therefore, E neurons may not terminate their activity in a timely manner when I neurons have begun firing, leading to the increased firing durations of both E and I neurons. The presence of a large number of phase-spanning neurons also supports it, as they would fire only during I phase if a fast phase transition took place in a brief period of time. This idea is also supported by neuronal activity during apneas, as none of them stops firing during apneas indicating that the apnea is likely to result from incomplete termination of E activity instead of a cessation of central I activity. Further supporting this idea are our data showing that enhancing endogenous GABAergic inhibition can correct firing patterns of the respiratory neurons in null rats.

Another novel finding in this study is the ectopic phrenic nerve activity of null rats during expiration, which is likely to derive from increased central I activity rather improper projections from E neurons for following reasons: 1) Its appearance time and firing course resemble the E-I phase-spanning neurons but not the E cells. Most of the ectopic phrenic discharge starts in the middle of expiration, when the phase-spanning neurons begin to fire. 2) Regarding ectopic phrenic activity running throughout expiration, its frequency increases at a time when phase-spanning neurons start firing (Fig. S4B). 3) Most E neurons within the cVRG and BötC start firing immediately after the I phase even with some overlaps with the post-I phase of phrenic activity. 4) Our experimental evidence indicates that some bulbospinal neurons have the E-I phase-spanning firing pattern.

The ectopic phrenic discharges are produced by a small number of motor neurons shown as a few single-unit phrenic activities in null rats. Although we did not find evident chest movements during the ectopic activity, their adverse effects are obvious. With these ectopic phrenic discharges, a portion of diaphragm may not be relaxed during expiration, making these muscle fibers vulnerable to fatigue. Without a total diaphragm relaxation, exhalation may not be well fulfilled, requiring active expiration mediated by internal intercostal muscles. The active expiration normally should occur only during forced ventilation in WT animals, which may potentially cause fatigue of the intercostal muscles as well. Thus, the ectopic phrenic activity resulting from of excessive central I neuronal activity seems to be an important contributor to symptom development in RTT, which is consistent with our finding that the ectopic phrenic activity occurs most frequently in animals reaching humane endpoint.

The demonstration of the extended firing activity of respiratory neurons with *Mecp2* disruption not only is a striking finding, but also suggests potential pharmacological interventions. Indeed, acute treatment of the null rats with the GABA uptake inhibitor NNC-711 significantly reduces the extended firing activity of the respiratory neurons, converts phase-spanning neurons to I type, and reduces the ectopic discharges of phrenic nerve. The

extrasynaptic $GABA_A$ receptor agonist THIP has similar neuronal effects which powerfully corrected the respiratory disorders in null rats. With the GABAergic interventions, the rhythmic phrenic activity is markedly improved, and rescued to the WT breathing phenotype. Indeed, the THIP treatment rescue 3 of 4 null rats that have reached humane endpoints. These suggest that the extended firing activity of medullary respiratory neurons plays a major part in respiratory disorders of null rats, and perhaps in people with RTT as well. Effective correction of such a general defect in the respiratory neurons appears to be a promising therapeutic strategy for the disease.

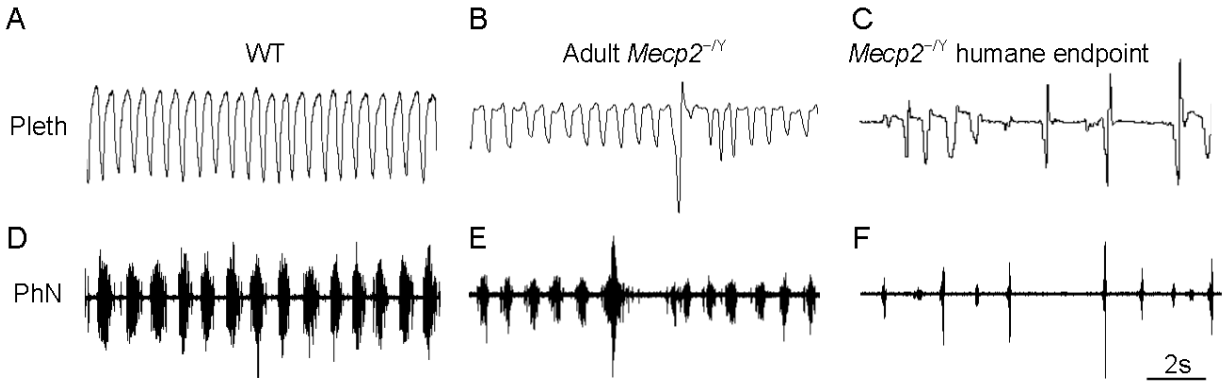

Figure 6.1 Breathing abnormalities in* Mecp2*-null rats.
Plethysmograph recording (Pleth, **A**-**C**) and phrenic activity (PhN, **D**-**F**) from WT and *Mecp2*-null rats. The latter exhibited variations in breathing frequency and amplitude as well as apnea starting from postnatal 4 weeks. The respiratory abnormalities became severe when animal reached humane endpoint.

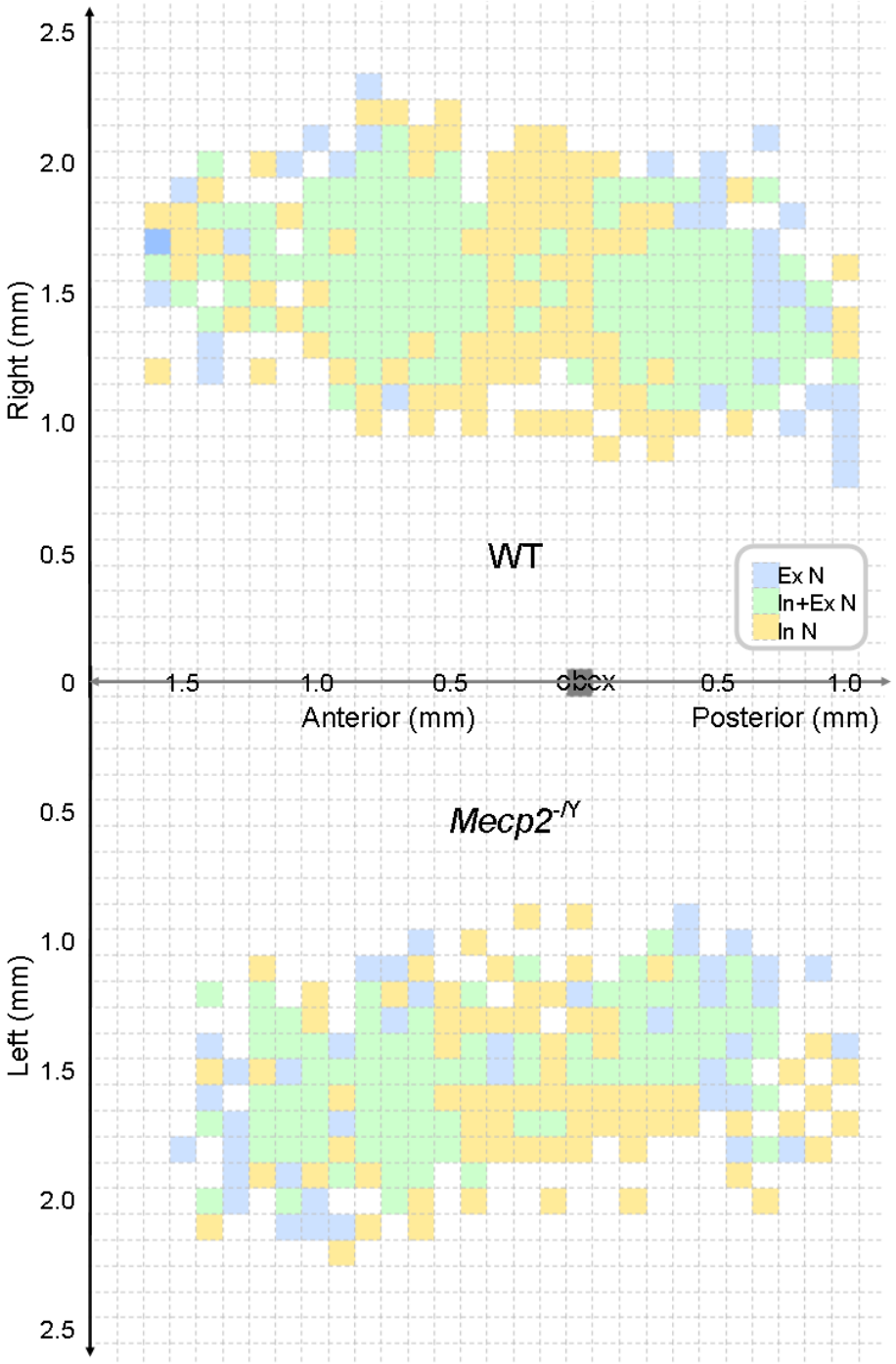

Figure 6.2 The localization of inspiratory (I) and expiratory (E) neurons in ventral respiratory column.

Location was measure from the obex on the left side of brainstem. Cells with different firing pattern were clearly separated into three areas with overlapping to some extent.

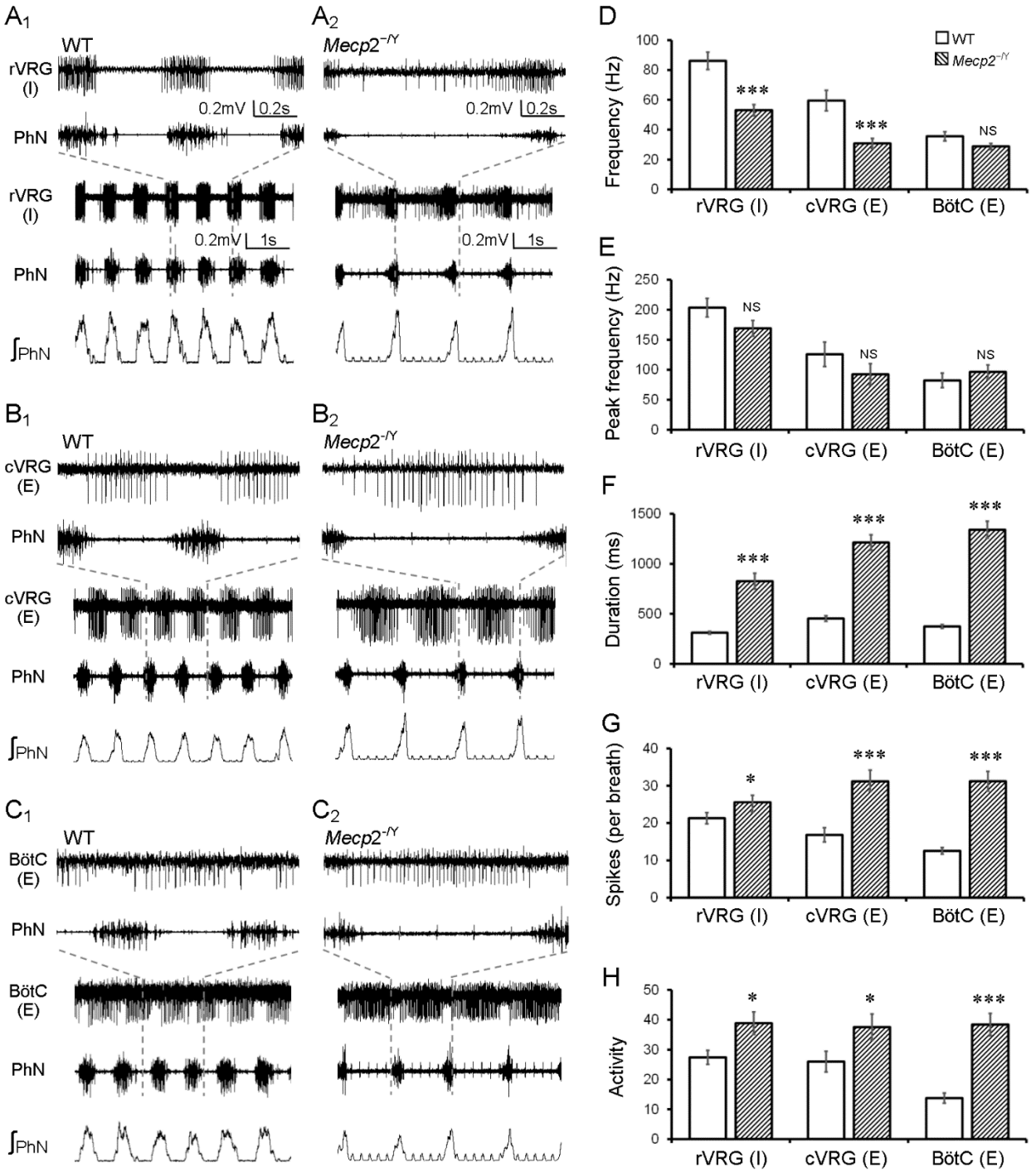

Figure 6.3 Firing activity and patterns of respiratory neurons.
(**A-C**) Neurons with expiratory (E) rhythm were recorded from cVRG and BötC, and cells with inspiratory (I) rhythm were found in rVRG. (**D**) Firing frequency of rVRG I neurons and cVRG E neurons was significantly lower in null rats than in WT rats, while firing frequency of BötC E neurons did not show significant difference between WT and null rats (I neurons in rVRG: n = 48 in WT and n = 63 in *Mecp2*-null rats, respectively; cVRG E neurons: n = 29 and n = 29; BötC E neurons: n = 43 and n = 65). (**E**) Peak frequency of all three groups of neurons had no

difference between WT and null rats. (**F**) Neuronal burst duration of all types of cells was measured with significant increase in null rats. (**G**) Spike number of each burst was measured in all groups of neurons, which was significantly higher in null rats than in WT rats. (**H**) Neuronal activity calculated as frequency (Hz) × duration (sec) was significantly higher in null rats than in the WT. *, $P<0.05$; **, $P<0.01$; ***, $P<0.001$ (Student's *t*-test); NS, no significance. Traces: phrenic nerve activity (PhN), integrated phrenic nerve discharge ($\int_{PhN}$). Note the presence of ECG activity in PhN.

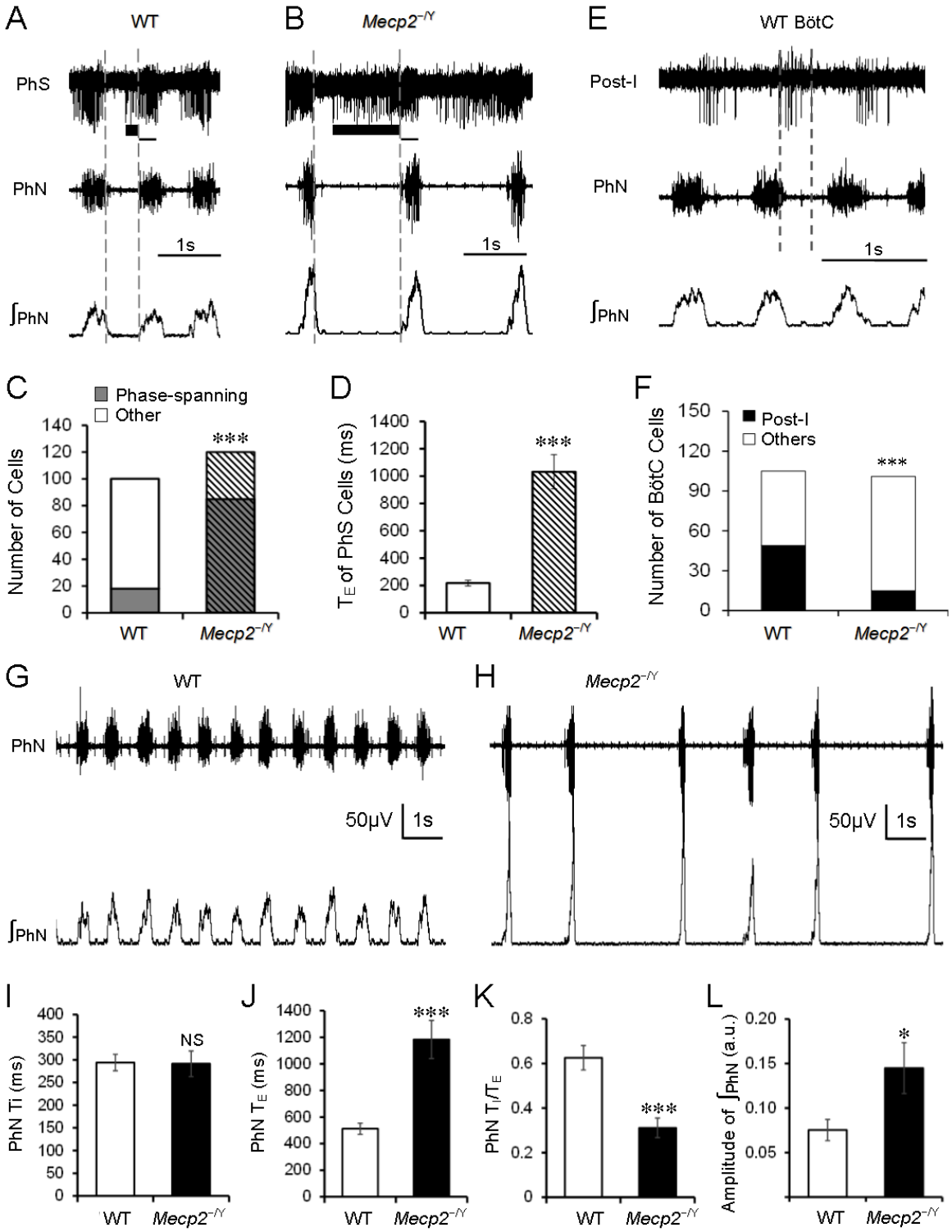

Figure 6.4 Phase-spanning, Post-I neurons and discharge patterns of phrenic nerve in WT and* Mecp2*-null rats.

(**A** and **B**) Neurons with E-I phase-spanning activity were recorded from rVRG in WT and *Mecp2*-null rats. Black bar, phase-spanning duration in expiration. (**C**) The number of E-I phase-spanning cells in rVRG was significantly greater in *Mecp2*-null rats than in the WT (***

P<0.001, χ^2 test). (**D**) The phase-spanning duration in expiration (T_E) was significantly longer in null rats as well (*P*<0.001, n = 43, Student's *t*-test). (**E** and **F**) Post-I neurons and its ratio with all other E cells in the BötC area (*** *P*<0.001, χ^2 test). (**G**) Phrenic discharge (PhN) and integrated phrenic activity ($\int_{PhN}$) recorded from a WT rat show relatively stable rhythmicity and amplitude. (**H**) In a *Mecp2*-null rat, such phrenic activity was slow and irregular with large amplitude. (**I**) Inspiratory duration (T_I) of phrenic activity did not show significant difference between WT and null rats (*P* = 0.936, measured in 21 WT and 18 *Mecp2*-null rats, with at least 20 phrenic bursts from each animal). (**J**) Expiratory duration (T_E) was significantly longer in null than WT rats (*P*<0.001). (**K**) The ratio of inspiration vs expiration duration (T_I/T_E) was significantly smaller in null rats than the WT (*P*<0.001). (**L**) The amplitude of integrated phrenic activity was larger in null rats than the WT at age 1.5 to 2.5 months (30 WT rats vs 21 *Mecp2*-null rats with *P* = 0.033). Arbitrary unit (a.u.). Student's *t*-test.

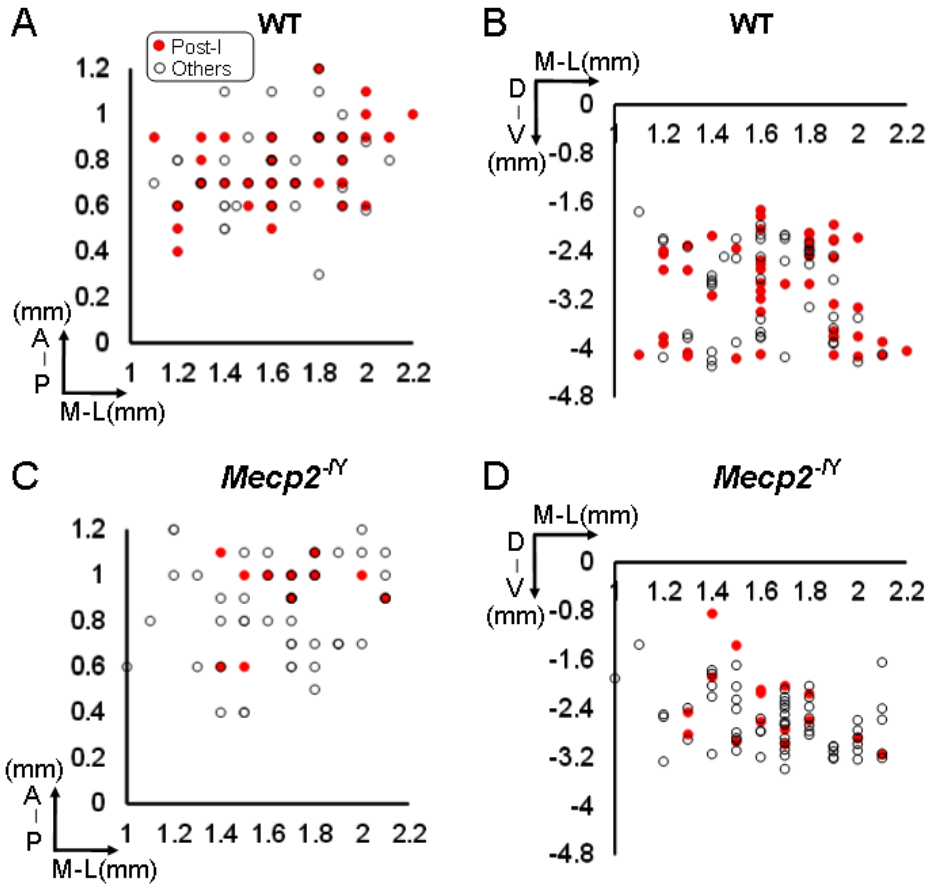

Figure 6.5 The localization of Post-I neurons in* Mecp2*-null and WT rats.
The axes indicate distances from obex (**A** and **C**) and the dorsal surface (**B** and **D**).

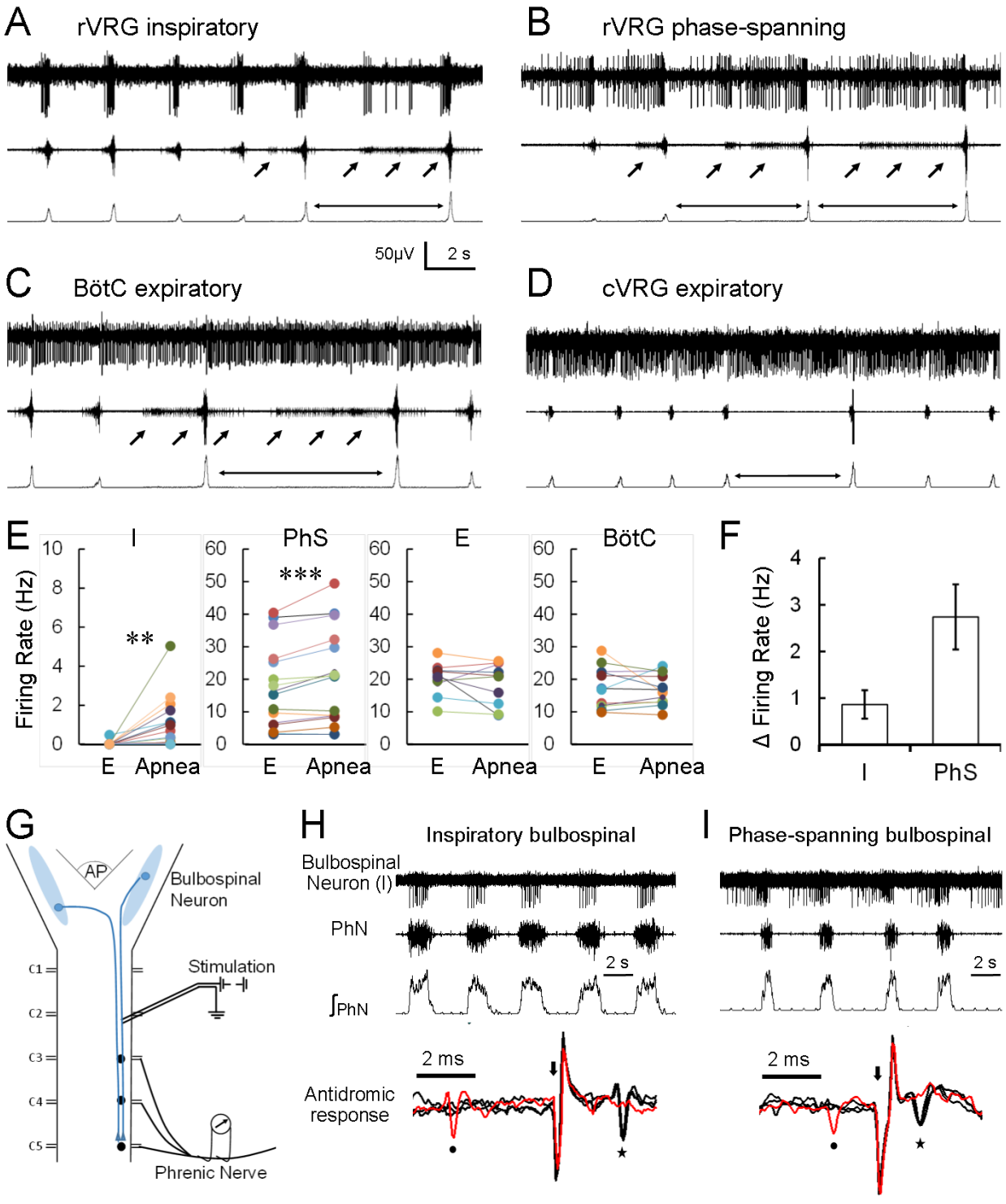

Figure 6.6 Neuronal activity during apneas in null rats.
(**A**) An inspiratory (I) neuron recorded in rVRG. It stopped firing completely during eupneic E phase, but started firing in the middle of apnea (double-head arrow). In the null rat, the phrenic nerve displayed single-unit discharges (arrows) during expiration. Such ectopic phrenic discharges were also seen during apnea. (**B**) An E-I phase-spanning cell recorded in rVRG.

During eupnea its firing started in the early E phase, and lasted to the end of I phase. During apnea, the cell started firing after a similar pause, and continued its firing throughout the apnea period. (**C** and **D**) E neurons in cVRG and BötC remained active during apnea. Note that ectopic phrenic discharges are seen in B and C, but not in D. (**E**) Parallel comparison of firing rates during eupneic expiration vs. apnea. Significant increases in firing rate was found in I and E-I phase-spanning (PhS) cells in rVRG. The firing rats of E neurons in cVRG and BötC did not show any significant difference between eupneic expiration and apnea (**, $P<0.01$; ***, $P<0.001$; paired Student's *t*-test). (**F**) The net difference of the firing rate between eupneic expiration and apnea in I and PhS cells. Data are obtained from E. ***G.*** Schematic of the antidromic stimulation experiment to identify bulbospinal neurons. (**H** and **I**) I and PhS cells with antidromic stimulation in the collision test. Lower panel: Both cells showed steady responses to antidromic stimulation (arrow) and collision test, i.e., the antidromic response (star) was eliminated with a prior action potential (dot) in a short latency.

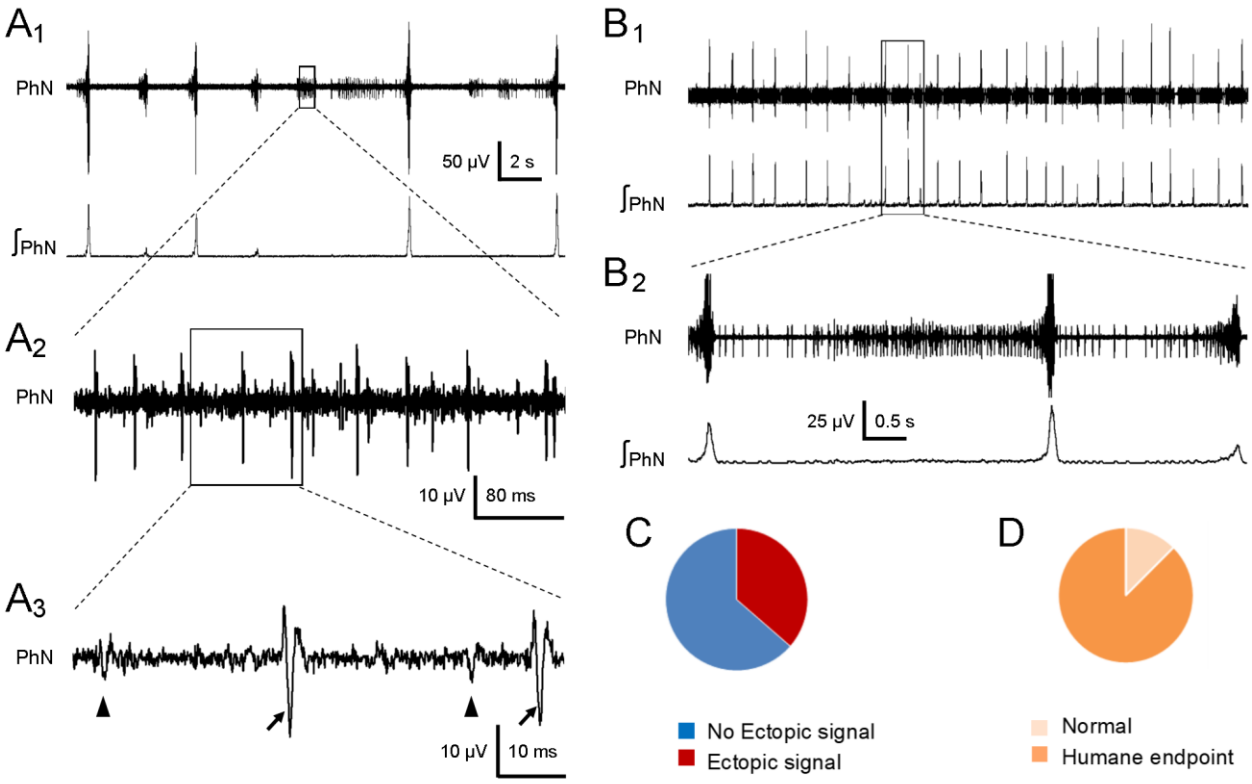

Figure 6.7 Ectopic phrenic activity in* Mecp2*-null rats.
(**A1**) Ectopic phrenic discharges occurred in the middle of expiration and apneas in a *Mecp2*-null rat that had reached humane endpoint. (**A2** and **A3**)With extended time scales, the ectopic phrenic ectopic activity consisted of three single units of action potentials with two of them shown in **A3** by arrows and arrow heads, respectively. (**B**) In another *Mecp2*-null rat, the ectopic phrenic discharges occurred throughout the expiration and apnea. (**C**) Eight out of 22 *Mecp2*-null rats had the phrenic ectopic signal. (**D**) Seven out of these 8 rats reached humane endpoint.

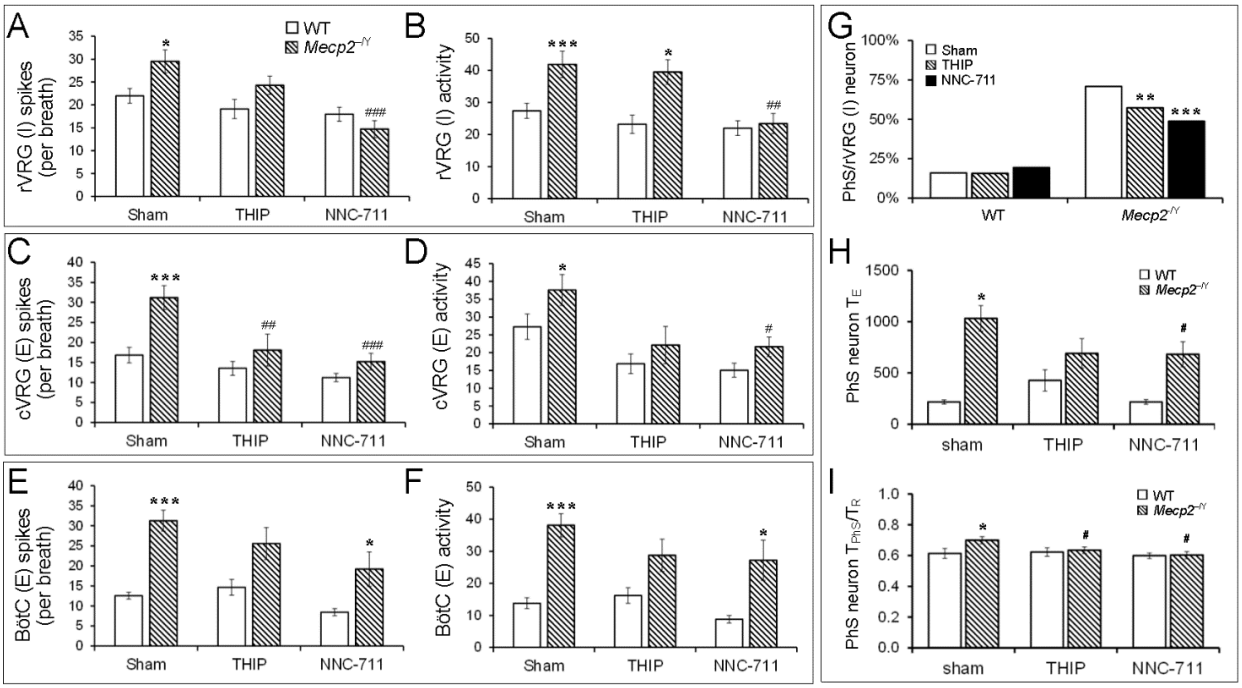

Figure 6.8 Effects of GABAergic augmentation on respiratory activities.
(**A-F**) Neuronal firing activities were tested with THIP or NNC-711. The drug treatments significantly reduced the differences between WT and *Mecp2*-null rats in burst spikes and firing activity of neurons. Spike number of THIP: rVRG: 19.1 ± 2.1, n = 45 in WT vs 24.3 ± 2.0, n = 41 in *Mecp2*-null; cVRG, 13.5 ± 1.7, n = 24 vs 18.1 ± 4.0, n = 14; BötC, 14.7 ± 2.0, n = 22 vs 25.6 ± 4.0, n = 16. Spike number of NNC-711: rVRG: 18.0 ± 1.5, n = 63 vs 14.7 ± 1.9, n = 30; cVRG, 11.2 ± 1.0, n = 41 vs 15.2 ± 2.1, n = 21; BötC, 8.4 ± 0.8, n = 31 vs 19.2 ± 4.3, n = 12. Activity of THIP: rVRG, 23.2 ± 2.9 vs 39.5 ± 3.9; cVRG, 16.9 ± 2.7 vs 22.1 ± 5.3; BötC, 16.2 ± 2.4 vs 28.7 ± 5.0. Activity of NNC-711: rVRG, 22.0 ± 2.3 vs 23.4 ± 3.2; cVRG, 15.0 ± 2.0 vs 21.7 ± 2.8; BötC, 8.8 ± 1.2 vs 27.2 ± 6.3. (**G**) The ratio of E-I neurons vs total rVRG cells was significantly reduced after THIP or NNC-711 treatment in *Mecp2*-null rats (χ^2 test). WT: 16% to 16% or 19%; *Mecp2*-null: 71% to 57% or 49%. (**H**) Duration of E-I neurons in *Mecp2*-null rats reduced by GABAergic augmentation. T_E of phase-spanning cells in WT changed from 217.3 ± 20.9 ms (n = 14) to 427.8 ± 103.4 ms (n = 11) or 217.7 ± 24.0 ms (n = 14) respectively after THIP or NNC-711 treatment, while T_E of phase-spanning cells in *Mecp2*-null reduced from 1031.5 ± 125.1 ms (n = 43) to 690.5 ± 144.7 ms (n = 38) or 682.4 ± 123.0 ms (n = 29). (**I**) Difference of normalized burst duration of E-I cells between *Mecp2*-null and WT disappeared after intervention of GABAergic augmentation. Normalized phase-spanning ratio of WT maintained similar (0.61 ± 0.03 to 0.62 ± 0.03 or 0.60 ± 0.02 respectively after THIP or NNC-711 treatment), while that of *Mecp2*-null reduced from 0.70 ± 0.02 to 0.64 ± 0.02 or 0.60 ± 0.02. (Two-way ANOVA followed by a Bonferroni post hoc test. *, significant difference comparing WT to *Mecp2*-null in same treatment group, #, significant difference comparing sham to THIP or NNC-711 groups within the same genetic background.)

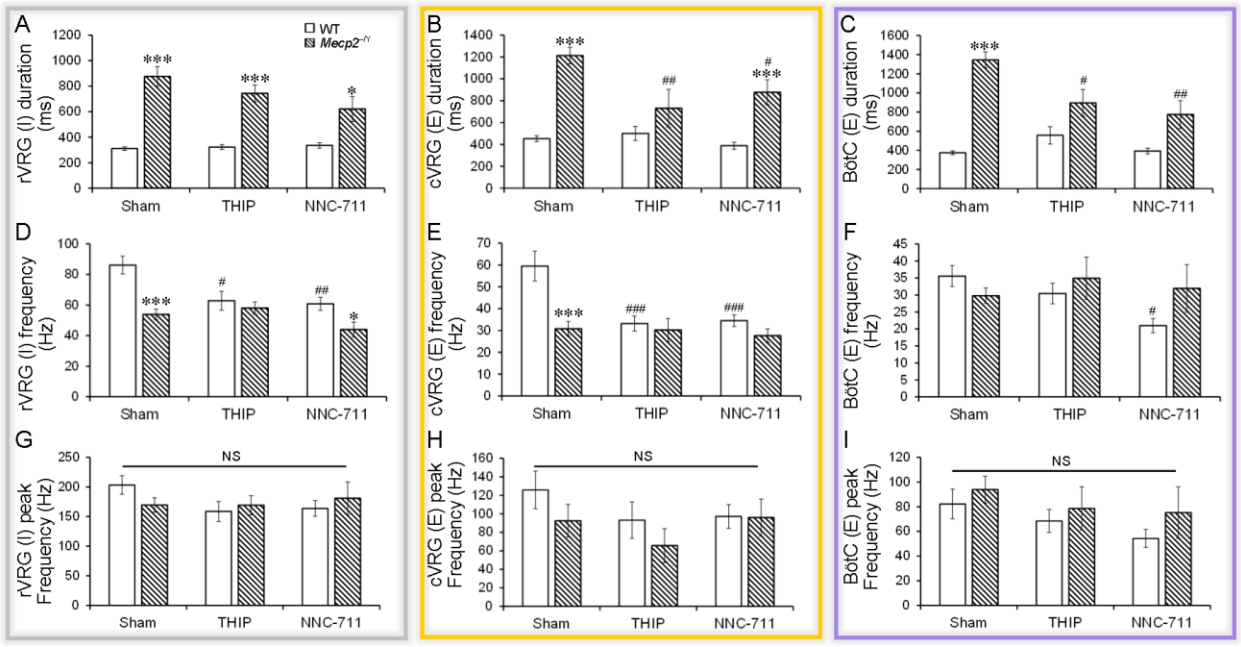

Figure 6.9 Neuronal firing pattern was changed by intervention of GABAergic augmentation. The THIP or NNC-711 treatment shortened the firing duration of *Mecp2*-null rats and reduced the difference of neuronal frequency between null and WT rats, while the peak frequency was intact. (**A**) Firing duration of WT in rVRG maintained at 322.3 ± 19.5 ms (n = 45) or 335.9 ± 21.0 ms (n = 63) respectively after THIP or NNC-711 treatment, and that of *Mecp2*-null reduced to 744.0 ± 66.6 ms (n = 41) or 621.4 ± 97.4 ms (n = 31). (**B**) Firing duration of WT in cVRG maintained at 501.2 ± 64.4 ms (n = 24) or 388.5 ± 31.6 ms (n = 41), and that of *Mecp2*-null reduced to 730.3 ± 173.5 ms (n = 14) or 876.6 ± 113.75 ms (n = 21). (**C**) Firing duration of WT in BötC maintained at 556.4 ± 90.66 ms (n = 22) or 392.5 ± 30.46 ms (n = 31) respectively, and that of *Mecp2*-null reduced to 895.6 ± 139.4 ms (n = 16) or 774.3 ± 144.5 (n = 12). (**D**) Firing frequency in rVRG reduced to 62.8 ± 6.2 Hz or 60.8 ± 4.2 Hz in WT vs 58.0 ± 4.0 or 44.0 ± 4.9 ms Hz in *Mecp2*-null respectively. (**E**) Firing frequency in cVRG reduced to 33.2 ± 3.5 Hz or 34.5 ± 2.6 Hz in WT vs 30.2 ± 5.2 Hz or 27.6 ± 3.2 Hz in *Mecp2*-null respectively. (**F**) Firing frequency in BötC didn't change much, only reduced to 30.4 ± 3.1 Hz or 21.0 ± 2.1 Hz in WT vs 34.9 ± 6.2 Hz or 31.9 ± 7.0 Hz in *Mecp2*-null respectively. (**G**-**I**) Peak frequency of all cells were not affected by drug treatments. Two-way ANOVA followed by a Bonferroni post hoc test.

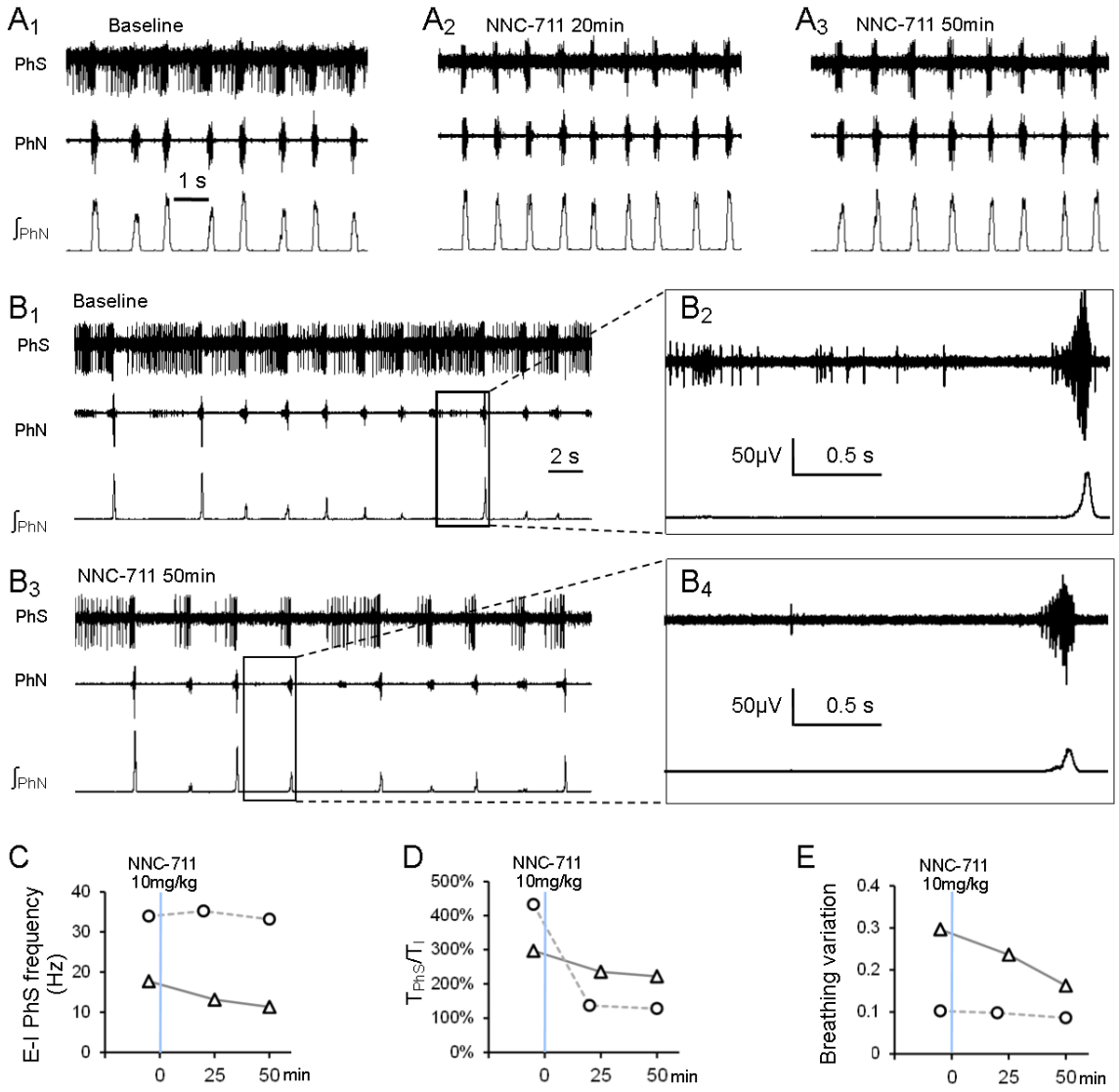

Figure 6.10 Firing pattern changes of phase-spanning neurons after NNC-711 treatment. (**A**) Continuous recordings from a phase-spanning neuron before and after NNC-711 injection (10 mg/kg, i.p.). The cell changed its firing pattern to I type 20 min after the injection, and maintained it throughout the rest of recording period. (**B**) Similar phenomenon was seen in another phase-spanning neuron from a different rat where phrenic recording showed severe irregularity, apneas and ectopic discharges. After NNC-711 injection, the cell changed its firing to a pattern more like I type with improvements of all other abnormalities in phrenic activity. (**C-E**) The NNC-711 treatment reduced firing frequency and burst duration of both the phase-spanning neurons as well as phrenic breathing variation. Circle, cell A; triangle, cell B.

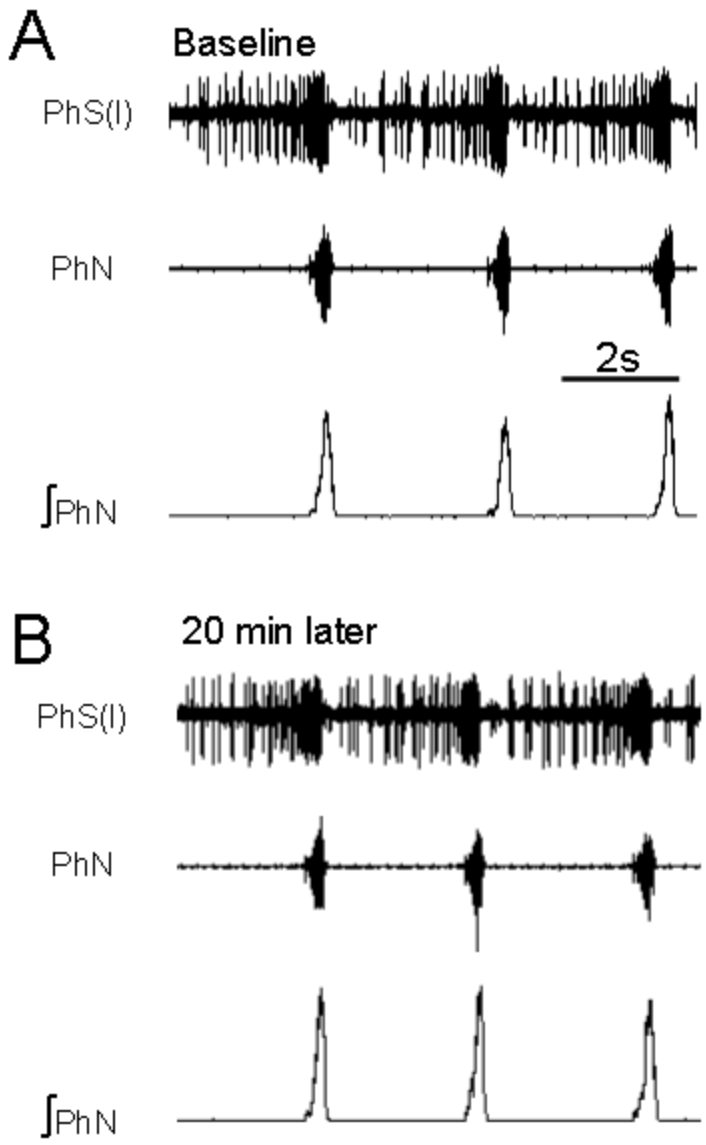

Figure 6.11 Saline injection had no effect on PhS activity in* Mecp2*-null.
Firing activity and pattern did not change in 20 min continuous recording.

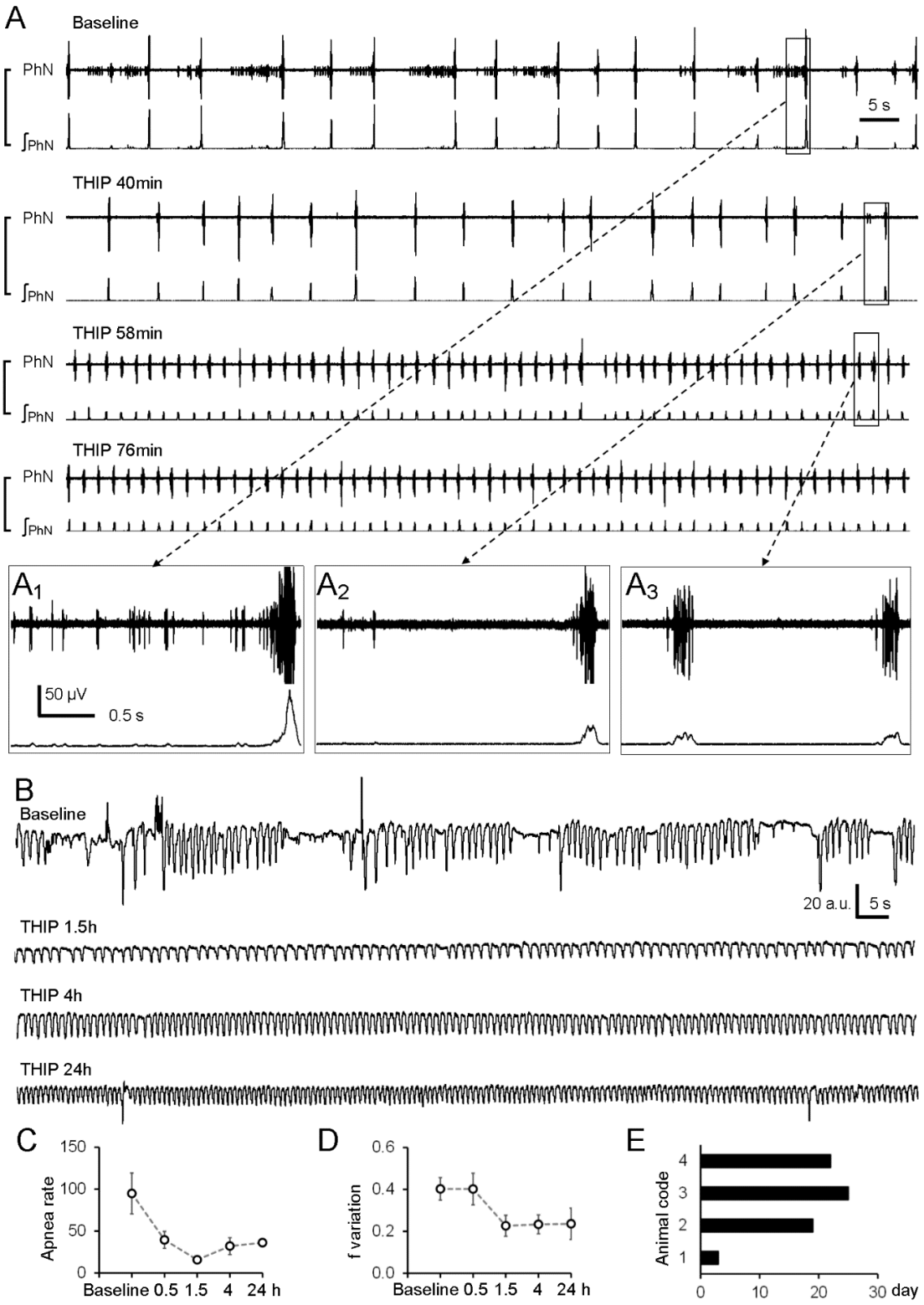

Figure 6.12 Rescue of phrenic activity and breathing pattern with THIP treatment.
(**A**) Continuous recording of phrenic activity from a *Mecp2*-null rat before and after THIP injection (20 mg/kg, i.p.). The rat had reached humane endpoint before the experiment. Its physical condition was confirmed by phrenic activity and discharge patterns, showing extremely

slow breathing, large variations in breathing rhythm and amplitude, widespread apneas, and severe ectopic phrenic activity. The first sign of symptomatic improvement was the robust inhibition of the ectopic phrenic activity 40 min after THIP injection (also compare **A_1** with **A_2**). A marked increase in breathing frequency and a reduction in the amplitude of integrated phrenic activity occurred 58 min after THIP injection with total elimination of the ectopic phrenic activity (**A_3**). The phrenic activity and discharge pattern resembled very much the WT with disappearance of apneas 76 min after the injection. (**B**) Breathing activity of an awake null rat was recorded using whole-body plethysmography at baseline and different time points after 20mg/kg THIP injection. The THIP treatment eliminated the abnormal breathing and rescued this *Mecp2*-null rat that had reached humane endpoints. The same study was done in 5 *Mecp2*-null rats reaching humane endpoints. A single dose of THIP injection (20mg/kg, i.p.) reduced their averaged apnea counts per hour (**C**), and breathing frequency variation (**D**). (**E**) After the THIP injection, 4 of the 5 rats were also treated with oral THIP in the drinking water (10mg/kg/day). Three of them extended the lifespans longer than 18 days.

7 RESULT 3: THE SUR2B SUBUNIT OF RAT VASCULAR KATP CHANNEL IS TARGETED BY MIR-9A-3P INDUCED BY PROLONGED EXPOSURE TO METHYLGLYOXAL

Published as "Shan-Shan Li,* **Yang Wu**,* Xin Jin,* and Chun Jiang. The SUR2B subunit of rat vascular K_{ATP} channel is targeted by miR-9a-3p induced by prolonged exposure to methylglyoxal. ***Am J Physiol Cell Physiol.*** 2015 Jan 15;308(2):C139-45."

* S-S. Li, Y. Wu, and X. Jin contributed equally to this study.

7.1 Acknowledgements

This work was supported by the National Institutes of Health (National Institute of Child Health and Human Development Grant HD-060959 and National Institute of Neurological Disorders and Stroke Grant NS-073875).

7.2 Abstract

ATP-sensitive K^+ (K_{ATP}) channels regulate plasma membrane excitability. The Kir6.1/SUR2B isoform of K_{ATP} channels is expressed in vascular smooth muscles and plays an important role in vascular tone regulation. This K_{ATP} channel is targeted by several reactive species. One of them is methylglyoxal (MGO), which is overly produced with persistent hyperglycemia and contributes to diabetic vascular complications. We have previously found that MGO causes posttranscriptional inhibition of the K_{ATP} channel, aggravating vascular tone regulation. Here we show evidence for the underlying molecular mechanisms. We screened microRNA databases and found several candidates. Of them, miR-9a-3p, increased its expression level by ~240% when the cultured smooth muscle cell line was exposed to micromolar concentrations of MGO. Treatments with exogenous miR-9a-3p downregulated the SUR2B but not Kir6.1 mRNA. Antisense nucleotides of miR-9a-3p alleviated the effects of MGO.

Quantitative PCR showed that the targeting sites of the miR-9a-3p were likely to be in the coding region of SUR2B. The effects of miR-9a-3p were mostly eliminated when the potential targeting site in SUR2B was site-specifically mutated. Our functional assays showed that K_{ATP} currents were impaired by miR-9a-3p induced with MGO treatment. These results suggest that MGO exposure raises the expression of miR-9a-3p, which subsequently downregulates the SUR2B mRNA, compromising K_{ATP} channel function in vascular smooth muscle.

7.3 Introduction

Diabetes mellitus is a major challenge to biomedical sciences [250]. Diabetes causes metabolic alterations leading to excessive production of various intermediary metabolites [180]. One of them is methylglyoxal (MGO), a highly reactive carbonyl species (RCS) [174,202,203]. MGO can react with proteins, nucleotides, and lipids, damaging these molecules and promoting inflammation and cell injuries [251-253]. Normally, MGO is rapidly detoxified by metabolic and redox enzymes so that it is maintained at a rather low level [254]. Under diabetic conditions, however, the increased production of precursor molecules and impaired carbonyl detoxification system result in overproduction and accumulation of this RCS [255]. The imbalance in the production and clearance of RCS then leads to carbonyl stress, which is known to play an important role in the development of diabetic complications, especially in the vasculature [256-258].

In the vasculature, an increase in MGO levels can impair structure and function of the vascular walls by acting on the vascular smooth muscle, endothelium, or both. This in turn disrupts the signaling network in these cells, triggers structural remodeling of the vascular wall, propagates vascular inflammation, and causes vascular dysfunction [259-261]. Indeed, our recent studies have shown that an important molecular target of MGO in the vasculature is the ATP-sensitive K^+ (K_{ATP}) channel [206].

The vascular K_{ATP} channel consisting of Kir6.1 and SUR2B subunit is expressed in VSM cells. This K_{ATP} channel is modulated by a number of vasoactive substances and metabolites [262]. Changes in channel activity in altered metabolic states affect membrane excitability as well as vascular tones and permeability [141,263,264]. Disruption of the K_{ATP} channel has severe consequences as shown in K_{ATP} channel-knockout mice [265-268]. In diabetic patients, K_{ATP} channel dependent vasodilation is impaired, suggesting that K_{ATP} channel dysfunction occurs under diabetic conditions [269,270]. In our recent studies, we have found that a prolonged exposure to MGO brings about inhibition of the K_{ATP} channel and augmentation of vasoconstriction responses [206]. However, the underlying mechanisms for the MGO-induced inhibition of K_{ATP} channel are still unclear.

MicroRNAs (miRs) are important regulators of gene expression especially in diseased conditions. In eukaryotes, miRs are encoded by nuclear DNA and transcribed as longer hairpin transcripts known as pre-miRs. After processed by the Drosha and Dicer enzymes, one strand of the hairpin duplex is loaded to an Argonaute family protein to form the core of miR-induced silencing complex that subsequently functions via base-pairing with complementary sequences of the target mRNA to regulate the mRNA life and its capability of translation. In the process, the binding of miRs to the target mRNA is important for their recognition. Most miR binding sites sufficient for the transcript silencing are located in the 3'-untranslated region (3'-UTR), while some are in the coding sequence (CDS). Our previous studies have suggested that MGO acts on the CDS of SUR2B mRNA, impairing their stability as well as K_{ATP} channel activity [206]. Thus, it is possible that under diabetic conditions, the reactive carbonyl stress raises the expression of miRs that subsequently target the K_{ATP} channel, and impair the vascular tone regulation. To test this hypothesis, we performed the present studies.

7.4 Results

7.4.1 Expression profiling of candidate miRNAs in reactive carbonyl stress.

In diabetic patients, persistent hyperglycemia leads to overproduction of MGO to ~400 µM [271,272]. In our previous study, we found that exposure to 300 µM MGO causes disruption of vascular K_{ATP} channels [206]. Therefore, we used this concentration of MGO in the present study.

We first screened the potential miR candidates targeting mRNAs of rat Kir6.1 and SUR2B subunits using bioinformatics, as our previous experiments were mostly done in the rat A10 VSM line. On the basis of their mammalian conservation and potential involvement in diabetes in existing literature, nine diabetes-associated miRs were found. Among them, three miRs were potentially targeting Kir6.1, and six miRs were potentially targeting SUR2B. Subsequently, the expression profiles of the nine mature miRs were determined in A10 VSM line following MGO exposure. Our qPCR analysis showed that the MGO treatment resulted in a significant increase of miR-9a-3p level by 2.4 ± 0.2-folds (n = 3 separated experiments with 3–6 samples each), while none of the other miRs increased their expression significantly (Fig. 7.2). We did not further study miRs that showed reductions in their expression as according to current literature they did not seem to have a direct effect on K_{ATP} channel inhibition by MGO exposure. Because of this and because miR-9a-3p is highly conserved in mammals (Fig. 7.1A), all further studies were performed on miR-9a-3p.

7.4.2 Inhibition of K_{ATP} channel expression by MGO and miR-9a-3p

To show whether miR-9a-3p affects K_{ATP} channel expression, one chemically synthesized and optimized double strand sequence to the mature endogenous miR-9a-3p. Also synthesized was one single-strand nucleotide complementary to the mature miR-9a-3p (anti-9).

We then transfected the A10 cells with these synthetic nucleotides and studied their effects on the expression of SUR2B subunit after MGO exposure.

Our qPCR analysis showed that the m-9 transfection caused suppression of the SUR2B mRNA expression (Fig. 7.3), which resembled the effect of MGO. Meanwhile, the effect of MGO was markedly diminished when the cells were transfected with anti-9 (Fig. 7.3). Consistent with qPCR results, Western blot analysis showed that m-9 inhibited SUR2B expression at the protein level, while anti-9 partially blocked the MGO effect (Fig. 7.4A,B). To determine whether m-9 also acts on Kir6.1 in the same conditions, we tested the expression of Kir6.1 at protein level. Our data showed that m-9 had no effect on Kir6.1 protein expression (Fig. 7.4C,D). These results suggest that miR-9a-3p regulates vascular K_{ATP} channel expression, which appears necessary for MGO to produce its effect.

7.4.3 Targeting at the CDS of SUR2B

Our bioinformatics analysis showed that a 9 seed-nucleotide region in the position 661–685 of rat SUR2B mRNA matches the miR-9a-3p, which also can be recognized in mouse (608–632) and human (2720 –2744) SUR2B mRNAs (Fig. 7.5A). Several constructs were made to demonstrate whether such a potential binding site interacts directly with miR-9a-3p. The mouse SUR2B mRNA was cloned into the pcDNA3.1 vector (SUR). Site-directed mutagenesis of two nucleotides at positions 622 and 625 without changing the amino acids (M-SUR) was also carried out using the same vector (Fig. 7.1C). We then cotransfected the HEK293 cells together with the M-SUR and m-9. The cotransfection of HEK293 cells with the SUR alone or scmiR was used as negative control. As shown in Fig. 7.5B, the cotransfection of HEK293 cells with the SUR and m-9 resulted in downregulation of SUR mRNA expression compared with controls, which is consistent with our findings in the A10 cells. This effect of m-9 was abrogated when the

miR-9a-3p binding site was mutated (Fig. 7.5B). Therefore, these results suggest that miR- 9a-3p is likely to target the SUR2B CDS, and the position 608–632 seems to be an important target site.

7.4.4 Inhibition of functional K_{ATP} currents by miR-9a-3p

To prove that exogenous m-9 and anti-9 had a functional impact on K_{ATP} channels, we studied its effects on heterologously expressed Kir6.1/SUR2B channels in HEK293 cells, in which K_{ATP} currents were relatively large and sufficient for a long-term analysis. Equal high concentrations of K^+ (145 mM) were applied to both sides of the membranes. The membrane potential was held at 0 mV and stepped to -80 mV every 3 s in voltage clamp. Pinacidil (Pin), a specific K_{ATP} opener, and glibenclamide (Glib), a K_{ATP} inhibitor, were used to set a window of K_{ATP} channel activity. At the basal level, K_{ATP} channel activity was low. Exposure to 10 μM Pin strongly activated K_{ATP} currents, which were subsequently suppressed by 10 μM Glib (Fig. 7.6A).

Consistent with our previous study [206], a marked inhibition in K_{ATP} currents occurred after cells were treated with MGO for 12 h (Fig. 7.6B). In cells transfected with anti-9, the MGO effect was drastically attenuated (Fig. 7.6C,D).

A significant inhibition in K_{ATP} currents was found after the cells were cotransfected with m-9 (Fig. 7.7B), to the degree similar to the effect of MGO on K_{ATP} currents (Fig. 7.6B). K_{ATP} current inhibition was reversed partially when the binding sites for miR-9a-3p were mutated in SUR2B (M-SUR) (Fig. 7.7C,D). In contrast, scmiR had no effect on K_{ATP} channel activity (data not shown).

7.5 Discussion

This is the first demonstration of regulation of K_{ATP} channel by miRs. The miR-9a-3p is upregulated in MGO-induced carbonyl stress. By targeting the CDS of SUR2B, the miR-9a-3p inhibits K_{ATP} channel expression, leading to a reduction in K_{ATP} channel activity.

In diabetic conditions, persistent hyperglycemia leads to overproduction of a variety of RCS including the highly reactive MGO, contributing to the development of diabetic complications. Acting on proteins, lipids, or nucleotides, excessive

MGO can cause carbonyl stress and cell damage. Our previous studies have shown that MGO acts on K_{ATP} channels in VSM cells, causing instability of Kir6.1 and SUR2B mRNAs, in which the 3'-UTR of Kir6.1 and the CDS of SUR2B are likely to be targeted [206]. As a result, a loss of functional K_{ATP} channels occurs followed by dysregulation of vascular tone [206].

Emerging evidence suggests that miRs contribute to the pathogenesis of diabetes and diabetic complications [273-276]. Since each miR has its potential targeting genes, information of miR involvement in diabetes is helpful for identification of the targeted molecules as well. The expression of these miRs may be upregulated by several pathological conditions in diabetes including the carbonyl stress. Therefore, it is reasonable to believe that the instability of Kir6.1 and SUR2B mRNAs shown in our previous studies is attributable to certain miRs.

With bioinformatics prediction, nine diabetes-associated miRs were selected for the profiling in carbonyl stress. With the information, we treated the A10 VSM cell line with 300 μM MGO, a concentration that is seen in serum of diabetic patients and also found effective for K_{ATP} disruption [206]. With the MGO treatment, we have found that miR-9a-3p is upregulated, while none of the other eight miRs show a significant increase in their expression levels. miR-9a-3p is highly conserved in mammals and has potential targeting sites in the human SUR2B gene

as well. Under diabetic conditions, miR-9 is suggested as being involved in insulin secretion by targeting Sirt1 in pancreatic β-islets [277]. However, no previous study has reported that miR-9a-3p is regulated by RCS under diabetic conditions. Therefore, our current study provides the first evidence for the upregulation of miR-9a-3p in reactive carbonyl stress.

In A10 cells, we overexpressed m-9 with/without MGO treatment and found inverse correlations between the exogenous miR-9a-3p and SUR2B mRNA levels. Consistently, antagonizing the endogenous miR-9a-3p with anti-9 reversed the MGO-induced reduction of SUR2B expression. In HEK cells, our qPCR and Western analysis further proved that the CDS of SUR2B was directly targeted by miR-9a-3p. These results thus indicate that miR-9a-3p is involved in MGO-induced disruption of vascular K_{ATP} channels by targeting at the CDS of SUR2B.

The SUR2B targeting by miR-9a-3p should have an impact on K_{ATP} channel activity. Our data indeed show that miR-9a-3p inhibits functional K_{ATP} currents to the degree similar to MGO treatment. The effects of MGO on K_{ATP} channel can partially be reversed when the endogenous miR-9a-3p was knocked down with anti-9, further supporting that miR-9a-3p mediates the modification of K_{ATP} channels in carbonyl stress. Our site-directed mutagenesis studies confirm that miR-9a-3p targets SUR2B mRNA at the CDS region.

In our previous studies, we have found that MGO causes instability of both Kir6.1 and SUR2B mRNAs [252]. Although miR-9a-3p is likely to target SUR2B, the Kir6.1-targeting miR(s) remains to be demonstrated. Since none of the three conserved miRs that we have studied seems to be the player, and since miR-9a-3p does not affect Kir6.1 expression either, we speculate that the Kir6.1 may be targeted by miRs that are either non-conserved or missing in the database. Alternatively, the Kir6.1 inhibition by MGO may not be mediated by miRs at all.

Mouse models of loss-of-function of SUR2 genes have shown the critical role of the vascular K_{ATP} channel in the coronary circulation. K_{ATP} channel dysfunction in mice leads to coronary vasospasm and sudden death [265,268]. Notably, in $SUR2^{-/-}$ mice, loss of hyperpolarizing K_{ATP} current causes abnormally elevated $[Ca^{2+}]_i$, leading to a reduction in coronary artery vasospasm [265]. Therefore, vascular K_{ATP} channel targeting by miR-9a-3p appears consistent with the adverse effects of MGO on vasculatures.

Recent studies indicate that the activity of the vascular isoform of K_{ATP} channels is necessary for the systemic responses in diabetes. The increased metabolic rate requires a corresponding elevation in cardiac output to meet the metabolic demands. Therefore, K_{ATP}-mediated vasodilation may act as compensatory role for several vital organs perfusion. Our studies indicate that miR-9a-3p modulates the K_{ATP} channel, which compromises the compensatory vasodilation in several vital organs and leads to inadequate perfusion, contributing to tissue hypoxia and cell injury. Therefore, our studies on miR mediated K_{ATP} channel regulation in diabetes may help in the understanding of diabetic organ dysfunction.

A number of diabetes-associated miRs have been identified. Some miRs are involved in tissue dysfunction, including retina, kidney, peripheral nerves, heart, and the vasculature. For instance, some miRs modulate the renin-angiotensin-aldosterone system, like miR-181a, miR-663, miR-155, miR-29b, miR-129-3p, and miR-132, and oxidative stress like miR-377, miR-23a/b, miR-27a, miR-24, miR-335, miR-205, and miR-210 in diabetic nephropathy [278]. Some miRs have been proved to be involved in vascular endothelial damage like miR-195, miR-503, and miR-146a in diabetic retinopathy [279-281], and some miRs like miR-34b, miR-34c, miR-199b, miR-210, miR-650, and miR-223 are shown to be dysregulated in diabetic ischemic heart failure patients [282]. Therefore, our present study illustrating the role of MGO-induced miR-9a-3p in

VSM cells helps in the understanding of the molecular mechanisms of vasculature dysfunction in diabetes.

At present, the mechanisms regulating miR expression and activity are still not fully understood. There is no information on the up- and downregulation of miRs by MGO in VSM cells either. Since the basic miR biogenesis pathways involve miR transcription, Drosha and Dicer processing, RNA editing, RNA modification, Argonaute loading, and RNA decay, MGO as a reactive carbonyl may act on one or some of these molecules affecting miR expression. Accumulating evidence suggests that aberrant DNA methylation of tumor suppressor genes occurs commonly in cancer, and events for miR hypermethylation/hypomethylation are found to play a role in human metastasis [283,284]. Indeed, MGO-mediated DNA demethylation has been found to alter the cellular redox balance in human cataract formation [285]. Similar mechanisms may work in the VSM cells in reactive carbonyl stress. Thus, our findings in the present study may stimulate further studies of the regulation of miRs by RCS as well as the resulting vascular complications in diabetes.

Other unidentified targets may exist as miR-9a-3p sequence has multiple partial matches with Abcc9, Kir6.1, and other mRNAs. Indeed, miR-9a-3p seed match regions are found at three places in rat Abcc9 (675-AGCTTTAT-682, 5404-GCTTTAT-5398, and 5978-GCTTTAT-5972). Thus, we cannot rule out the possibility that other sites may also be targeted by miR-9a-3p in rat SUR2B and perhaps Kir6.1 as well.

In conclusion, the present study provides the first evidence for regulation of K_{ATP} channels by miRs. Our results indicate that miR-9a-3p plays an important role in the regulation of vascular K_{ATP} channels in reactive carbonyl stress, acting on the CDS of the SUR2B and

inhibiting K_{ATP} channel activity. Therefore, the stabilization of miR-9a-3p levels may be a novel strategy for clinical treatment of diabetic vascular complications.

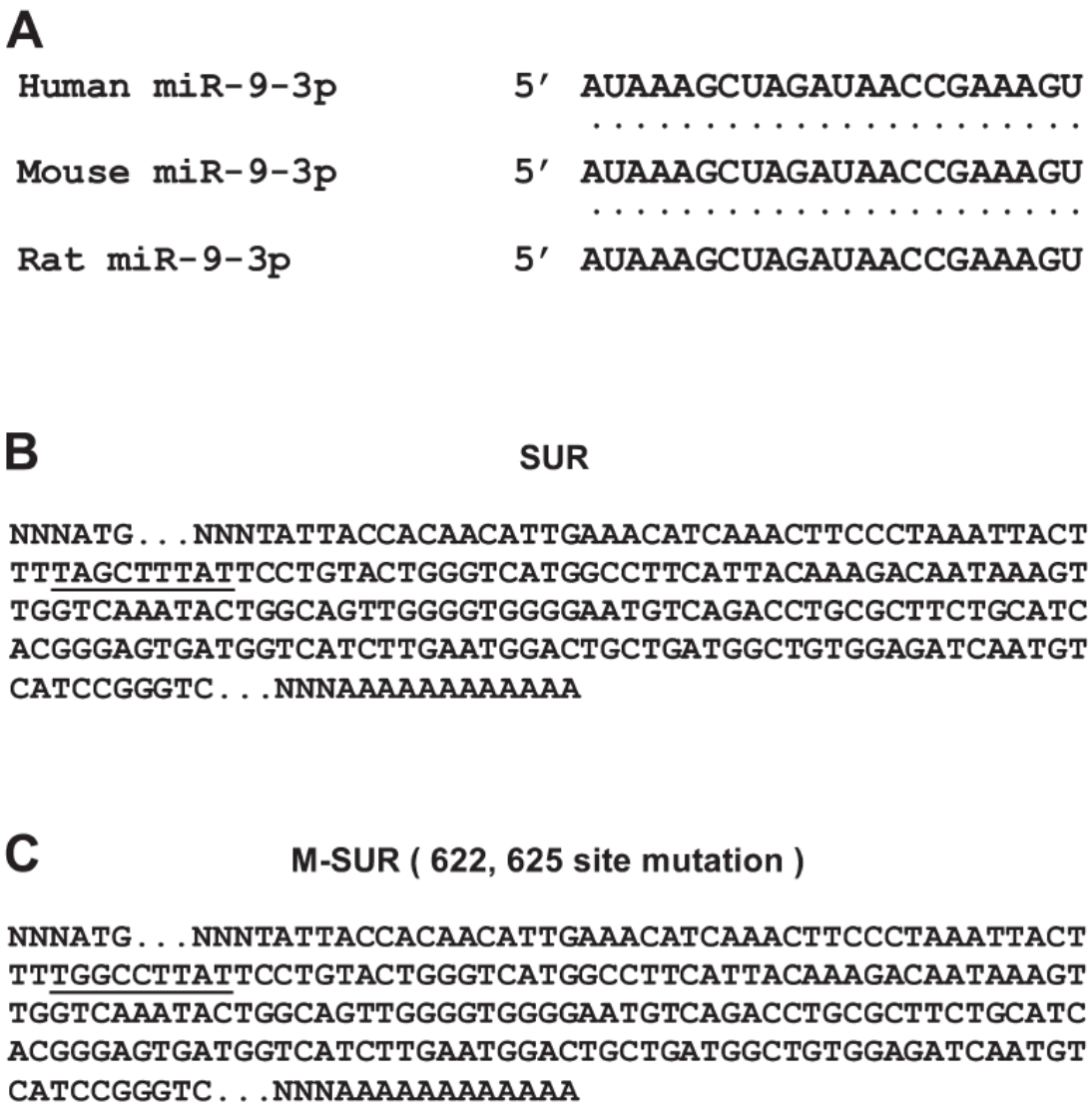

Figure 7.1 Mutation sites in Kir6.1 and SUR2B mRNA.
(A) Evolutionary conservation of miR-9a-3p among mammals. **(B)** Sequences of SUR2B mRNA (SUR). **(C)** Sequences of mutated SUR2B mRNA (M-SUR). Mutated sites were numbered in SUR2B mRNA. Some omitted sequences are represented with "N". Underlined letters are targeting sites for miR-9a-3p.

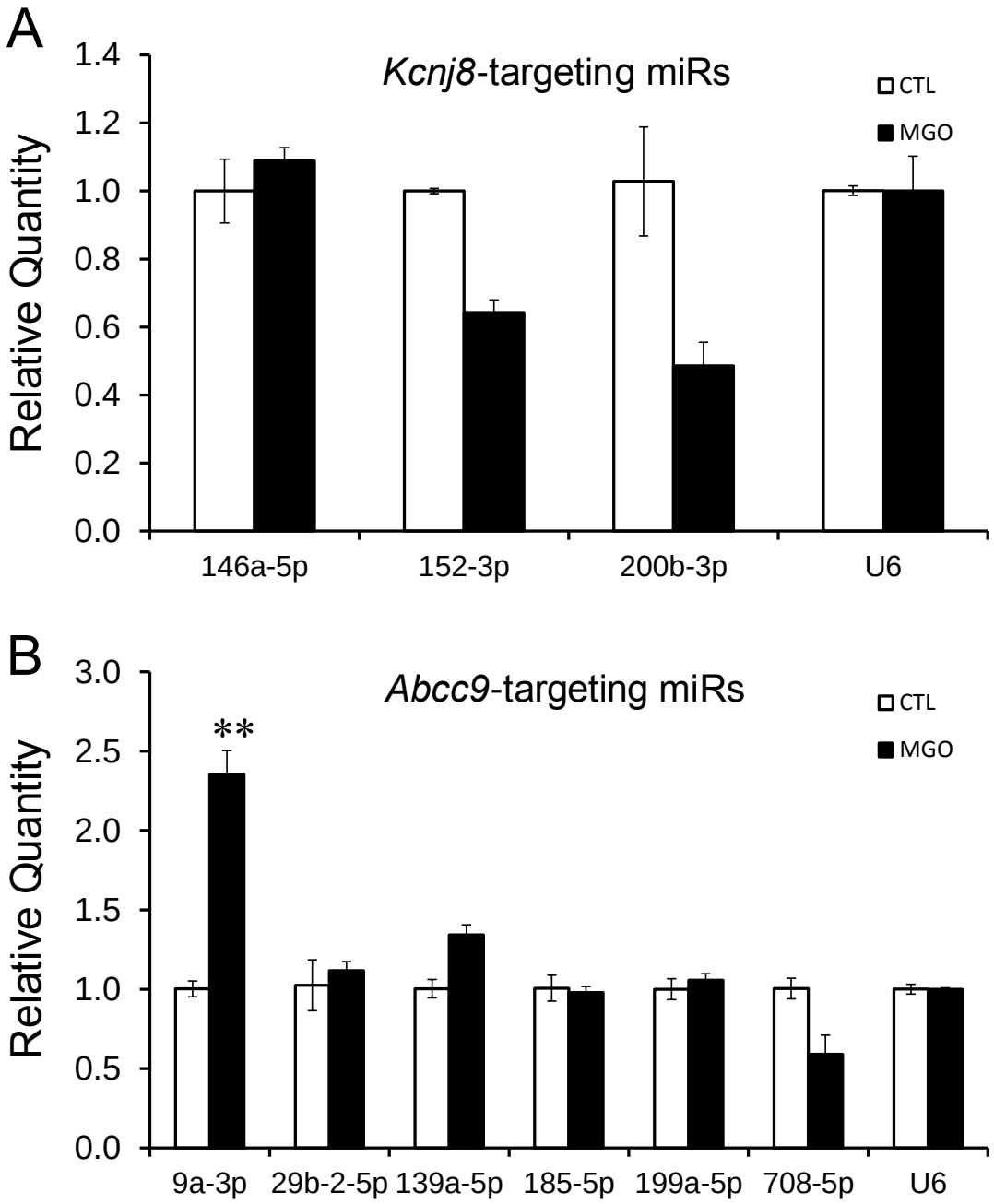

Figure 7.2 Profiling of MGO-regulated microRNAs (miRs) in A10 cells.

A10 cells were treated with 300 μM MGO for 6h. Real-time quantitative PCR (qPCR) analysis then was performed to show changes in expression levels of candidate miRs targeting on Kir6.1 (**A**) and SUR2B mRNA (**B**). U6 was used for normalization. **, P <0.01 (n = 3 separated experiments with 3-6 samples each). 9a-3p, miR-9a-3p; 29b-2-5p, miR-29b-2-5p; 139a-5p, miR-139a-5p; 146a-5p, miR-146a-5p; 152-3p, miR-152-3p; 185-5p, miR-185-5p; 199a-5p, miR-199a-5p; 200b-3p, miR-200b-3p; 708-5p, miR-708-5p; U6, RNU6.

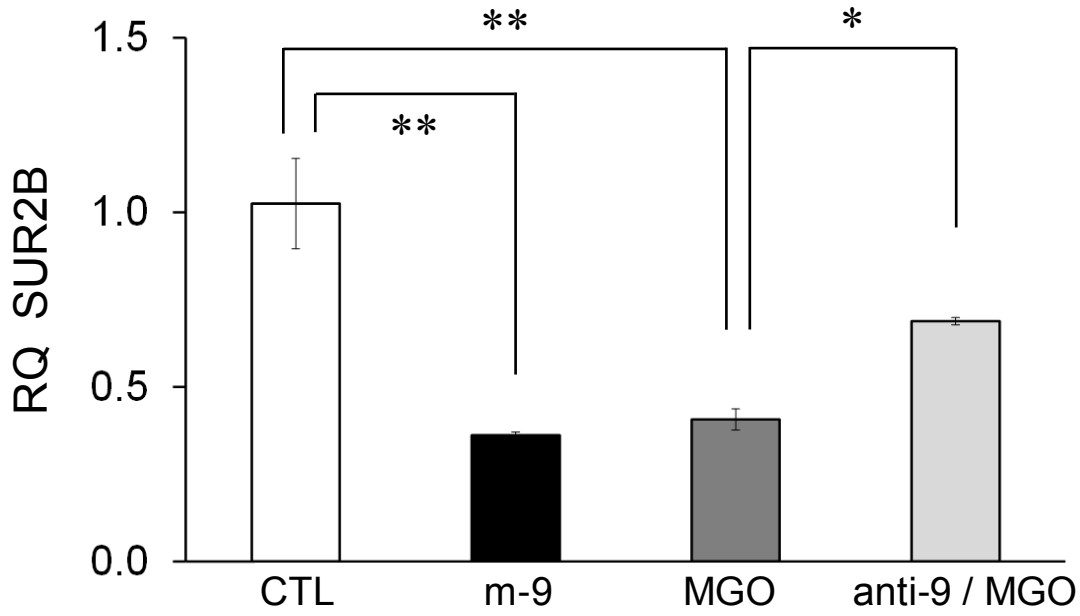

Figure 7.3 Inhibitions of SUR2B mRNA expressions by MGO and exogenous miR-9a-3p. After transfection with m-9, A10 cells were cultured for 12-24h. Cells transfected with anti-9 were also treated with 300 μM MGO and cultured under the same condition. A marked reduction in the relative quantity (RQ) of SUR2B mRNA was found in cells transfected with m-9, to the similar degree as the effect of 300 μM MGO treatment. The effect of MGO was significantly reduced in cells transfected with anti-9. Cells transfected with scrambled RNA (scmiR) were used as control. GAPDH was used for internal normalization. *, $P < 0.05$; **, $P < 0.01$ ($n = 4$).

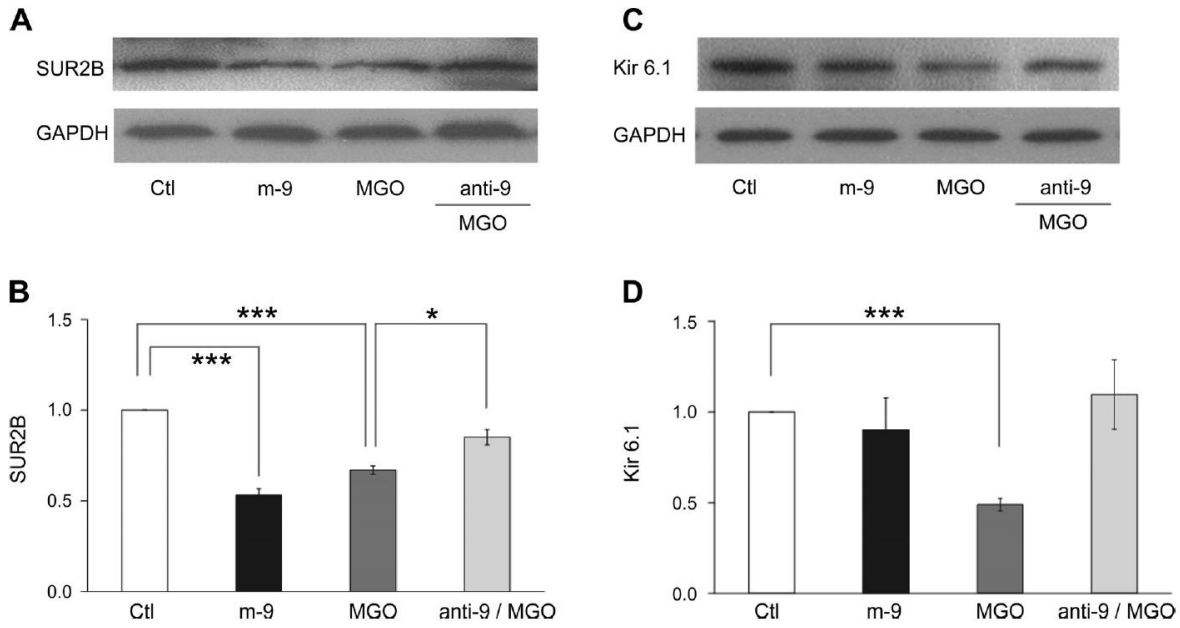

Figure 7.4: Effects of miR-9a-3p on MGO-induced inhibition of SUR2B/Kir6.1 expression at the protein level.

After transfection with m-9, A10 cells were cultured for 12–24 h. Cells transfected with anti-9 were also treated with 300 μM MGO and cultured under the same conditions. Cells transfected with scmiR were used as negative control, and GAPDH was used for normalization. **(A, C)** Western blot assay of expression of protein levels of SUR2B **(A)** and Kir6.1 **(C)**. **(B, D)** bar graphs represent the photodensity of each protein. *, $P < 0.05$; ***, $P < 0.001$ (n = 3–4).

A

```
Human Abcc9 CDS(2720-2744)  5′ AACCAAAGATGTTGAGCTTTATGAA
                                    .........
Mouse Abcc9 CDS(608-632)    5′ CCTAAATTACTTTTAGCTTTATTCC
                                    .........
Rat Abcc9 CDS(661-685)      5′ CCTAAATTACTTTTAGCTTTATTCC
                                    |||||||||
Rat miR-9                   3′ UGAAAGCCAAUAGAUCGAAAUA
```

B

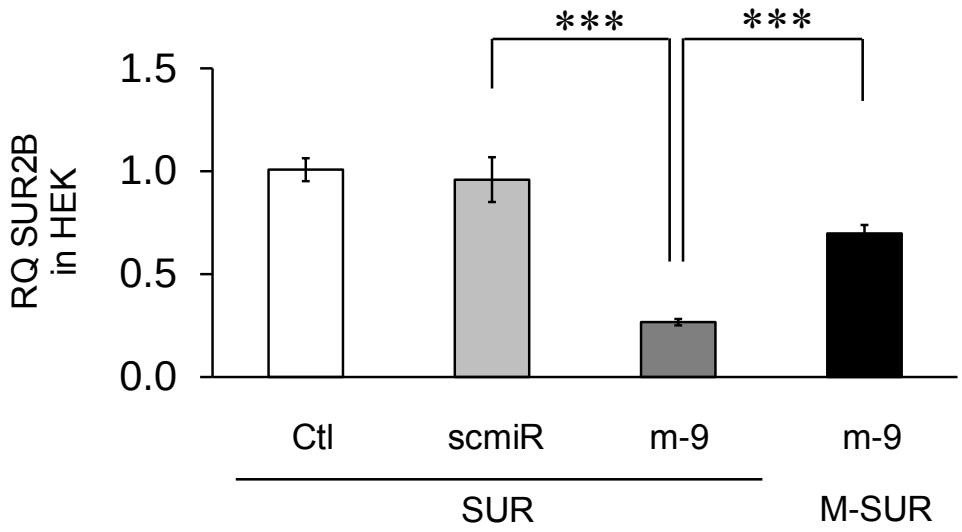

Figure 7.5 Targeting sites in SUR2B mRNAs by miR-9a-3p.

(A) Seed matches region of miR-9a-3p to the SUR2B mRNA. The seed regions were numbered in positions of SUR2B mRNA. The conserved seed matches in different species were represented with dots. **(B)** qPCR assay for SUR2B mRNA reduction by CDS targeting. Cotransfection of HEK293 cells with m-9 and the SUR2B mRNA construct (SUR) led to significant inhibition of SUR2B expression level. Such inhibition was abrogated when cells were cotransfected with m-9 and M-SUR (2 site mutations in SUR2B mRNA). ***, $P < 0.001$ ($n = 3$).

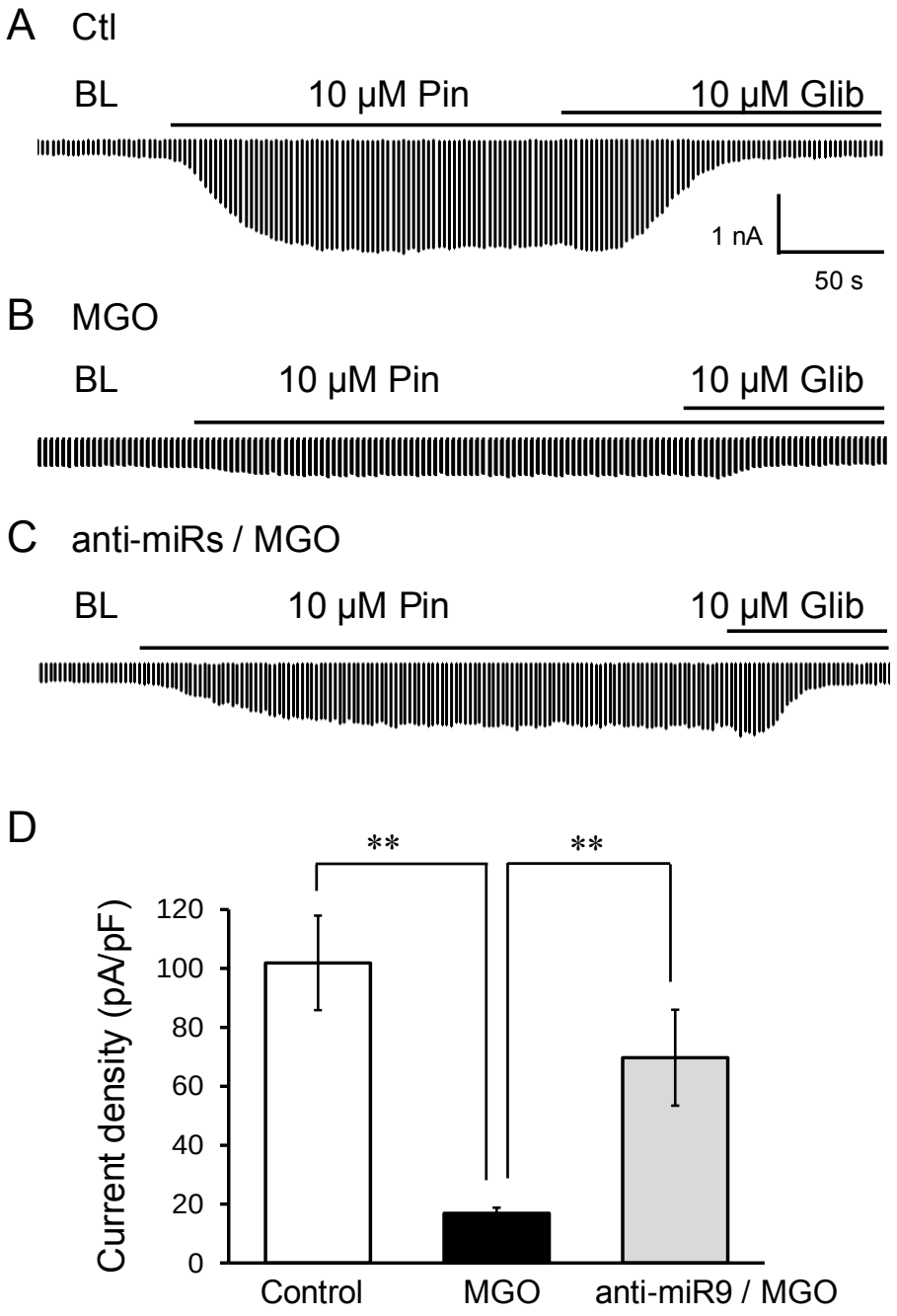

Figure 7.6 Effects of MGO and miR-9a-3p on functional K_{ATP} currents.

One day after Kir6.1/SUR2B channels were expressed in HEK293 cells, the cells transfected with anti-9 were treated with 300 μM MGO and cultured for 12-24h. Cells transfected with scmiR was used as negative control. **(A)** K_{ATP} currents were recorded using symmetric K^+ concentration of internal and bath solutions. Inward K^+ currents were elicited with voltage commands from 0 to -80 mV every 3 s. The K_{ATP} currents were strongly activated by 10 μM pinacidil (Pin) and were inhibited by 10 μM glibenclamide (Glib). **(B)** MGO treatment significantly suppressed K_{ATP} current in HEK cellS. **(C)** MGO-induced reduction of K_{ATP}

currents was reversed in anti-9-transfected cells. **(D)** Current density was represented as the bar graph. **, P <0.01 (n = 8-10 cells).

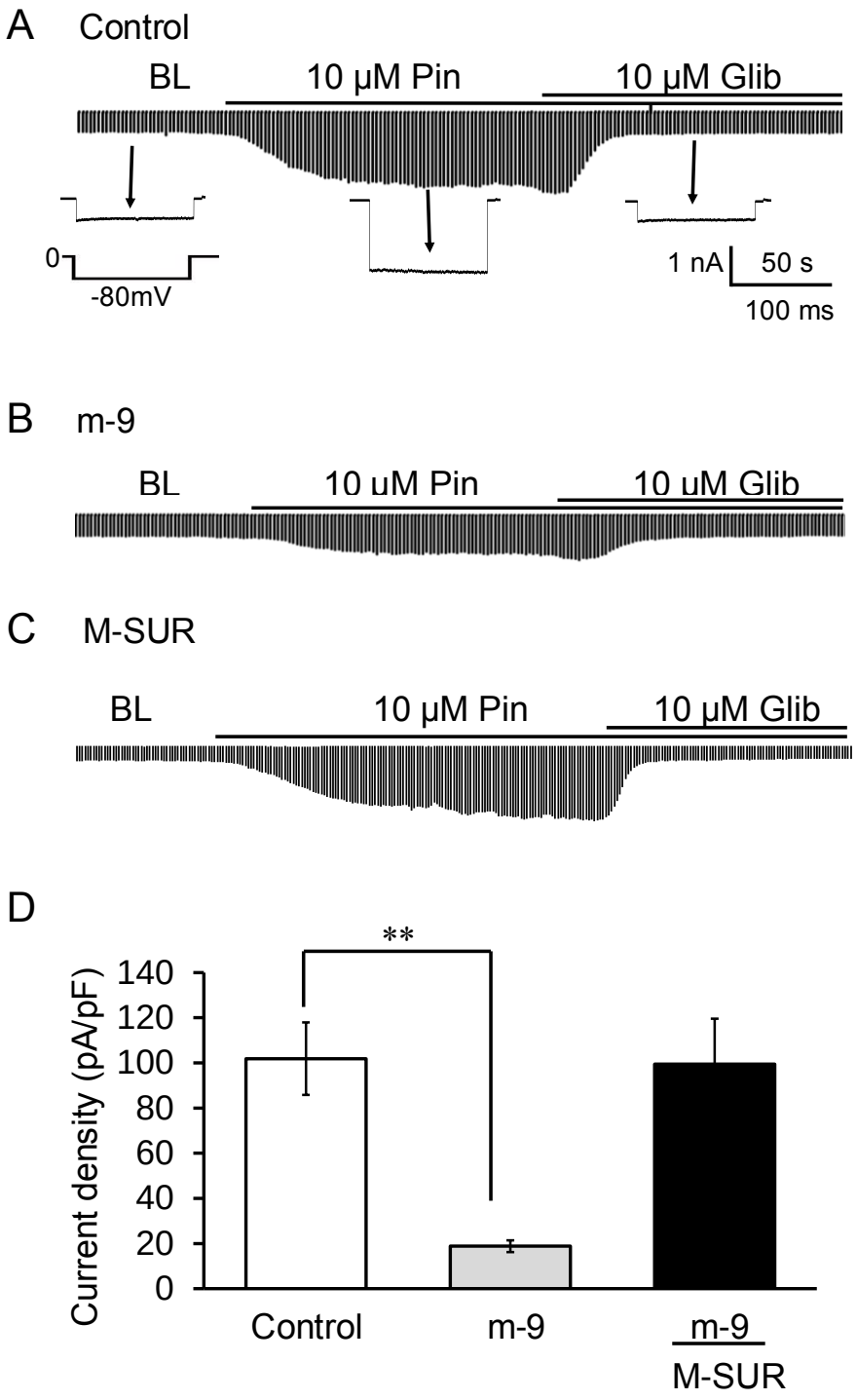

Figure 7.7 Inhibitions of K_{ATP} currents by miR-9a-3p.
Experiments were done as described in Fig. 7.6. Cells transfected with scmiR was used as negative control. **(A)** K_{ATP} Currents were recorded from the negative control (Ctl). **(B)** Pin-induced currents became much smaller in m-9 transfected cells. **(C)** The m-9 induced current inhibitions were abrogated when their targeting sites in SUR2B subunit was mutated. **(D)** Effect of miR-9a-3p on the current density was represented in the bar graph. **, P <0.01 (n = 8 to 10 cells).

8 RESULT 4: OPTOGENETIC APPROACH FOR FUNCTIONAL ASSAYS OF THE CARDIOVASCULAR SYSTEM BY LIGHT ACTIVATION OF THE VASCULAR SMOOTH MUSCLE

Published as "**Yang Wu**, Shan-Shan Li, Xin Jin, Ningren Cui, Shuang Zhang and Chun Jiang. Optogenetic approach for functional assays of the cardiovascular system by light activation of the vascular smooth muscle. ***Vascul Pharmacol***. 2015 Aug;71:192-200."

8.1 Acknowledgements

This work was supported by National Institutes of Health [grant number R01-NS-073875].

8.2 Abstract

Cardiovascular diseases are the major challenge to modern medicine. Intervention to cardiovascular cells is crucial for treatment of the diseases. Here we report a novel intervention to VSMCs by optogenetics. Channelrhodopsin in a tandem with YFP was selectively expressed in smooth muscle of transgenic mice in which YFP fluorescence was found in arterial walls of various tissues. In dissociated VSM cells from the mice blue light evoked inward currents, leading to depolarization and contraction. In isolated mesenteric arterial rings, optostimulation produced vasoconstriction that was reproducible, sustained, light intensity-dependent and comparable to popular vasoconstrictors. Blue light raised robustly coronary resistance without significant effects on heart rate and pulse pressure. Optostimulation produced renal vasoconstriction as well. The optical vasoconstriction had temporal resolutions less than 40s in these organs. These results indicate that optical vasoconstriction can be effectively produced in various organs with channelrhodopsin expression in VSM cells.

8.3 Introduction

Cardiovascular diseases are the leading causes of deaths worldwide. According to the National Vital Statistics Reports by the Center for Disease Control in 2010, 29.4% of total causes of death in the USA involve the cardiovascular and cerebrovascular systems. One limitation for therapeutic intervention is the accessibility to the cardiovascular system, especially to the vasculature. At present, treatments of the cardiovascular diseases heavily rely on pharmacological agents. Thus, more accessibility to the cardiovascular system is needed for development of effective therapies, especially those with better temporal and spatial resolutions.

Recent development in optogenetics suggests a new way to access the cardiovascular system. The optogenetics is a research approach based on transgenic expression of photosensitive opsins to one group or a few groups of cells, and then these cells are available for optical activation and inhibition [190,286]. Such an optical control of cellular activity has been demonstrated to be highly effective in the manipulation of excitability of individual neurons and recruitment of cells in selective neuronal networks [287-292]. Indeed, the optogenetics has been rapidly applied to studies of a number of types of neurons and glial cells [190,286-294]. However, research in the cardiovascular field has barely taken the advantage of the newly developed cell-selective optical intervention. To our knowledge, there is no report on the application of optogenetics to the blood vessels, although optogenetic control of myocardium has been recently demonstrated [193,195,295].

Therefore, we generated a novel mouse strain with expression of a variant of channelrhodopsin2 (ChR2 H134R) in VSMCs. Using tissues from the mice, we tested the expression, membrane excitability, contraction of VSM cells, and vascular tone regulation in several organs. Our results indicate that optical activation of VSM cells can produce potent

vasoconstriction that is fast, reproducible, light intensity-dependent and comparable in strength to popular vasoconstrictors.

8.4 Results

8.4.1 VSM expression of ChR2

We developed a new strain of transgenic mice, in which ChR2 was selectively expressed in smooth muscle cells. Genotyping shows that the offspring of ChR-loxP and Tagln-cre mice are supposed to express ChR2 with the present of Cre recombinase under the control of Tagln promoter (Fig. 8.1).In various tissues, we have systematically examined the expression of YFP engineered in frame with ChR2. All arteries in the heart, skeletal muscle, kidney and intestine showed YFP fluorescence in the Tagln-ChR mice but none in the control mice (Fig. 8.2). Similar expression of YFP was found in dissociated individual VSM cells from Tagln-ChR mice (Fig. 8.4A). In the Tagln-ChR mice YFP fluorescence was also observed in smooth muscle in the intestine and uterus (Fig. 8.2K-R).

8.4.2 Optical activation of acutely dissociated VSM cells

Whole-cell currents were studied in VSM cells acutely dissociated from aorta. In voltage clamp, the aortic VSM cells exhibited typical voltage-dependent outward currents with the membrane potential held at -50 mV and stepped from -100 to 40 mV (Fig. 8.3A). Under this condition, exposure of the VSM cells obtained from Tagln-ChR mice to 10 ms pulses of blue light (470 nm) evoked large inward currents (Fig. 8.3B). The photo currents had a fast onset (0.7 ± 0.04 ms by 10%-90% peak, n = 6 cells) and slow decay with the time constant (30.8 ± 1.7 ms by 90%-10% peak, n = 6 cells). The slow decay was apparently produced by passive membrane properties, as the photo currents showed very little inactivation. With prolonged optical stimulations in 200 ms and 300 ms, blue light evoked persistent inward photo currents showing

very little adaptation or inactivation over the time periods (Fig. 8.3C). In the current-voltage (I-V) relationship, the photo currents had the reversal potential ~0 mV with moderate inward rectification (Fig. 8.3D). In current-clamp, 300 ms blue light stimulation produced depolarization reliably (Fig. 3E), which significantly changed the membrane potentials of VSM cells from -45.4 ± 1.5 mV to -35.1 ± 2.1 mV (n = 5 cells, $P<0.01$) (Fig. 8.3F).

8.4.3 Blue light evoked VSM cell contraction

The light-evoked depolarization was expected to affect the contractility of VSM cells. Therefore, we measured the length of isolated VSM cells with and without 470nm light exposure. In Tagln-ChR mice, 10 s blue light exposure shortened individual aortic VSM cells. Typical VSM contraction was the shortening in the longitudinal axis of the VSM cells. The contraction was quantified by measurement of the size in the longitudinal axis of VSM cells. The blue light produced significant shortening in the VSM cells from the Tagln-ChR mice ($P<0.01$, n = 8) (Fig. 8.4A, B), which could have been even greater if there had been a way to add a preload to the cells. No change in cell shape from WT mice was observed (Fig. 8.4C). Cell length was recovered to about original level within 2 min ($P<0.01$, n = 8). The contractility was tested by additional 20 mM KCl with further length shrinkage observed (Fig. 8.4B, C).

8.4.4 Optostimulation initiated contractions of isolated and perfused mesenteric arteries

The light-evoked VSM contraction should have impact on vascular tones. To demonstrate this, we studied vascular constriction in isolated and perfused mesenteric arterial rings from control and Tagln-ChR mice. Vasoconstriction was observed with the blue light exposure (Fig. 8.5A). Using high intensity and long-lasting (up to 1 hr) optical stimulation, we studied the kinetics of vasoconstriction. The vasoconstriction started fast with a 100 ms latency, reached the peak level within 10 s, and was maintained at the level throughout the photo stimulation period

with only a slight decline in the contractile force (Fig. 8.5A, F). Clear vasoconstriction occurred with the light intensity ~10 mW/mm2, and stronger photo stimulations produced stronger vasoconstrictions (Fig. 8.5B). The contractile force generated by blue light (~24 mW/mm2) was comparable to that produced by 1 μM phenylephrine [296], a selective α-adrenergic receptor agonist, and even larger than that produced by 60 mM KCl (Fig. 8.5C, E). To test the contraction reversibility, we repetitively stimulated the rings by 1 min light followed by 2 min time interval. As shown in the figure (Fig. 8.5C), the repetitive optical stimulations triggered repetitive vasoconstrictions with modest augmentation in the contractile force to subsequent stimulations. After each photo constriction, baseline contractile force was slightly elevated, which dropped to original level in 1-2 min (Fig. 8.5C). In contrast, the rings from control (Tagln-cre) mice showed no response to any optostimulation (Fig. 8.5D). Contractile force which was produced by 1 μM PE (0.26 ± 0.03 g, n = 7), 60 mM KCl (0.19 ± 0.04 g, n = 7) and light (0.23 ± 0.02 g, n = 7) were compared (Fig. 8.5E). No significant differences were found among these groups. The vasoconstriction force at the peak level of light exposure (0.24 ± 0.03 g, n = 7) was not significantly different from the force in the plateau (0.23 ± 0.02 g, n = 7) (Fig. 8.5F). The optostimulation had no significant residual effect on subsequent PE- and KCl- induced vasoconstrictions (Fig. 8.5G). Long-lasting optostimulation (1 hr) produced sustained vasoconstriction without any relaxation (Fig. 8.5H). Indeed, the contractile force increased by 24.7 ± 17 % (n = 4) at the end of the 1 hr simulation (Fig. 8.5I). The sustained vasoconstriction was reversible, and vascular tension returned the baseline level within 10 min after light was turned off (Fig. 8.5H).

8.4.5 Manipulation of coronary arterial tones with optical stimulation

To further test the effects of light-controlled vascular tones on tissue perfusion at the organ-typical level, we studied coronary vascular responses using the Langendorff heart preparation [297]. The heart was prepared to enable the coronary circulation at a constant perfusion volume. The basal perfusion volume was firstly determined at the arterial pressure 80 cm H_2O. Then the perfusion volume was maintained constantly at this level, and the pressure of the coronary arteries was measured with a force-electricity transducer. The viability of the preparation was verified in each heart by the stable heart rate >200 bpm (beat/min) and the vasodilation response to isoproterenol, a β-adrenergic receptor agonist [297-299].

The heart rate averaged 300 bpm at about 35°C, consistent with previous observations in isolated heart preparations [187,300]. In the Tagln-ChR heart, optostimulation produced a marked increase in coronary resistance which stands for the coronary resistance with the constant pump output (Fig. 8.6A), which was not seen in the control heart (Fig. 8.6B). In both hearts, PE (10 μM) gave rise to a small increase of coronary resistance (Fig. 8.6A, B). The exposure to 10 μM isoproterenol brought about a clear vasodilation of coronary arteries with increases in the heart rate and the pulse pressure (Fig. 8.6A, B). Optostimulation (3 min) did not have any evident effects on the heart rate and pulse pressure in both groups of hearts (Fig. 8.6A, B). In comparison, the light exposure raised the coronary pressure by 20.1 ± 1.6 cm H_2O with ~20 mW/mm2 intensity (n = 11 hearts), while 10 μM PE increased the pressure by 15.1 ± 3.1 cm H2O (n = 11) (Fig. 8.6C).

The temporal resolution was studied by measuring the onset and offset times for the coronary vasoconstriction (Fig. 8.6D). The onset latency was 1.1 ± 0.2 s (n = 7), and the time to 90% peak vasoconstriction was 29.5 ± 8.4 s (n = 6). The offset latency was 1.1 ± 0.3 s (n = 7),

and the time of withdrawal to 10% peak vasoconstriction was even shorter as 15.0 ± 3.1 s (n = 7). These indicate that the optical vasoconstriction has a high temporal resolution in isolated hearts.

With a prolonged period (30 min) optostimulation, the increase in coronary resistance was well maintained showing only modest or no relaxation (Fig. 8.6E, F). However, such a long-lasting optostimulation had an effect on the heart rate. Arrhysmia occurred after 10 min, and became very severe at 20 min (Fig. 8.6G), suggesting that coronary perfussin is indeed restrained.

8.4.6 Light stimulation increased vessel resistance in perfused kidneys

In isolated and perfused kidneys from Tagln-ChR and Tagln-cre mice, renal vascular tension was measured with a constant perfusion flow that produced the renal pressure 100 cm H2O at baseline. The viability of kidney was tested by 10 μM PE and 10 μM isoproterenol. In the Tagln-ChR kidney, optostimulation with ~20 mW/mm2 intensity raised the renal pressure by 20-30 cm H_2O (Fig. 8.7A). Such a light response was not seen in control kidney (Fig. 8.7B), although its PE response was the same to the Tagln-ChR kidney. Vasodilation effects of 10 μM isoproterenol were relatively small in both groups of kidneys, likely due to the lack of expression of β2 adrenoceptors [301]. In comparison, the Tagln-ChR kidney responded to light with an increase of renal pressure by 27.2 ± 2.5 cm H_2O (n = 7), while the pressure reached 126.9 ± 12.0 cm H_2O with 10 μM PE exposure (Fig. 8.6C). The temporal resolution was 38.3 ± 8.7 s (n = 6) for the onset time of 90% peak vasoconstriction, and 30.4 ± 4.43 s (n = 6) for the time to return to baseline (10% peak vasoconstriction) (Fig. 8.7D).

The renal vasoconstriction was well maintained with prolonged optostimulation (up to 30 min). After the peak pressure increase was reached at about 4 min, renal vascular pressure

dropped modestly at 30 min followed by a full recovery (Fig. 8.7E). On average the renal resistance did not significantly decline by the end of 30 min of opteostimulation (Fig. 8.7F).

8.5 Discussion

This is the first demonstration of optical vasoconstriction using an optogenetic approach. By taking the advantage of Cre-Lox mice, we have generated a new strain of transgenic mice that express ChR in VSMs. This allows us to stimulate the VSM cells and produce optical vasoconstriction. The optical vasoconstriction is robust, reproducible, light intensity-dependent, and superb in temporal resolution, which we have observed in various tissues.

8.5.1 Successful generation of VSM optogenetic mice

The *Tagln* gene encodes the protein transgelin, an actin cross-linking protein found in smooth muscle cells. Tagln mRNA is detected in the aorta, uterus, intestine and lung at high levels, especially in the SMC lines [302,303]. The promoter *Tagln* has been well characterized, and used previously to deliver genes in the tissue-specific manner [304-306]. By cross-breeding mice with *Cre* driven by the *Tagln* promoter with LoxP-ChR2 mice, we have developed a new mouse strain, in which ChR is expressed in VSM cells. This is supported by our morphological studies of YFP fluorescence in various tissues. Strong YFP fluorescence is found only in vessel walls, although several tissues in both control and Tagln-ChR mice have weak background fluorescence that can be easily distinguished by the fluorescence intensity. Weak YFP fluorescence has been observed in veins of Tagln-ChR mice, especially large veins that have a thin layer of smooth muscle as well. In addition to VSM, we also examined YFP fluorescence in the skeletal muscle, heart, kidney, intestine and uterus. YFP fluorescence is negative in skeletal muscle, adipocyte, heart, and kidney, and is weak in intestine and uterus. In kidney tissues where

pericytes and intraglomerular mesangial cells are located, we did not find any YFP fluorescence, suggesting that ChR may not be expressed in these cells.

8.5.2 Characteristics of the optical activation of VSM cells

Photo currents have been recorded in VSM cells dissociated from aorta of Tagln-ChR mice in voltage clamp. These are inward currents seen more clearly at hyperpolarized membrane potentials. Their reversal potential is close to 0 mV, indicating that the currents are carried by cations non-selectively. These currents show very little adaptation/inactivation with a prolonged light exposure, and show moderate inward rectification in the I-V relationship, which are consistent with our results of optical vasoconstriction showing little/no adaption as well. In current clamp, optical activation of these currents produces depolarization known to be necessary for VSM contraction. The VSM cells in our study seem to have a high level of ChR2 expression although the critical expression intensity for activation individual VSM cell is unknown. All these indicate that ChR has been successfully expressed in VSM cells of the Tagln-ChR mice [306,307].

8.5.3 Effective vasoconstriction by optical stimulation

We have studied the effects of optostimulation on vascular tones in several tissues. In isolated VSM cells from the aorta, shortening in cell length is seen. We believe that the optical activation effect is under-presented in the dissociated cell preparation. The VSM cell contraction could be greater if there were a preload added to the cells. It is known that the preload can drastically enhance muscle contraction according the muscle length-tension relationship.

Indeed, the optical vasoconstriction is found quite robust in the isolated and perfused mesenteric rings. The force produced by the optical vasoconstriction is comparable to 1 μM PE or 60 mM KCl, both of which are known to contract VSMs in mesenteric rings potently. The

optical vasoconstriction is reproducible, which is seen with repetitive optical stimulation, and shows no decline in the contractile force. The optical vasoconstriction is light intensity-dependent, which is seen with blue light as low as ~10 mW/mm^2.

We have observed optical vasoconstriction in isolated and perfused heart and kidney. Light penetration is limited in these organs, allowing the blood vessels on and close to the surface to be stimulated. Even with the poor transparence, optostimulation produces strong vasoconstriction. In the coronary circulation, the optical vasoconstriction is more potent than the vasoconstrictions produced by 10 μM PE. In addition to the robustness, optical vasoconstriction has an extraordinarily high temporal resolution in isolated organs. The onset and offset times (measured as the 10-90% peak value) are within 40 s, which cannot be achieved by any non-invasive approaches at present. The optical vasoconstriction is weaker in the renal circulation, which is likely to be due to anatomical nature of the kidney. Unlike the heart, the kidney is not a hollow organ in which substantial blood vessels may be not accessible to surface light. In perfused heart, light source was positioned on the surface of the heart, adjacent to aortic root from which left and right coronary arteries branch off. About 30% of the superficial vessels of the heart can be directly illuminated (single beam, 3mm diameter light guide). In contrast, the coverage area of the light accounts for up to 35% of the entire kidney surface. Attenuation coefficients of solid portion of heart and kidney at 470 nm are similar [308]. Therefore hollow chamber of the heart helps the heart to gain better light transmittance. In addition, a change in the tissue thickness from 1.0 to 1.1 mm leads to a 10% decrease of light intensity. Thus, only a small proportion of blood vessels near to the surface are activated by optical stimulation. As a result, optostimulation may not lead to strong vasoconstriction.

No evident injury or side effect was seen in the vasculature even after repetitive and long-lasting optostimulation (1 hr in rings and 30 min in perfused organs). This is consistent with the fact that VSM cells unlike neurons can survive relatively hight Ca^{2+} load to maintain persistent contractile forces [309].

8.5.4 Potential usage in biomedical research

The preparation of optical vasoconstriction has several potentials for research applications. Firstly, owing to the nature of optical stimulation, blood vessels in a well-defined region can be activated, an approach that is not currently available with systemic administration of vasoconstrictors. Such an approach can be useful for the understanding of cortical functions of the brain. The spatial accuracy of optical vasoconstriction could be used to reveal the mechanism of neuron-astrocyte-vascular coupling in certain brain areas, such nucleus regulating breathing [293,310]. Secondly, the temporal resolution and robustness of optical vasoconstriction may allow a better control of vascular tension where timing is critical. The approach may be useful for the study of microcirculation when precision controls of the arteriole tone are needed. In the presence of a basal level of vasodilator, optical vasoconstriction may allow a fast manipulation of the arteriole tone to desired levels. Thirdly, the optical vasoconstriction can be used to set a basal vascular tone for further vasodilation by potential therapeutic agents. The optogenetic approach does not involve vasoconstrictors, many of which may interfere with the vasodilators to be studied. Finally, the optical vasoconstriction may be useful to manipulate the metabolic rate temporospatially by reducing O_2 and nutrient supplies to certain tissue. This even allow clinical applications when rhodopsins can be delivered to a specific tissue. Our findings thus may open an avenue for future studies to achieve such a therapeutic objective.

In conclusion, this study shows a novel intervention to vascular tones by optical activation of VSM cells that express ChR. In dissociated VSM cells, blue light evokes large inward currents, leading to depolarization and contraction. In isolated mesenteric arterial rings, optostimulation produces vasoconstriction that is reproducible, sustained and light intensity-dependent. In isolated and perfused heart, blue light raises coronary resistance even more potently than that produced by 10 μM PE with fast onset and offset responses. These results indicate that the optogenetics can be effectively applied to the vasculature, and thus opens a brand new avenue for intervention to the cardiovascular system.

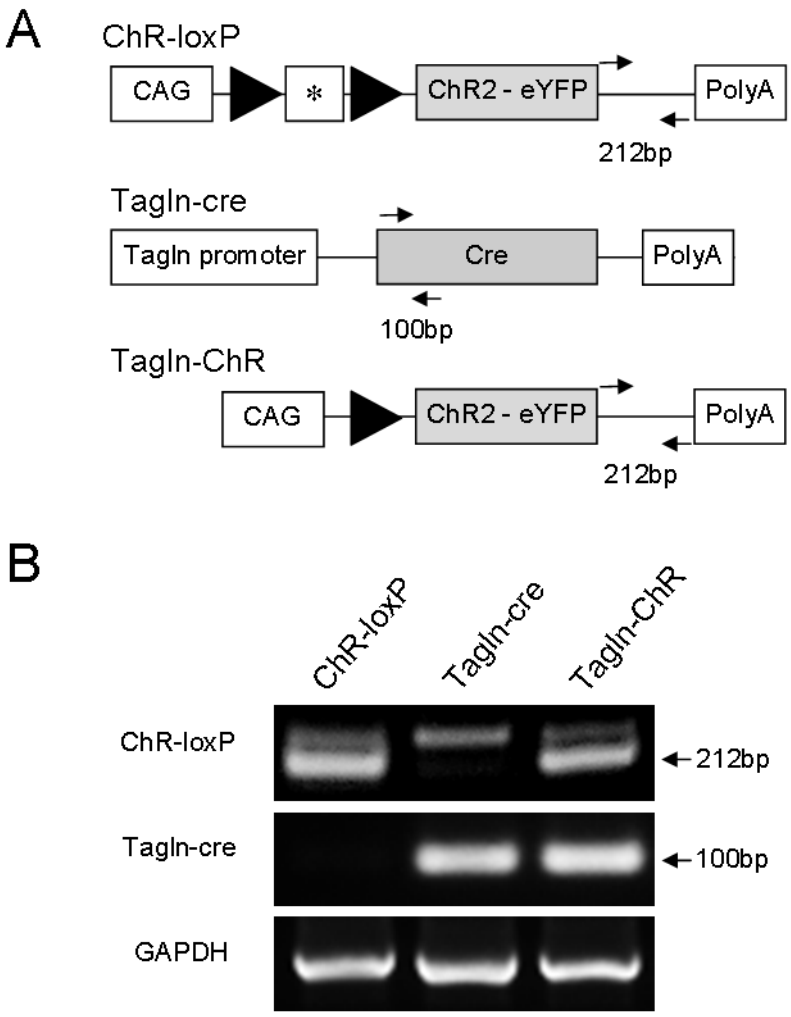

Figure 8.1 Design and genotyping of transgenic mice.
(A) Constructs of parental ChR-LoxP and Tagln-cre mice as well as the expected offspring that express both ChR-loxP and Tagln-cre by removal of the stop codon (asterisk) flanked by loxP (solid triangle). This led to expression of ChR2-eYFP in a tandem driven by the CAG promoter in Tagln-ChR mice. **(B)** Mice were genotyped with primers provided by Jackson Laboratory, which are targeted at the 3" UTR with a 212 bp expected product. The presence of the 212 bp band indicated ChR2-eYFP mRNA expression in ChR-loxP and Tagln-ChR mice. Note that a 300 bp non-specific band was found in all mice. Another pair of primers yielding a 100bp PCR product in the cre sequence, which was found in Tagln-cre and Tagln-ChR mice. Abbreviations: CAG, cytomegalovirus-immediate-early (CMV-IE) enhancer/chicken β-actin/rabbit β -globin hybrid promoter; PolyA, bovine growth hormone polyadenylation signal and flippase recognition target flanked phosphoglycerate kinase-Neo-polyA cassette; GAPDH, glyceraldehyde 3-phosphate dehydrogenase.

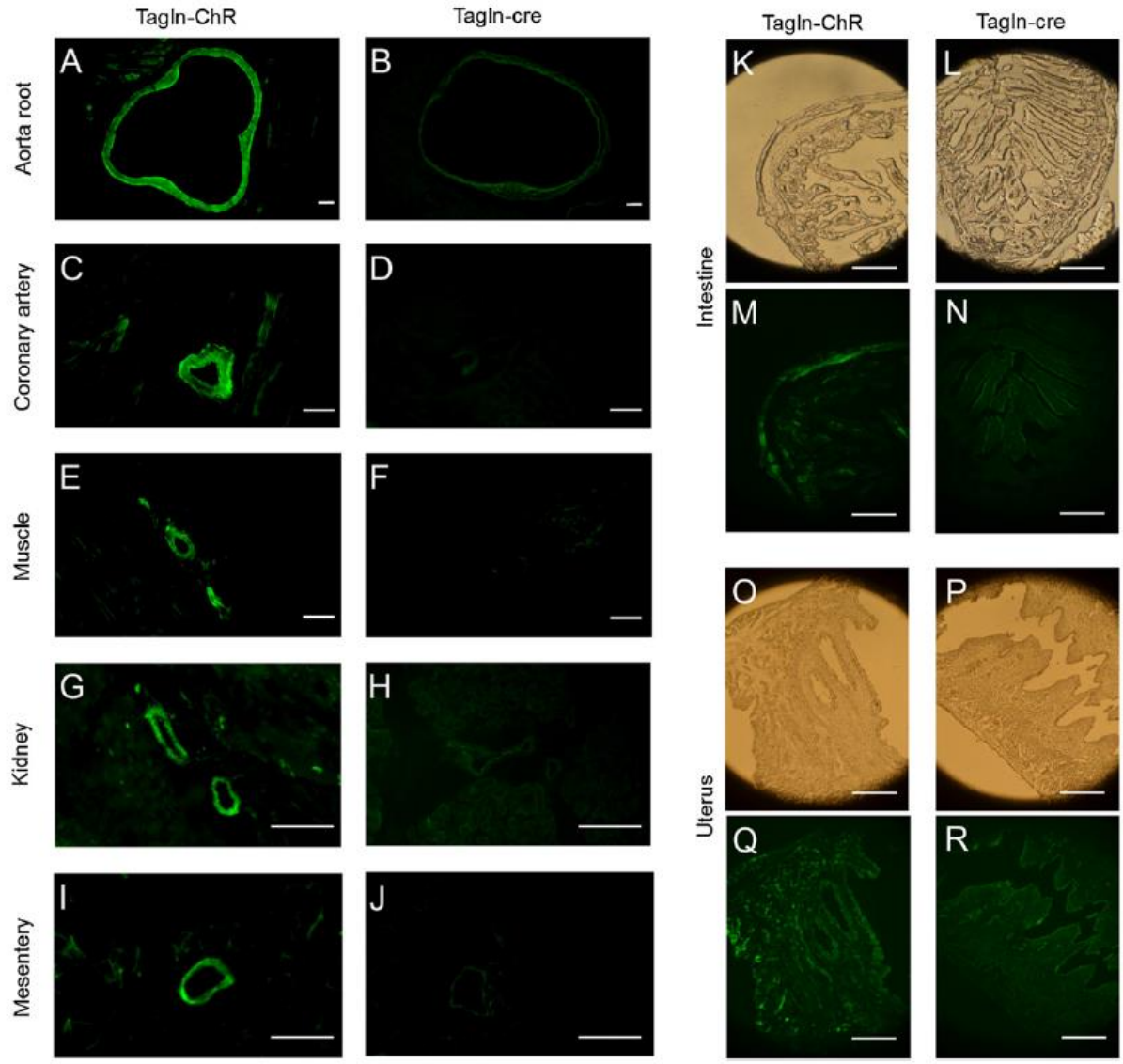

Figure 8.2 Comparison of YFP fluorescence in various tissues between Tagln-ChR and Tagln-cre mice.

In Tagln-ChR mice **(A, C, E, G, I)**, strong YFP fluorescence was found on arterial walls of the aorta, coronary arteries, skeletal muscle, kidney and gastrointestinal arteries, respectively. In Tagln-cre mice **(B, D, F, H, J)**, arteries in these tissues showed no or rather weak background fluorescence. YFP fluorescence was found in the muscularis externa of small intestine in Tagln-ChR mice **(K, M)** but not in Tagln-cre mice **(L, N)** (The lower panel was obtained in the same field of the upper one). Blood vessels in the mucosa were also fluorescent in the Tagln-ChR mice. Similar YFP fluorescence expression was seen in the uterus of the Tagln-ChR mice **(O, Q)** but not of the Tagln-cre mice **(P, R)**. Scale bars are 200 μm.

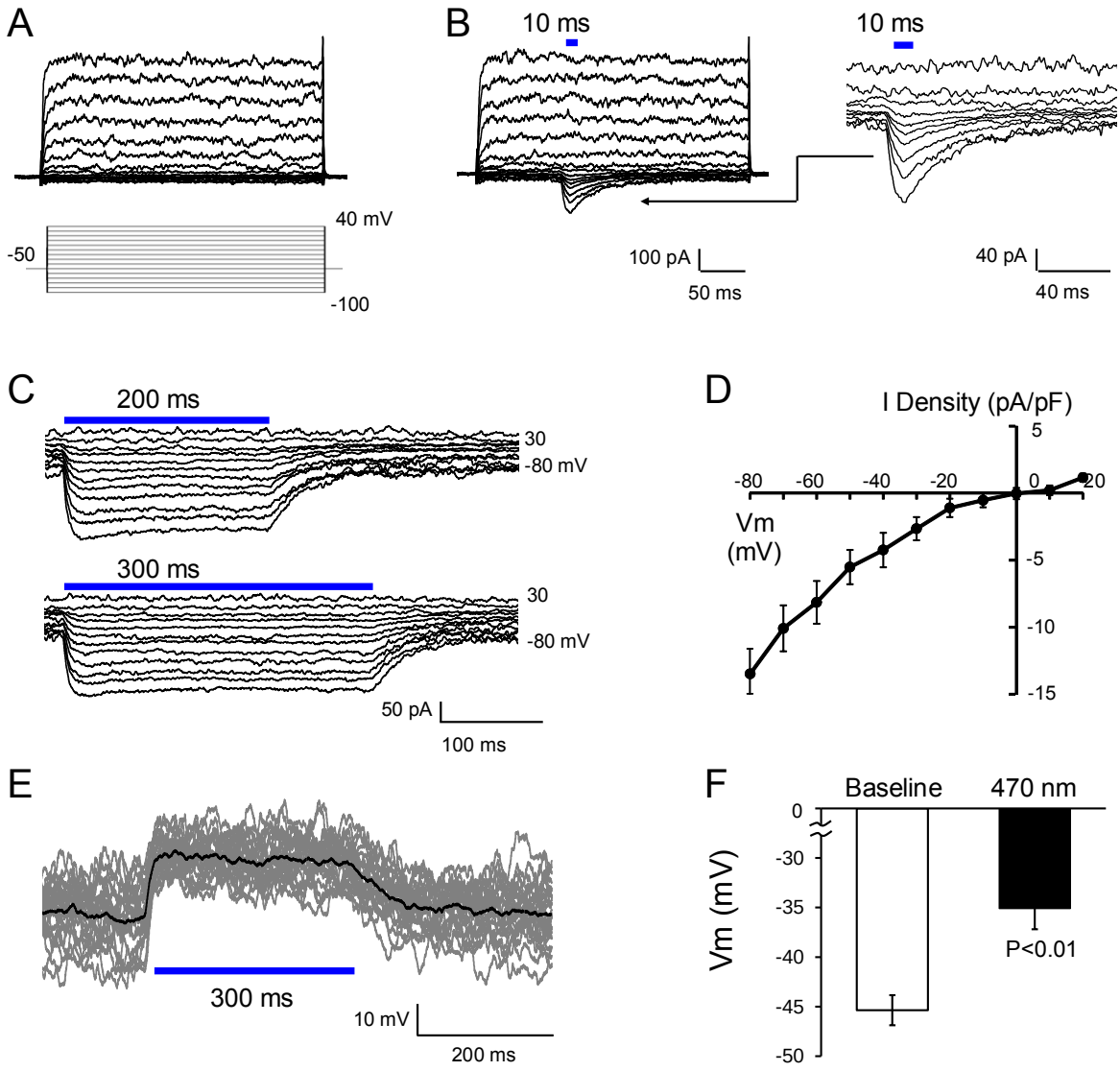

Figure 8.3 Optical excitation of dissociated VSM cells.
(A) Whole-cell currents were recorded from a VSM cell dissociated from aorta of a Tagln-ChR mouse in voltage clamp. Steps of voltage commands (from -100 to 40 mV with a 10 mV increment) were applied to the cell at a holding potential of -50 mV. **(B)** Stimulation of the VSM cell with 10 ms pulses of blue light (470 nm) (~24 mW/mm^2) evoked inward currents. The photo currents onset rapidly, and decayed slowly with the light on and off, which are better seen in the expanded display on the right panel. **(C)** Responses of another VSM cell to longer durations of blue light stimulations. The inward photo currents induced by 200 ms and 300 ms blue light showed only modest reduction in current amplitudes. **(D)** Current-voltage (I-V) relationship of the photo currents showed a reversal potential at 5 mV with moderate inward rectification. **(E)** In current clamp, blue light stimulation produced large depolarization in a VSM cell. **(F)** Comparison of membrane potentials before and during light exposure. Data are presented as means ± s.e. ($P<0.01$, Student's t-test; n = 5 cells).

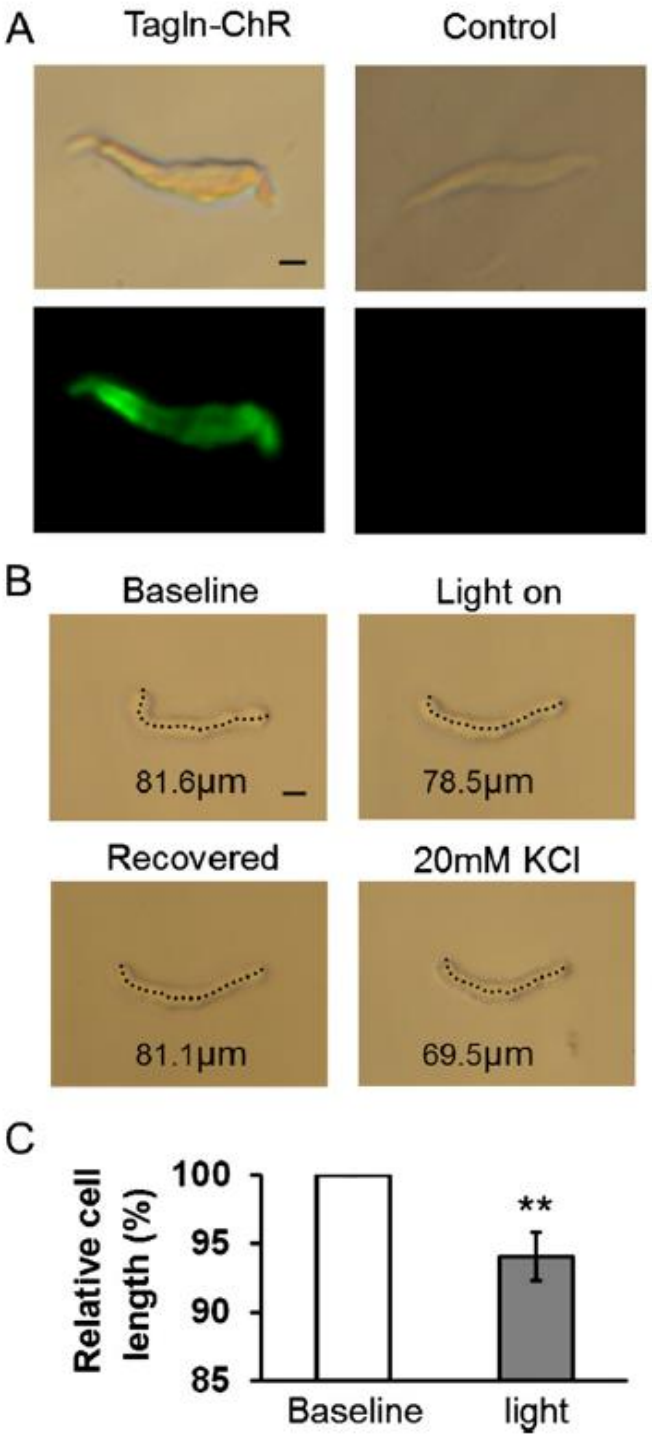

Figure 8.4 Contraction of the dissociated VSM cell by optostimulation.
(A) Fluorescence expression of dissociated individual VSM cells was compared between Tagln-ChR and control groups. **(B)** Longitudinal length of a VSM cell for a Tagln-ChR mouse was measured with and without light stimulation (~24 mW/mm^2). Complete recovery was seen 2 min after light stimulation. Final length was measured 5 min after addition of 20 mM KCl. **(C)** Statistically, the blue light produced significant shortening in the longitudinal length (**, $P<0.01$, $n = 8$). Scale bar in A is 10 µm.

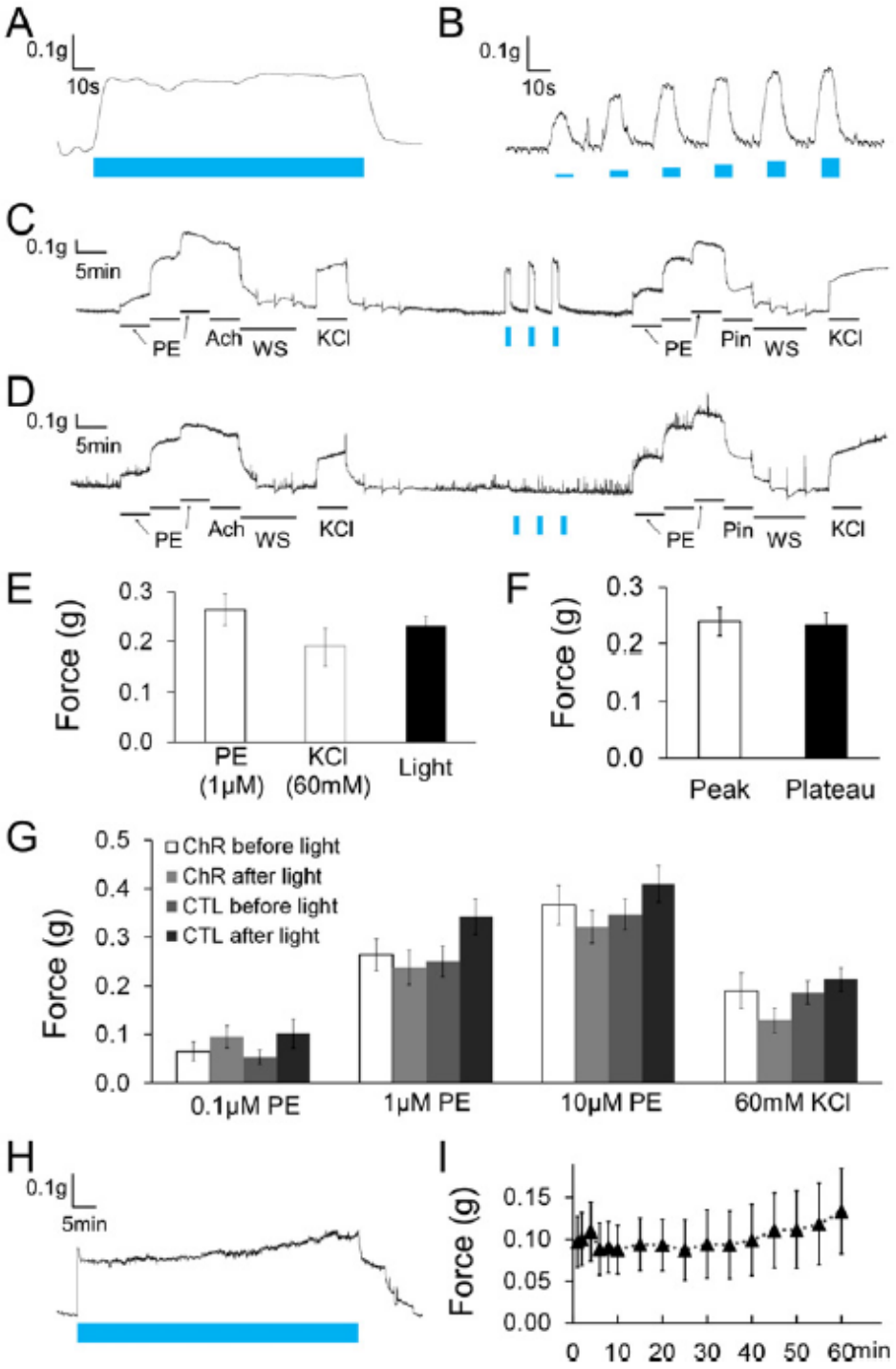

Figure 8.5 Characterization of optical vasoconstriction in isolated mesenteric arterial rings. (**A)** A mesenteric ring was obtained from a Tagln-ChR mouse and studied *in-vitro* with a 0.3 g preload. Exposure of the ring to blue light (~24 mW/mm^2) produced vasoconstriction that started fast when the light was on, was maintained roughly at the same level during the light exposure, and returned to the baseline level rapidly. **(B)** Graded increases in the light intensity led to graded increases in forces of vasoconstriction (from ~10 mW/mm^2 to ~24 mW/mm^2). **(C)** In another ring from a Tagln-ChR mouse, vasoconstriction was first produced with PE at 0.1, 1 and

10 μM, followed by the vasodilator acetylcholine (Ach, 1 μM) and washout (WS). The lack of Ach effect indicated that endothelium was denuded. Exposures to 60 mM KCl also produced vasoconstriction. Subsequently, the ring was exposed to three pulses of blue light, each of which led to vasoconstriction. The amplitude of the light-evoked vasoconstriction increased slightly in the 2^{nd} and 3^{rd} exposures. After 15 min rest, the PE and KCl vasoconstrictions were repeated, and the same results were shown. Pinacidil (10 μM), a vasodilator, relaxed rings. **(D)** The same experiments were done in another ring from control mice. The ring showed the same responses to all treatments except light. **(E)** Contractile force was produced by PE, KCl and light. No significant differences were found among these treatments. **(F)** The vasoconstriction force at the beginning of light exposure (peak) was not significantly different from the force in the later steady level. **(G)** Comparison of vasoconstrictions by PE and KCl. The vasoconstriction forces at all tested concentrations of PE and KCl showed no significant difference before and after light exposure. Constant optical stimulation was indicated as blue bars. **(H)** Long-term stimulation (~24 mW/mm^2, 1 hr) produced vasoconstriction that started fast when the light was on and did not decline during the light exposure. The vascular tension returned to the initial baseline level within 10 min after light off. **(I)** With the long-lasting optical stimulation, the stable contractile force lasted for 1 hr without decline (n = 4).

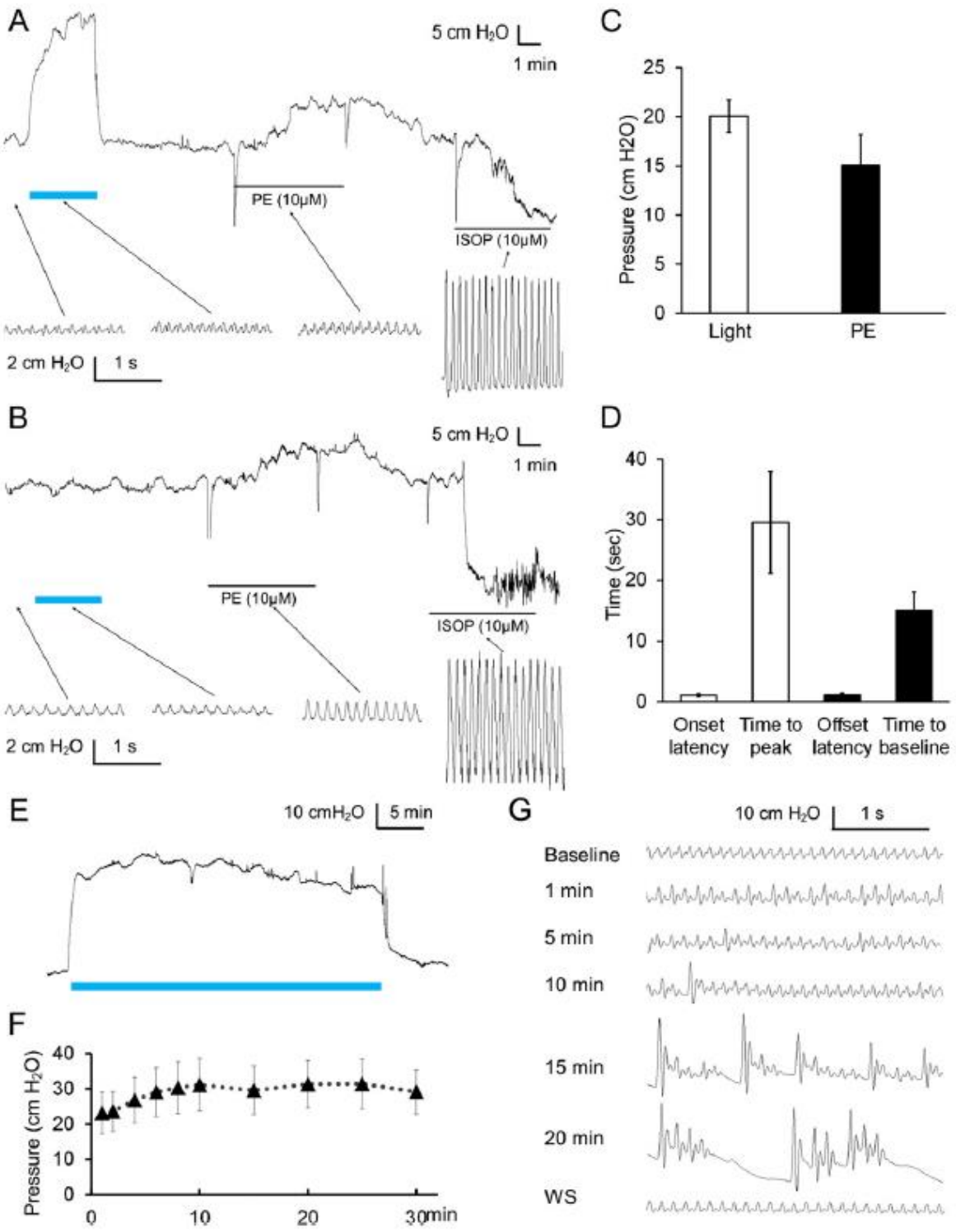

Figure 8.6 Constriction of coronary arteries by optical stimulation.
(A) In an isolated and perfused heart from a Tagln-ChR mouse, a marked increase in coronary perfusion resistance was produced by blue light followed by PE and isoproterenol (Isop) treatments. Note that the optical vasoconstriction with ~20 mW/mm^2 blue light was much greater than that produced by 10 μM PE. The optical coronary vasoconstriction did not cause evident changes in heart rate and pulse pressure, while both were augmented by Isop. The heart rate and

pulse pressure were obtained from areas indicated by arrows. **(B)** In a control heart, light did not produce coronary vasoconstriction. **(C)** In comparison, the vasoconstriction force was greater by light than by 10 μM PE (n = 11). **(D)** Time responses of the optostimulation. **(E)** long-term stimulation (30 min) raised coronary pressure to a relatively stable level with a slight decline. The coronary perfusion resistance went back to the initial baseline level in a few minutes after optostimulation. **(F)** The coronary resistance was maintained at a relative stable level during a 30 min optostimulation without obvious decline (n = 4). **(G)** long-lasting light stimulation induced the cardiac arrhythmia. Severe arrhythmia was observed after 15 min optical stimulation, such as heart block and cardiac arrest.

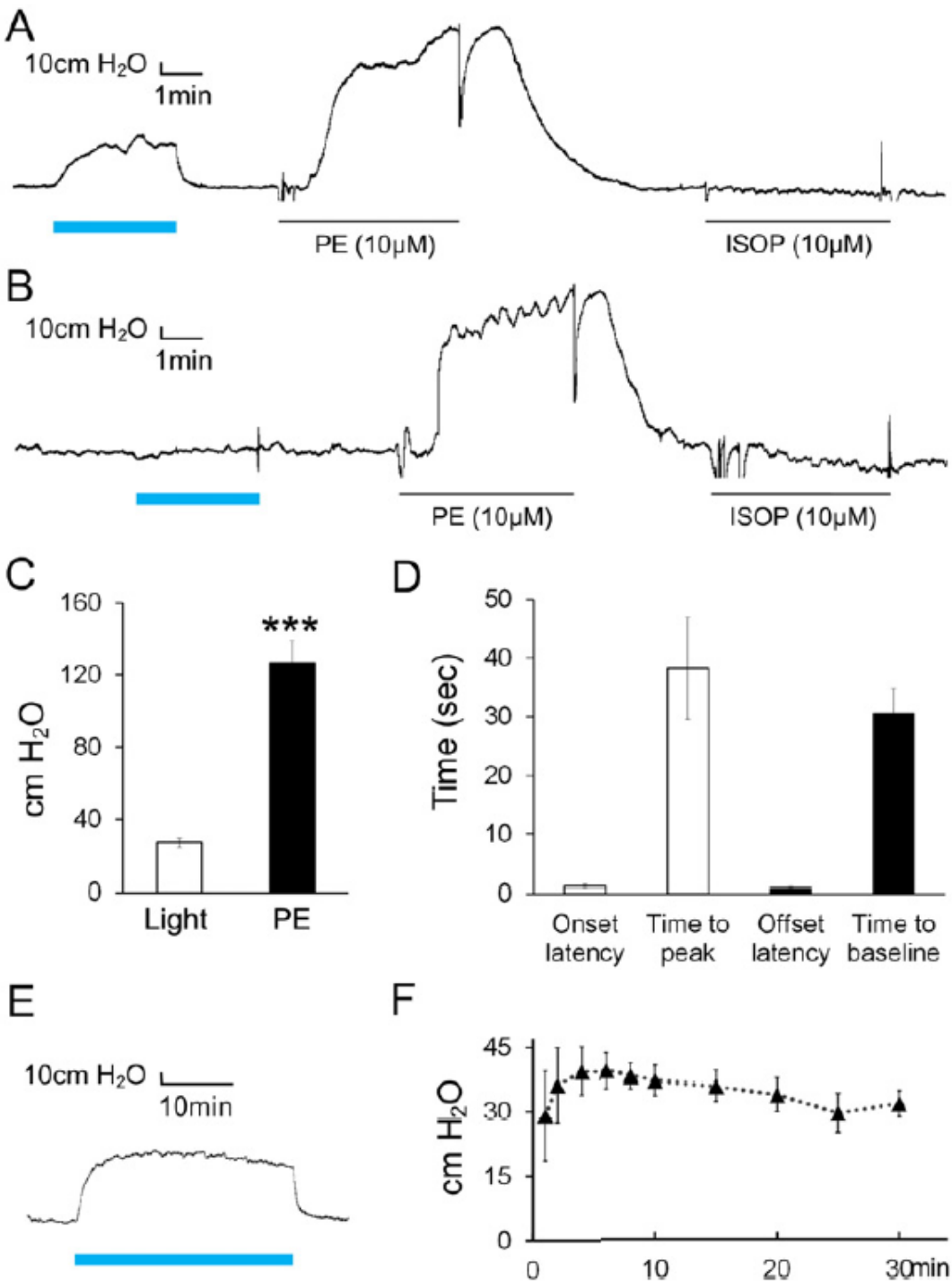

Figure 8.7 Optical vasoconstriction in isolated kidney.
(A, B) Optical vasoconstriction was observed in an isolated and perfused kidney from a Tagln-ChR mouse but not that from a control mouse. **(C)** The optical renal vasoconstriction was compared with that produced by 10 μM PE. **(D)** Onset/offset time responses to optostimulation. **(E)** Long-lasting optical stimulation (30 min) induced a prolonged increase in vessel resistance. **(F)** The renal vascular resistance took about 4 min to reach the peak level and slightly declined (by 19 %, n = 4) at the end of 30 min stimulation.

9 GENERAL DISCUSSIONS

Excitable cells rely on the excitation status to generate their functions. In peripheral tissues, excitation arises from motor neurons receiving central regulation. Such neural controls can be voluntary as in most somatic motor activity, involuntary as in cardiovascular function, and both as in breathing. Multiple excitable tissues including central nerves, peripheral nerves and muscles are involved during this process. Disorders in either may result in changes in excitation status. Therefore, information of cellular excitability control under certain physiological and pathophysiological conditions helps the understanding of diseases in the ANS. And novel approaches to cellular excitability have great impacts on the ANS diseases as well. These are indeed what are presented in this thesis study.

9.1 Respiratory dysfunction and intervention: from the view of RTT

9.1.1 Alternation of respiratory neurons excitability in Mecp2 rat model

With the transgenic animal models, many progresses in RTT research have been made in RTT showing widespread disorders in motor, social and respiratory behaviors. Our study indicates that the over excitation or prolonged discharge of both I and E respiratory neurons in VRC caused by *Mecp2* mutation may contribute to the slow breathing rate and frequent apnea. Additionally, the disruption of cellular excitation is not only found in VRC, but also in LC in our studies, which is consistent with the literatures that attributes the respiratory disorders such as apneas, air swallowing and periodic breathing to obvious prolonged and enhanced respiratory activity [94,110]. Consistent with our findings in rats, *Mecp2* mouse exhibits hyperexcitability of brainstem neurons and depressed spontaneous inhibitory synaptic currents. The alternations of neuronal excitability may affect the functional integrity of the brainstem respiratory network.

The disrupted coordination of the respiratory oscillators in brainstem become noticeable only when the animals reach certain age. In our study, the normal and abnormal breathing appears alternatively on *Mecp2*-null rats. The obvious breathing abnormalities were detected around 2 months after birth through plethysmography tests. However, our neuronal recording indicates the enhanced or prolonged neuronal activity appears not only when apnea or breathing variation occurs, but also during relatively normal breathing. In addition, the ectopic phrenic discharge only appears at the latter stage of life. These indicate that the molecular changes happen before the symptoms can be detected, and the change of overall cellular excitability is a step by step process. The molecular changes caused by *Mecp2* disruption in different brain regions contribute to the alternation of the neuronal excitability. In brain, these molecular changes include the changes of neurotransmission. Normal autonomic functions depend on the fine control of neuron activities in different brain regions via neurotransmission which is impaired by *Mecp2* disruption. The animal body may be able to do certain adjustment to adapt the minor changes at early stage. With the progress of the disease, the severity excesses the compensatory mechanism making the symptoms detectable.

As a multifunctional protein, MeCP2 regulates many gene expression and influences various biological metabolism. Neuronal excitabilities in different brain region can be altered with *Mecp2* disruption. Seizure and tremor were not analyzed in our studies, but also can be seen on *Mecp2*-null animals, which may be also caused by alternation of neuronal excitability. *Mecp2* disruption in the forebrain lead to cortical hyperexcitation represented as spontaneous seizures associated with a defect of GABAergic transmission [117]. And tremor or striking myoclonic jerk on forelimbs and paws was observed simultaneously with hyperactive cortical electroencephalographic (EEG) signal in mice expressing a truncated MeCP2 protein [119]. By

using the rat models, the underlying molecular mechanisms causing these excitability changes are expected to be uncovered, and the development of the potential therapeutic strategies of RTT becomes possible.

9.1.2 Transgenic and pharmacological interventions of RTT

Although the molecular pathogenesis of respiratory dysfunction is still not fully understood due to the complicity of the downstream regulation of MeCP2, the therapeutic interventions can be developed and help to alleviate the RTT symptoms with information generated in this and other studies. It is encouraging that developmental absence of MeCP2 does not cause irreversibly damage of neurons [237]. Therefore, the expression of normal MeCP2 during a specific time window might reverse RTT. The mature gene therapy or alternative therapy to restore the MeCP2 level is still missing. Therefore, potential RTT treatment could be focused on maintaining the hemostasis of neurotransmission by using existing agents. THIP, also known as Gaboxadol, has promising effects on the alleviation of RTT-like phenotypes in both mouse models and our rat model. This agent is considered in the treatment of insomnia [311]. Although it reached a phase III trial before it was called off with safety and efficacy concerns, animal experiments on THIP shows it effectively rescues the neurophysiological and behavioral deficits in fragile X syndrome and Angelman Syndrome [312-314]. The pilot study on THIP as hypnotics supplies precise knowledge to guide its usage on other diseases. In our study, THIP rescuing the *Mecp2*-null rats suggests the possibility of certain GABA enhancers as RTT treatment reagents. NNC-711 is another agent having delightful and potent rescuing effects on RTT phenotypes. Although the side effects of these GABA enhancers including sedation, dizziness, confusion and hallucination are reported, these drugs may still be used under restrictive control, and their side effects seem less important when considering its life-rescuing effects. In addition, systemic

division of RTT subtypes based on phenotypes and severity is needed to make medication guideline. Hopefully, technical development in future will allow more accurate application of transgenic or pharmacological intervention to avoid unnecessary side effects and to target specifically the subdivided phenotypes of this disease.

9.2 Vascular dysfunction and intervention: from the view of *VSMC*

9.2.1 Alternation of VSMCs excitability in MGO model

Besides influence on CNS, alternation of membrane excitability on executive cells such as VSMCs, cardiomyocytes and other smooth muscle cells can also lead to autonomic dysfunctions. The excitability of these cells is influenced by the membrane potential. The transmembrane proteins, such as ion transporters and ion channels, are the key setters of the electrical potential across the membrane. Membrane potential is used by the excitable cells to transmit electric signals in the cells. The opening and closing of ion channels producing a local electric change on the membrane influence the membrane potential, and determine the activation status of the cell. The resting membrane potential established by Na^+/K^+-ATPase is affected by K^+ channels, such as K_{ATP} channels, to a large extent. In the case of the K_{ATP} dysfunction, reduced outflow of K^+ ions will lead to a depolarized membrane potential, and increase vasoconstrictor-induced vasoconstriction [206]. We demonstrated that the cumulated MGO targeted on mRNAs of K_{ATP} channels in VSMCs via miRs, causing instability of Kir6.1 and SUR2B transcripts. This suggests that the function of the widely-expressed K_{ATP} channels can be impaired by excessive MGO in diabetes leading to abnormalities of cellular excitability of VSMCs, which contributes to the diabetic vascular disorders including hypertension [204,205] and cardiovascular complications including ischemic coronary artery disease and stroke [202,315]. Indeed, increased contractility of VSMCs was demonstrated under diabetic conditions [316,317].

Emerging evidence suggests that hyperglycemia and high MGO level affects the miRs expression in vascular tissues, and this may be associated with the altered vascular reactivity. The relation between excessive MGO and altered expression of several miRs is studied firstly in dysfunction of endothelial cells. For example, reduced level of miR-190a is reported associated with impaired aortic endothelial insulin resistance [318]. The dysfunction of umbilical vein endothelial cells is induced by miR-221 in persistent hyperglycemia [319]. Our study demonstrates that VSMC is also involved in miRs-caused vascular dysfunction in hyperglycemia. Downregulation of SUR2B mRNA in VSMCs is induced by elevation of miR-9a-3p in high MGO exposure. Besides miR-9a-3p, miR-29 is another miRs increasing VSMC contractile phenotypes in hyperglycemic conditions [320]. It directly interacts with mRNA of a transcription factor called KLF4 which is a potent inhibitor of cell proliferation, causing downregulation of KLF4, inducing vascular smooth muscle contractile markers calponin, and leading to consequent proliferation of VSMCs. Therefore, there are possibly more miRs besides mi9-9a-3p induced by high glucose or excessive reactive species involving in diabetic vascular dysfunctions. And Kir6.1 subunit may be targeted by other undetected miRs, together with mi9-9a-3p, contributing to downregulation of the K_{ATP} channels. The consequences include hypotension and insufficient blood flow to main organs when sympathetic system is activated.

Specific miRs regulate cellular excitability by affecting the genetic programs. In our study, increased mi9-9a-3p triggered by MGO influences the VSMCs excitability via impairing the function of the K_{ATP} channels. Evidence suggests that increased mi9-9a-3p is detected in human epileptic plasma samples [321]. The blood mi9-9a-3p may be a putative biomarkers of epilepsy. Although it needs to be proved, we have a bold guess that mi9-9a-3p might affect the

neuronal excitability in the brain and increase the risk of epilepsy via its impact on K_{ATP} channels as well.

9.2.2 Transgenic interventions of vascular tone

Traditional intervention to vasculature intensively depends on the usage of pharmacological agents. Here, two novel transgenic approaches could be used as alternatives to vascular system. One is through manipulation of miRs which supplies a systemic intervention, the other is through optogenetic engineering which enable the spatiotemporal controlling of vascular tone.

Manipulation of miRs may offer a novel therapeutic intervention in vascular diseases. It is feasible to use miRs as a therapeutic tool in vascular system. Evidence suggests that exosomes may contain miRs which can be delivered to another cell and function in the new location [322]. Furthermore, miRs can be detected in circulation as potential biomarkers of epilepsy [321]. These suggested miRs delivery can be used as a minimally invasive tool to intervene vascular system with specificity. Pilot studies on therapeutic miRs delivery as a replacement therapy have some success in the suppression of liver tumorigenesis with adeno-associated virus (AAV) [323]. Our study demonstrated that elevated miRs in disease condition can be lowered down with antisense oligonuecleotides complementary to the target mature miRs. These approved that miRs level can be manipulated using replacement therapy or antisense oligoneucleotides depending on endogenous miRs levels in disease conditions. Although, at current stage, further studies are needed to gain insight into the miRs expression pattern in vascular system, manipulation of miRs provides attractive therapeutic targets for the treatment of vascular diseases.

The application of optogenetics in vascular system supplies an exquisite tool in vascular manipulation. Different from pharmacological and miRs intervention, this transgenic method

produces quick onset and withdrawal without obvious sequela. And the potency of vasoconstriction triggered by optostimulation is comparable with endogenous vasoconstrictor PE. The coupling of the cerebral blood flow and neuronal activation makes Tagln-ChR mice an ideal model in studies of the neuronal function. Furthermore, it may useful in regulating the filtration of glomerulus by controlling the vasoconstriction of renal afferent and efferent arterioles, where the blood pressure may be influenced without other unwanted ANS interference. Although we did complete in vitro test to approve the optogenetic approach has the potential in the studies of the relation of reginal blood flow and neuronal activity in CNS, subsequent experiment encountered bottleneck when we tried to reveal the mechanism of RTN chemosensitivity in *in vivo* studies because of the limited resolution of light source and the unwanted heat radiation generated by laser stimulator. Before these problems can be solved, the applications of optogenetics will be limited in vascular system. Currently, some labs are dedicated to break through the technique issues. Hopefully, with the development of light delivery technique, such as a high resolution integrated image-stimulation system [324], optical modulation of vasoconstriction can be achieved on living animals with low damage to blood vessels and local tissues.

10 CONCLUSION

In these studies aimed at addressing regulation of autonomic system, specifically respiratory and vascular systems, we have found that the alternation of the cellular excitability is the key reason for ANS dysfunctions. The novel *Mecp2*-null rat model recapitulates many RTT phenotypes and is ideal in the studies of cellular mechanisms. With the RTT rat model, we have demonstrated that RTT type of breathing is likely due to increased excitability of the respiratory neurons in brainstem, which can be rescued by augmentation of GABAergic synaptic inhibition. The change in cellular excitability plays equally important role in VSMCs where dysfunction of the vascular K_{ATP} channels is caused by elevation of miR-9a-3p during oxidative stress. Because of the importance of the cellular excitability, we have tried to control the excitability of VSMCs using the optogenetic approach that appears helpful in laboratory research. Therefore, these thesis studies demonstrate the relationship between the hemostasis of the cellular excitability and the molecular mechanism of RTT respiratory disorders as well as the vascular dysfunction under oxidative stress. Furthermore, this dissertation also provides a good perspective on the potential usage of transgenic tools including transgenic animal, miRs and optogenetics in basic studies and potential therapeutical interventions to ANS dysfunctions.

REFERENCES

1 Nozdrachev, A. D. [Structuro-functional organization of the vegetative (autonomic) nervous system]. *Fiziol Zh SSSR Im I M Sechenova* **66**, 937-961 (1980).

2 Wakade, A. R. & Wakade, T. D. Contribution of nicotinic and muscarinic receptors in the secretion of catecholamines evoked by endogenous and exogenous acetylcholine. *Neuroscience* **10**, 973-978 (1983).

3 Hu, Y., Converse, C., Lyons, M. C. & Hsu, W. H. Neural control of sweat secretion: a review. *Br J Dermatol*, doi:10.1111/bjd.15808 (2017).

4 Bell, C. Dopamine release from sympathetic nerve terminals. *Prog Neurobiol* **30**, 193-208 (1988).

5 Xiao, R. P. *et al.* Coupling of beta2-adrenoceptor to Gi proteins and its physiological relevance in murine cardiac myocytes. *Circ Res* **84**, 43-52 (1999).

6 Bulbring, E. & Tomita, T. Catecholamine action on smooth muscle. *Pharmacol Rev* **39**, 49-96 (1987).

7 Graham, R. M., Perez, D. M., Hwa, J. & Piascik, M. T. alpha 1-adrenergic receptor subtypes. Molecular structure, function, and signaling. *Circ Res* **78**, 737-749 (1996).

8 MacDonald, E. & Scheinin, M. Distribution and pharmacology of alpha 2-adrenoceptors in the central nervous system. *J Physiol Pharmacol* **46**, 241-258 (1995).

9 Civantos Calzada, B. & Aleixandre de Artinano, A. Alpha-adrenoceptor subtypes. *Pharmacol Res* **44**, 195-208, doi:10.1006/phrs.2001.0857 (2001).

10 Molinoff, P. B. Alpha- and beta-adrenergic receptor subtypes properties, distribution and regulation. *Drugs* **28 Suppl 2**, 1-15 (1984).

11 Fitzpatrick, D. P., Dale; Augustine, George. *Neuroscience*. Third Edition edn, Table 20:2 (Sinauer 2004).

12 Bulloch, J. M. & Daly, C. J. Autonomic nerves and perivascular fat: interactive mechanisms. *Pharmacol Ther* **143**, 61-73, doi:10.1016/j.pharmthera.2014.02.005 (2014).

13 Qin, K., Dong, C., Wu, G. & Lambert, N. A. Inactive-state preassembly of G(q)-coupled receptors and G(q) heterotrimers. *Nat Chem Biol* **7**, 740-747, doi:10.1038/nchembio.642 (2011).

14 Volpicelli, L. A. & Levey, A. I. Muscarinic acetylcholine receptor subtypes in cerebral cortex and hippocampus. *Prog Brain Res* **145**, 59-66, doi:10.1016/S0079-6123(03)45003-6 (2004).

15 Jordan, D. Central nervous pathways and control of the airways. *Respir Physiol* **125**, 67-81 (2001).

16 Song, G. & Poon, C. S. Functional and structural models of pontine modulation of mechanoreceptor and chemoreceptor reflexes. *Respir Physiol Neurobiol* **143**, 281-292, doi:10.1016/j.resp.2004.05.009 (2004).

17 Shannon, R. & Lindsey, B. G. Expiratory neurons in the region of the retrofacial nucleus: inhibitory effects of intercostal tendon organs. *Exp Neurol* **97**, 730-734 (1987).

18 Smith, J. C., Ellenberger, H. H., Ballanyi, K., Richter, D. W. & Feldman, J. L. Pre-Botzinger complex: a brainstem region that may generate respiratory rhythm in mammals. *Science* **254**, 726-729 (1991).

19 Schwarzacher, S. W., Smith, J. C. & Richter, D. W. Pre-Botzinger complex in the cat. *J Neurophysiol* **73**, 1452-1461, doi:10.1152/jn.1995.73.4.1452 (1995).

20 Gerrits, P. O. & Holstege, G. Pontine and medullary projections to the nucleus retroambiguus: a wheat germ agglutinin-horseradish peroxidase and autoradiographic tracing study in the cat. *J Comp Neurol* **373**, 173-185, doi:10.1002/(SICI)1096-9861(19960916)373:2<173::AID-CNE2>3.0.CO;2-0 (1996).

21 Schreihofer, A. M., Stornetta, R. L. & Guyenet, P. G. Evidence for glycinergic respiratory neurons: Botzinger neurons express mRNA for glycinergic transporter 2. *J Comp Neurol* **407**, 583-597 (1999).

22 Bongianni, F., Mutolo, D. & Pantaleo, T. Depressant effects on inspiratory and expiratory activity produced by chemical activation of Botzinger complex neurons in the rabbit. *Brain Res* **749**, 1-9 (1997).

23 Bongianni, F., Mutolo, D., Cinelli, E. & Pantaleo, T. Respiratory responses induced by blockades of GABA and glycine receptors within the Botzinger complex and the pre-Botzinger complex of the rabbit. *Brain Res* **1344**, 134-147, doi:10.1016/j.brainres.2010.05.032 (2010).

24 Alheid, G. F., Milsom, W. K. & McCrimmon, D. R. Pontine influences on breathing: an overview. *Respir Physiol Neurobiol* **143**, 105-114, doi:10.1016/j.resp.2004.06.016 (2004).

25 Gautier, H. & Bertrand, F. Respiratory effects of pneumotaxic center lesions and subsequent vagotomy in chronic cats. *Respir Physiol* **23**, 71-85 (1975).

26 Song, G., Yu, Y. & Poon, C. S. Cytoarchitecture of pneumotaxic integration of respiratory and nonrespiratory information in the rat. *J Neurosci* **26**, 300-310, doi:10.1523/JNEUROSCI.3029-05.2006 (2006).

27 Dutschmann, M. & Dick, T. E. Pontine mechanisms of respiratory control. *Compr Physiol* **2**, 2443-2469, doi:10.1002/cphy.c100015 (2012).

28 Richter, D. W. Generation and maintenance of the respiratory rhythm. *J Exp Biol* **100**, 93-107 (1982).

29 Richter, D. W., Ballanyi, K. & Schwarzacher, S. Mechanisms of respiratory rhythm generation. *Curr Opin Neurobiol* **2**, 788-793 (1992).

30 Onimaru, H., Arata, A. & Homma, I. Neuronal mechanisms of respiratory rhythm generation: an approach using in vitro preparation. *Jpn J Physiol* **47**, 385-403 (1997).

31 von Euler, C. On the central pattern generator for the basic breathing rhythmicity. *J Appl Physiol Respir Environ Exerc Physiol* **55**, 1647-1659, doi:10.1152/jappl.1983.55.6.1647 (1983).

32 Salmoiraghi, G. C. & Burns, B. D. Notes on mechanism of rhythmic respiration. *J Neurophysiol* **23**, 14-26, doi:10.1152/jn.1960.23.1.14 (1960).

33 Feldman, J. L., Del Negro, C. A. & Gray, P. A. Understanding the rhythm of breathing: so near, yet so far. *Annu Rev Physiol* **75**, 423-452, doi:10.1146/annurev-physiol-040510-130049 (2013).

34 Anderson, T. M. & Ramirez, J. M. Respiratory rhythm generation: triple oscillator hypothesis. *F1000Res* **6**, 139, doi:10.12688/f1000research.10193.1 (2017).

35 Suzue, T. Respiratory rhythm generation in the in vitro brain stem-spinal cord preparation of the neonatal rat. *J Physiol* **354**, 173-183 (1984).

36 Smith, J. C., Abdala, A. P., Koizumi, H., Rybak, I. A. & Paton, J. F. Spatial and functional architecture of the mammalian brain stem respiratory network: a hierarchy of three oscillatory mechanisms. *J Neurophysiol* **98**, 3370-3387, doi:10.1152/jn.00985.2007 (2007).

37 Janczewski, W. A. & Feldman, J. L. Distinct rhythm generators for inspiration and expiration in the juvenile rat. *J Physiol* **570**, 407-420, doi:10.1113/jphysiol.2005.098848 (2006).

38 Gray, P. A., Janczewski, W. A., Mellen, N., McCrimmon, D. R. & Feldman, J. L. Normal breathing requires preBotzinger complex neurokinin-1 receptor-expressing neurons. *Nat Neurosci* **4**, 927-930, doi:10.1038/nn0901-927 (2001).

39 McKay, L. C., Janczewski, W. A. & Feldman, J. L. Sleep-disordered breathing after targeted ablation of preBotzinger complex neurons. *Nat Neurosci* **8**, 1142-1144, doi:10.1038/nn1517 (2005).

40 Pena, F. & Ramirez, J. M. Substance P-mediated modulation of pacemaker properties in the mammalian respiratory network. *J Neurosci* **24**, 7549-7556, doi:10.1523/JNEUROSCI.1871-04.2004 (2004).

41 Pena, F. & Aguileta, M. A. Effects of riluzole and flufenamic acid on eupnea and gasping of neonatal mice in vivo. *Neurosci Lett* **415**, 288-293, doi:10.1016/j.neulet.2007.01.032 (2007).

42 Brockhaus, J. & Ballanyi, K. Synaptic inhibition in the isolated respiratory network of neonatal rats. *Eur J Neurosci* **10**, 3823-3839 (1998).

43 Ren, J. & Greer, J. J. Modulation of respiratory rhythmogenesis by chloride-mediated conductances during the perinatal period. *J Neurosci* **26**, 3721-3730, doi:10.1523/JNEUROSCI.0026-06.2006 (2006).

44 Shao, X. M. & Feldman, J. L. Respiratory rhythm generation and synaptic inhibition of expiratory neurons in pre-Botzinger complex: differential roles of glycinergic and GABAergic neural transmission. *J Neurophysiol* **77**, 1853-1860, doi:10.1152/jn.1997.77.4.1853 (1997).

45 Onimaru, H. & Homma, I. A novel functional neuron group for respiratory rhythm generation in the ventral medulla. *J Neurosci* **23**, 1478-1486 (2003).

46 Guyenet, P. G. *et al.* Retrotrapezoid nucleus, respiratory chemosensitivity and breathing automaticity. *Respir Physiol Neurobiol* **168**, 59-68, doi:10.1016/j.resp.2009.02.001 (2009).

47 Wang, S., Shi, Y., Shu, S., Guyenet, P. G. & Bayliss, D. A. Phox2b-expressing retrotrapezoid neurons are intrinsically responsive to H+ and CO2. *J Neurosci* **33**, 7756-7761, doi:10.1523/JNEUROSCI.5550-12.2013 (2013).

48 Onimaru, H. & Homma, I. Two modes of respiratory rhythm generation in the newborn rat brainstem-spinal cord preparation. *Adv Exp Med Biol* **605**, 104-108, doi:10.1007/978-0-387-73693-8_18 (2008).

49 Pagliardini, S. *et al.* Active expiration induced by excitation of ventral medulla in adult anesthetized rats. *J Neurosci* **31**, 2895-2905, doi:10.1523/JNEUROSCI.5338-10.2011 (2011).

50 Anderson, T. M. *et al.* A novel excitatory network for the control of breathing. *Nature* **536**, 76-80, doi:10.1038/nature18944 (2016).

51 Dutschmann, M. & Herbert, H. The Kolliker-Fuse nucleus gates the postinspiratory phase of the respiratory cycle to control inspiratory off-switch and upper airway resistance in rat. *Eur J Neurosci* **24**, 1071-1084, doi:10.1111/j.1460-9568.2006.04981.x (2006).

52 Subramanian, H. H. & Holstege, G. Midbrain and medullary control of postinspiratory activity of the crural and costal diaphragm in vivo. *J Neurophysiol* **105**, 2852-2862, doi:10.1152/jn.00168.2011 (2011).

53 Winter, S. M. *et al.* Glycinergic interneurons are functionally integrated into the inspiratory network of mouse medullary slices. *Pflugers Arch* **458**, 459-469, doi:10.1007/s00424-009-0647-1 (2009).

54 Richter, D. W. & Smith, J. C. Respiratory rhythm generation in vivo. *Physiology (Bethesda)* **29**, 58-71, doi:10.1152/physiol.00035.2013 (2014).

55 Smith, J. C., Abdala, A. P., Borgmann, A., Rybak, I. A. & Paton, J. F. Brainstem respiratory networks: building blocks and microcircuits. *Trends Neurosci* **36**, 152-162, doi:10.1016/j.tins.2012.11.004 (2013).

56 Tan, W., Pagliardini, S., Yang, P., Janczewski, W. A. & Feldman, J. L. Projections of preBotzinger complex neurons in adult rats. *J Comp Neurol* **518**, 1862-1878, doi:10.1002/cne.22308 (2010).

57 Janczewski, W. A., Tashima, A., Hsu, P., Cui, Y. & Feldman, J. L. Role of inhibition in respiratory pattern generation. *J Neurosci* **33**, 5454-5465, doi:10.1523/JNEUROSCI.1595-12.2013 (2013).

58 Del Negro, C. A., Morgado-Valle, C. & Feldman, J. L. Respiratory rhythm: an emergent network property? *Neuron* **34**, 821-830 (2002).

59 Del Negro, C. A. *et al.* Sodium and calcium current-mediated pacemaker neurons and respiratory rhythm generation. *J Neurosci* **25**, 446-453, doi:10.1523/JNEUROSCI.2237-04.2005 (2005).

60 Feldman, J. L. & Del Negro, C. A. Looking for inspiration: new perspectives on respiratory rhythm. *Nat Rev Neurosci* **7**, 232-242, doi:10.1038/nrn1871 (2006).

61 Morgado-Valle, C., Baca, S. M. & Feldman, J. L. Glycinergic pacemaker neurons in preBotzinger complex of neonatal mouse. *J Neurosci* **30**, 3634-3639, doi:10.1523/JNEUROSCI.3040-09.2010 (2010).

62 Kuwana, S. *et al.* Electrophysiological and morphological characteristics of GABAergic respiratory neurons in the mouse pre-Botzinger complex. *Eur J Neurosci* **23**, 667-674, doi:10.1111/j.1460-9568.2006.04591.x (2006).

63 Ezure, K., Tanaka, I. & Kondo, M. Glycine is used as a transmitter by decrementing expiratory neurons of the ventrolateral medulla in the rat. *J Neurosci* **23**, 8941-8948 (2003).

64 Montandon, G. *et al.* PreBotzinger complex neurokinin-1 receptor-expressing neurons mediate opioid-induced respiratory depression. *J Neurosci* **31**, 1292-1301, doi:10.1523/JNEUROSCI.4611-10.2011 (2011).

65 Boom, M. *et al.* Non-analgesic effects of opioids: opioid-induced respiratory depression. *Curr Pharm Des* **18**, 5994-6004 (2012).

66 Manzke, T. *et al.* 5-HT4(a) receptors avert opioid-induced breathing depression without loss of analgesia. *Science* **301**, 226-229, doi:10.1126/science.1084674 (2003).

67 Manzke, T. *et al.* Serotonin targets inhibitory synapses to induce modulation of network functions. *Philos Trans R Soc Lond B Biol Sci* **364**, 2589-2602, doi:10.1098/rstb.2009.0068 (2009).

68 Amir, R. E. *et al.* Rett syndrome is caused by mutations in X-linked MECP2, encoding methyl-CpG-binding protein 2. *Nat Genet* **23**, 185-188, doi:10.1038/13810 (1999).

69 Caballero, I. M. & Hendrich, B. MeCP2 in neurons: closing in on the causes of Rett syndrome. *Hum Mol Genet* **14 Spec No 1**, R19-26, doi:10.1093/hmg/ddi102 (2005).

70 Nieto-Barrera, M., Nieto-Jimenez, M. & Siljestrom, M. L. [Clinical phenotypes of classic Rett syndrome]. *Rev Neurol* **36 Suppl 1**, S146-152 (2003).

71 Glaze, D. G., Frost, J. D., Jr., Zoghbi, H. Y. & Percy, A. K. Rett's syndrome: characterization of respiratory patterns and sleep. *Ann Neurol* **21**, 377-382, doi:10.1002/ana.410210410 (1987).

72 Julu, P. O. *et al.* Characterisation of breathing and associated central autonomic dysfunction in the Rett disorder. *Arch Dis Child* **85**, 29-37 (2001).

73 Weese-Mayer, D. E. *et al.* Autonomic dysregulation in young girls with Rett Syndrome during nighttime in-home recordings. *Pediatr Pulmonol* **43**, 1045-1060, doi:10.1002/ppul.20866 (2008).

74 Katz, D. M., Dutschmann, M., Ramirez, J. M. & Hilaire, G. Breathing disorders in Rett syndrome: progressive neurochemical dysfunction in the respiratory network after birth. *Respir Physiol Neurobiol* **168**, 101-108, doi:10.1016/j.resp.2009.04.017 (2009).

75 Guy, J., Hendrich, B., Holmes, M., Martin, J. E. & Bird, A. A mouse Mecp2-null mutation causes neurological symptoms that mimic Rett syndrome. *Nat Genet* **27**, 322-326, doi:10.1038/85899 (2001).

76 Pelka, G. J. *et al.* Mecp2 deficiency is associated with learning and cognitive deficits and altered gene activity in the hippocampal region of mice. *Brain* **129**, 887-898, doi:10.1093/brain/awl022 (2006).

77 Chen, R. Z., Akbarian, S., Tudor, M. & Jaenisch, R. Deficiency of methyl-CpG binding protein-2 in CNS neurons results in a Rett-like phenotype in mice. *Nat Genet* **27**, 327-331, doi:10.1038/85906 (2001).

78 Goffin, D. *et al.* Rett syndrome mutation MeCP2 T158A disrupts DNA binding, protein stability and ERP responses. *Nat Neurosci* **15**, 274-283, doi:10.1038/nn.2997 (2011).

79 Schaevitz, L. R., Gomez, N. B., Zhen, D. P. & Berger-Sweeney, J. E. MeCP2 R168X male and female mutant mice exhibit Rett-like behavioral deficits. *Genes Brain Behav* **12**, 732-740, doi:10.1111/gbb.12070 (2013).

80 Yasui, D. H. *et al.* Mice with an isoform-ablating Mecp2 exon 1 mutation recapitulate the neurologic deficits of Rett syndrome. *Hum Mol Genet* **23**, 2447-2458, doi:10.1093/hmg/ddt640 (2014).

81 Voituron, N., Zanella, S., Menuet, C., Dutschmann, M. & Hilaire, G. Early breathing defects after moderate hypoxia or hypercapnia in a mouse model of Rett syndrome. *Respir Physiol Neurobiol* **168**, 109-118, doi:10.1016/j.resp.2009.05.013 (2009).

82 Ward, C. S. *et al.* MeCP2 is critical within HoxB1-derived tissues of mice for normal lifespan. *J Neurosci* **31**, 10359-10370, doi:10.1523/JNEUROSCI.0057-11.2011 (2011).

83 Zhong, W. *et al.* Methyl CpG Binding Protein 2 Gene Disruption Augments Tonic Currents of gamma-Aminobutyric Acid Receptors in Locus Coeruleus Neurons: IMPACT ON NEURONAL EXCITABILITY AND BREATHING. *J Biol Chem* **290**, 18400-18411, doi:10.1074/jbc.M115.650465 (2015).

84 Wu, Y. *et al.* Characterization of Rett Syndrome-like phenotypes in Mecp2-knockout rats. *J Neurodev Disord* **8**, 23, doi:10.1186/s11689-016-9156-7 (2016).

85 Braunschweig, D., Simcox, T., Samaco, R. C. & LaSalle, J. M. X-Chromosome inactivation ratios affect wild-type MeCP2 expression within mosaic Rett syndrome and Mecp2-/+ mouse brain. *Hum Mol Genet* **13**, 1275-1286, doi:10.1093/hmg/ddh142 (2004).

86 Young, J. I. & Zoghbi, H. Y. X-chromosome inactivation patterns are unbalanced and affect the phenotypic outcome in a mouse model of rett syndrome. *Am J Hum Genet* **74**, 511-520, doi:10.1086/382228 (2004).

87 Samaco, R. C. *et al.* Female Mecp2(+/-) mice display robust behavioral deficits on two different genetic backgrounds providing a framework for pre-clinical studies. *Hum Mol Genet* **22**, 96-109, doi:10.1093/hmg/dds406 (2013).

88 Patterson, K. C., Hawkins, V. E., Arps, K. M., Mulkey, D. K. & Olsen, M. L. MeCP2 deficiency results in robust Rett-like behavioural and motor deficits in male and female rats. *Hum Mol Genet* **25**, 3303-3320, doi:10.1093/hmg/ddw179 (2016).

89 Veeraragavan, S. *et al.* Loss of MeCP2 in the rat models regression, impaired sociability and transcriptional deficits of Rett syndrome. *Hum Mol Genet* **25**, 3284-3302, doi:10.1093/hmg/ddw178 (2016).

90 Mironov, S. L. *et al.* Remodelling of the respiratory network in a mouse model of Rett syndrome depends on brain-derived neurotrophic factor regulated slow calcium buffering. *J Physiol* **587**, 2473-2485, doi:10.1113/jphysiol.2009.169805 (2009).

91 Kline, D. D., Ogier, M., Kunze, D. L. & Katz, D. M. Exogenous brain-derived neurotrophic factor rescues synaptic dysfunction in Mecp2-null mice. *J Neurosci* **30**, 5303-5310, doi:10.1523/JNEUROSCI.5503-09.2010 (2010).

92 Kron, M., Zhang, W. & Dutschmann, M. Developmental changes in the BDNF-induced modulation of inhibitory synaptic transmission in the Kolliker-Fuse nucleus of rat. *Eur J Neurosci* **26**, 3449-3457, doi:10.1111/j.1460-9568.2007.05960.x (2007).

93 Thoby-Brisson, M., Cauli, B., Champagnat, J., Fortin, G. & Katz, D. M. Expression of functional tyrosine kinase B receptors by rhythmically active respiratory neurons in the pre-Botzinger complex of neonatal mice. *J Neurosci* **23**, 7685-7689 (2003).

94 Abdala, A. P., Dutschmann, M., Bissonnette, J. M. & Paton, J. F. Correction of respiratory disorders in a mouse model of Rett syndrome. *Proc Natl Acad Sci U S A* **107**, 18208-18213, doi:10.1073/pnas.1012104107 (2010).

95 Toward, M. A., Abdala, A. P., Knopp, S. J., Paton, J. F. & Bissonnette, J. M. Increasing brain serotonin corrects CO2 chemosensitivity in methyl-CpG-binding protein 2 (Mecp2)-deficient mice. *Exp Physiol* **98**, 842-849, doi:10.1113/expphysiol.2012.069872 (2013).

96 Roux, J. C., Panayotis, N., Dura, E. & Villard, L. Progressive noradrenergic deficits in the locus coeruleus of Mecp2 deficient mice. *J Neurosci Res* **88**, 1500-1509, doi:10.1002/jnr.22312 (2010).

97 Taneja, P. *et al.* Pathophysiology of locus ceruleus neurons in a mouse model of Rett syndrome. *J Neurosci* **29**, 12187-12195, doi:10.1523/JNEUROSCI.3156-09.2009 (2009).

98 Zhang, X. *et al.* Intrinsic membrane properties of locus coeruleus neurons in Mecp2-null mice. *Am J Physiol Cell Physiol* **298**, C635-646, doi:10.1152/ajpcell.00442.2009 (2010).

99 Zanella, S. *et al.* Oral treatment with desipramine improves breathing and life span in Rett syndrome mouse model. *Respir Physiol Neurobiol* **160**, 116-121, doi:10.1016/j.resp.2007.08.009 (2008).

100 Roux, J. C., Dura, E., Moncla, A., Mancini, J. & Villard, L. Treatment with desipramine improves breathing and survival in a mouse model for Rett syndrome. *Eur J Neurosci* **25**, 1915-1922, doi:10.1111/j.1460-9568.2007.05466.x (2007).

101 El-Khoury, R. *et al.* GABA and glutamate pathways are spatially and developmentally affected in the brain of Mecp2-deficient mice. *PLoS One* **9**, e92169, doi:10.1371/journal.pone.0092169 (2014).

102 Zhang, L., He, J., Jugloff, D. G. & Eubanks, J. H. The MeCP2-null mouse hippocampus displays altered basal inhibitory rhythms and is prone to hyperexcitability. *Hippocampus* **18**, 294-309, doi:10.1002/hipo.20389 (2008).

103 Medrihan, L. *et al.* Early defects of GABAergic synapses in the brain stem of a MeCP2 mouse model of Rett syndrome. *J Neurophysiol* **99**, 112-121, doi:10.1152/jn.00826.2007 (2008).

104 Kron, M. *et al.* Brain activity mapping in Mecp2 mutant mice reveals functional deficits in forebrain circuits, including key nodes in the default mode network, that are reversed with ketamine treatment. *J Neurosci* **32**, 13860-13872, doi:10.1523/JNEUROSCI.2159-12.2012 (2012).

105 Patrizi, A. *et al.* Chronic Administration of the N-Methyl-D-Aspartate Receptor Antagonist Ketamine Improves Rett Syndrome Phenotype. *Biol Psychiatry* **79**, 755-764, doi:10.1016/j.biopsych.2015.08.018 (2016).

106 Jin, X., Cui, N., Zhong, W., Jin, X. T. & Jiang, C. GABAergic synaptic inputs of locus coeruleus neurons in wild-type and Mecp2-null mice. *Am J Physiol Cell Physiol* **304**, C844-857, doi:10.1152/ajpcell.00399.2012 (2013).

107 Abdala, A. P., Toward, M. A., Dutschmann, M., Bissonnette, J. M. & Paton, J. F. Deficiency of GABAergic synaptic inhibition in the Kolliker-Fuse area underlies respiratory dysrhythmia in a mouse model of Rett syndrome. *J Physiol* **594**, 223-237, doi:10.1113/JP270966 (2016).

108 Chao, H. T. *et al.* Dysfunction in GABA signalling mediates autism-like stereotypies and Rett syndrome phenotypes. *Nature* **468**, 263-269, doi:10.1038/nature09582 (2010).

109 Dani, V. S. *et al.* Reduced cortical activity due to a shift in the balance between excitation and inhibition in a mouse model of Rett syndrome. *Proc Natl Acad Sci U S A* **102**, 12560-12565, doi:10.1073/pnas.0506071102 (2005).

110 Stettner, G. M. *et al.* Breathing dysfunctions associated with impaired control of postinspiratory activity in Mecp2-/y knockout mice. *J Physiol* **579**, 863-876, doi:10.1113/jphysiol.2006.119966 (2007).

111 Zhang, X. *et al.* The disruption of central CO2 chemosensitivity in a mouse model of Rett syndrome. *Am J Physiol Cell Physiol* **301**, C729-738, doi:10.1152/ajpcell.00334.2010 (2011).

112 Viemari, J. C. *et al.* Mecp2 deficiency disrupts norepinephrine and respiratory systems in mice. *J Neurosci* **25**, 11521-11530, doi:10.1523/JNEUROSCI.4373-05.2005 (2005).

113 Pintaudi, M. *et al.* Epilepsy in Rett syndrome: clinical and genetic features. *Epilepsy Behav* **19**, 296-300, doi:10.1016/j.yebeh.2010.06.051 (2010).

114 Glaze, D. G. Neurophysiology of Rett syndrome. *J Child Neurol* **20**, 740-746, doi:10.1177/08830738050200090801 (2005).

115 Jian, L. *et al.* Seizures in Rett syndrome: an overview from a one-year calendar study. *Eur J Paediatr Neurol* **11**, 310-317, doi:10.1016/j.ejpn.2007.02.008 (2007).

116 Cardoza, B. *et al.* Epilepsy in Rett syndrome: association between phenotype and genotype, and implications for practice. *Seizure* **20**, 646-649, doi:10.1016/j.seizure.2011.06.010 (2011).

117 Zhang, W., Peterson, M., Beyer, B., Frankel, W. N. & Zhang, Z. W. Loss of MeCP2 from forebrain excitatory neurons leads to cortical hyperexcitation and seizures. *J Neurosci* **34**, 2754-2763, doi:10.1523/JNEUROSCI.4900-12.2014 (2014).

118 Temudo, T. *et al.* Stereotypies in Rett syndrome: analysis of 83 patients with and without detected MECP2 mutations. *Neurology* **68**, 1183-1187, doi:10.1212/01.wnl.0000259086.34769.78 (2007).

119 Shahbazian, M. *et al.* Mice with truncated MeCP2 recapitulate many Rett syndrome features and display hyperacetylation of histone H3. *Neuron* **35**, 243-254 (2002).

120 Zhong, W. *et al.* Effects of chronic exposure to low dose THIP on brainstem neuronal excitability in mouse models of Rett syndrome: Evidence from symptomatic females. *Neuropharmacology* **116**, 288-299, doi:10.1016/j.neuropharm.2017.01.002 (2017).

121 Zhong, W. *et al.* Effects of early-life exposure to THIP on brainstem neuronal excitability in the Mecp2-null mouse model of Rett syndrome before and after drug withdrawal. *Physiol Rep* **5**, doi:10.14814/phy2.13110 (2017).

122 Zhong, W. *et al.* Effects of early-life exposure to THIP on phenotype development in a mouse model of Rett syndrome. *J Neurodev Disord* **8**, 37, doi:10.1186/s11689-016-9169-2 (2016).

123 Lo, F. S., Blue, M. E. & Erzurumlu, R. S. Enhancement of postsynaptic GABAA and extrasynaptic NMDA receptor-mediated responses in the barrel cortex of Mecp2-null mice. *J Neurophysiol* **115**, 1298-1306, doi:10.1152/jn.00944.2015 (2016).

124 Levitt, E. S., Hunnicutt, B. J., Knopp, S. J., Williams, J. T. & Bissonnette, J. M. A selective 5-HT1a receptor agonist improves respiration in a mouse model of Rett syndrome. *J Appl Physiol (1985)* **115**, 1626-1633, doi:10.1152/japplphysiol.00889.2013 (2013).

125 Chapleau, C. A. *et al.* Recent Progress in Rett Syndrome and MeCP2 Dysfunction: Assessment of Potential Treatment Options. *Future Neurol* **8**, doi:10.2217/fnl.12.79 (2013).

126 Landi, S. *et al.* The short-time structural plasticity of dendritic spines is altered in a model of Rett syndrome. *Sci Rep* **1**, 45, doi:10.1038/srep00045 (2011).

127 Ogier, M. *et al.* Brain-derived neurotrophic factor expression and respiratory function improve after ampakine treatment in a mouse model of Rett syndrome. *J Neurosci* **27**, 10912-10917, doi:10.1523/JNEUROSCI.1869-07.2007 (2007).

128 Guyenet, P. G. The sympathetic control of blood pressure. *Nat Rev Neurosci* **7**, 335-346, doi:10.1038/nrn1902 (2006).

129 Brayden, J. E. & Nelson, M. T. Regulation of arterial tone by activation of calcium-dependent potassium channels. *Science* **256**, 532-535 (1992).

130 Thomas, G. D. Neural control of the circulation. *Adv Physiol Educ* **35**, 28-32, doi:10.1152/advan.00114.2010 (2011).

131 Gordan, R., Gwathmey, J. K. & Xie, L. H. Autonomic and endocrine control of cardiovascular function. *World J Cardiol* **7**, 204-214, doi:10.4330/wjc.v7.i4.204 (2015).

132 Missale, C., Nash, S. R., Robinson, S. W., Jaber, M. & Caron, M. G. Dopamine receptors: from structure to function. *Physiol Rev* **78**, 189-225, doi:10.1152/physrev.1998.78.1.189 (1998).

133 Pablo Huidobro-Toro, J. & Veronica Donoso, M. Sympathetic co-transmission: the coordinated action of ATP and noradrenaline and their modulation by neuropeptide Y in human vascular neuroeffector junctions. *Eur J Pharmacol* **500**, 27-35, doi:10.1016/j.ejphar.2004.07.008 (2004).

134 Yee, A. H., Burns, J. D. & Wijdicks, E. F. Cerebral salt wasting: pathophysiology, diagnosis, and treatment. *Neurosurg Clin N Am* **21**, 339-352, doi:10.1016/j.nec.2009.10.011 (2010).
135 Patil, J., Heiniger, E., Schaffner, T., Muhlemann, O. & Imboden, H. Angiotensinergic neurons in sympathetic coeliac ganglia innervating rat and human mesenteric resistance blood vessels. *Regul Pept* **147**, 82-87, doi:10.1016/j.regpep.2008.01.006 (2008).
136 Hu, X. Q. & Zhang, L. Function and regulation of large conductance Ca(2+)-activated K+ channel in vascular smooth muscle cells. *Drug Discov Today* **17**, 974-987, doi:10.1016/j.drudis.2012.04.002 (2012).
137 Ledoux, J., Werner, M. E., Brayden, J. E. & Nelson, M. T. Calcium-activated potassium channels and the regulation of vascular tone. *Physiology (Bethesda)* **21**, 69-78, doi:10.1152/physiol.00040.2005 (2006).
138 Guia, A., Wan, X., Courtemanche, M. & Leblanc, N. Local Ca2+ entry through L-type Ca2+ channels activates Ca2+-dependent K+ channels in rabbit coronary myocytes. *Circ Res* **84**, 1032-1042 (1999).
139 Lu, T. *et al.* Regulation of coronary arterial BK channels by caveolae-mediated angiotensin II signaling in diabetes mellitus. *Circ Res* **106**, 1164-1173, doi:10.1161/CIRCRESAHA.109.209767 (2010).
140 Reeve, H. L., Weir, E. K., Archer, S. L. & Cornfield, D. N. A maturational shift in pulmonary K+ channels, from Ca2+ sensitive to voltage dependent. *Am J Physiol* **275**, L1019-1025 (1998).
141 Shi, W. W., Yang, Y., Shi, Y. & Jiang, C. K(ATP) channel action in vascular tone regulation: from genetics to diseases. *Sheng Li Xue Bao* **64**, 1-13 (2012).
142 Yang, Y. *et al.* Molecular basis and structural insight of vascular K(ATP) channel gating by S-glutathionylation. *J Biol Chem* **286**, 9298-9307, doi:10.1074/jbc.M110.195123 (2011).
143 Vanelli, G., Hussain, S. N. & Aguggini, G. Glibenclamide, a blocker of ATP-sensitive potassium channels, reverses endotoxin-induced hypotension in pig. *Exp Physiol* **80**, 167-170 (1995).
144 Landry, D. W. & Oliver, J. A. The ATP-sensitive K+ channel mediates hypotension in endotoxemia and hypoxic lactic acidosis in dog. *J Clin Invest* **89**, 2071-2074, doi:10.1172/JCI115820 (1992).
145 Vanhoutte, P. M., Shimokawa, H., Feletou, M. & Tang, E. H. Endothelial dysfunction and vascular disease - a 30th anniversary update. *Acta Physiol (Oxf)* **219**, 22-96, doi:10.1111/apha.12646 (2017).
146 Shimokawa, H. & Matoba, T. Hydrogen peroxide as an endothelium-derived hyperpolarizing factor. *Pharmacol Res* **49**, 543-549, doi:10.1016/j.phrs.2003.10.016 (2004).
147 Shimokawa, H. & Godo, S. Diverse Functions of Endothelial NO Synthases System: NO and EDH. *J Cardiovasc Pharmacol* **67**, 361-366, doi:10.1097/FJC.0000000000000348 (2016).
148 Klein, R. Hyperglycemia and microvascular and macrovascular disease in diabetes. *Diabetes Care* **18**, 258-268 (1995).
149 Fiorentino, T. V., Prioletta, A., Zuo, P. & Folli, F. Hyperglycemia-induced oxidative stress and its role in diabetes mellitus related cardiovascular diseases. *Curr Pharm Des* **19**, 5695-5703 (2013).

150 Thannickal, V. J. & Fanburg, B. L. Reactive oxygen species in cell signaling. *Am J Physiol Lung Cell Mol Physiol* **279**, L1005-1028, doi:10.1152/ajplung.2000.279.6.L1005 (2000).
151 Gutterman, D. D., Miura, H. & Liu, Y. Redox modulation of vascular tone: focus of potassium channel mechanisms of dilation. *Arterioscler Thromb Vasc Biol* **25**, 671-678, doi:10.1161/01.ATV.0000158497.09626.3b (2005).
152 Ardanaz, N. & Pagano, P. J. Hydrogen peroxide as a paracrine vascular mediator: regulation and signaling leading to dysfunction. *Exp Biol Med (Maywood)* **231**, 237-251 (2006).
153 Vasquez-Vivar, J. *et al.* Superoxide generation by endothelial nitric oxide synthase: the influence of cofactors. *Proc Natl Acad Sci U S A* **95**, 9220-9225 (1998).
154 Pendyala, S. & Natarajan, V. Redox regulation of Nox proteins. *Respir Physiol Neurobiol* **174**, 265-271, doi:10.1016/j.resp.2010.09.016 (2010).
155 Son, S. M. Reactive oxygen and nitrogen species in pathogenesis of vascular complications of diabetes. *Diabetes Metab J* **36**, 190-198, doi:10.4093/dmj.2012.36.3.190 (2012).
156 Montezano, A. C. & Touyz, R. M. Reactive oxygen species and endothelial function--role of nitric oxide synthase uncoupling and Nox family nicotinamide adenine dinucleotide phosphate oxidases. *Basic Clin Pharmacol Toxicol* **110**, 87-94, doi:10.1111/j.1742-7843.2011.00785.x (2012).
157 Yang, Y., Shi, W., Cui, N., Wu, Z. & Jiang, C. Oxidative stress inhibits vascular K(ATP) channels by S-glutathionylation. *J Biol Chem* **285**, 38641-38648, doi:10.1074/jbc.M110.162578 (2010).
158 Suzuki, L. A., Poot, M., Gerrity, R. G. & Bornfeldt, K. E. Diabetes accelerates smooth muscle accumulation in lesions of atherosclerosis: lack of direct growth-promoting effects of high glucose levels. *Diabetes* **50**, 851-860 (2001).
159 Fukumoto, H., Naito, Z., Asano, G. & Aramaki, T. Immunohistochemical and morphometric evaluations of coronary atherosclerotic plaques associated with myocardial infarction and diabetes mellitus. *J Atheroscler Thromb* **5**, 29-35 (1998).
160 Stentz, F. B., Umpierrez, G. E., Cuervo, R. & Kitabchi, A. E. Proinflammatory cytokines, markers of cardiovascular risks, oxidative stress, and lipid peroxidation in patients with hyperglycemic crises. *Diabetes* **53**, 2079-2086 (2004).
161 Giulietti, A. *et al.* Monocytes from type 2 diabetic patients have a pro-inflammatory profile. 1,25-Dihydroxyvitamin D(3) works as anti-inflammatory. *Diabetes Res Clin Pract* **77**, 47-57, doi:10.1016/j.diabres.2006.10.007 (2007).
162 Kanter, J. E. *et al.* Diabetes promotes an inflammatory macrophage phenotype and atherosclerosis through acyl-CoA synthetase 1. *Proc Natl Acad Sci U S A* **109**, E715-724, doi:10.1073/pnas.1111600109 (2012).
163 Hansson, G. K., Robertson, A. K. & Soderberg-Naucler, C. Inflammation and atherosclerosis. *Annu Rev Pathol* **1**, 297-329, doi:10.1146/annurev.pathol.1.110304.100100 (2006).
164 Gilardini Montani, M. S. *et al.* High glucose and hyperglycemic sera from type 2 diabetic patients impair DC differentiation by inducing ROS and activating Wnt/beta-catenin and p38 MAPK. *Biochim Biophys Acta* **1862**, 805-813, doi:10.1016/j.bbadis.2016.01.001 (2016).

165 Razavi Nematollahi, L. *et al.* Proinflammatory cytokines in response to insulin-induced hypoglycemic stress in healthy subjects. *Metabolism* **58**, 443-448, doi:10.1016/j.metabol.2008.10.018 (2009).
166 Mittal, M., Siddiqui, M. R., Tran, K., Reddy, S. P. & Malik, A. B. Reactive oxygen species in inflammation and tissue injury. *Antioxid Redox Signal* **20**, 1126-1167, doi:10.1089/ars.2012.5149 (2014).
167 Griffith, B. *et al.* NOX enzymes and pulmonary disease. *Antioxid Redox Signal* **11**, 2505-2516, doi:10.1089/ARS.2009.2599 (2009).
168 Guzik, T. J. *et al.* Mechanisms of increased vascular superoxide production in human diabetes mellitus: role of NAD(P)H oxidase and endothelial nitric oxide synthase. *Circulation* **105**, 1656-1662 (2002).
169 Kim, J. A., Montagnani, M., Koh, K. K. & Quon, M. J. Reciprocal relationships between insulin resistance and endothelial dysfunction: molecular and pathophysiological mechanisms. *Circulation* **113**, 1888-1904, doi:10.1161/CIRCULATIONAHA.105.563213 (2006).
170 Tesfamariam, B., Brown, M. L. & Cohen, R. A. Elevated glucose impairs endothelium-dependent relaxation by activating protein kinase C. *J Clin Invest* **87**, 1643-1648, doi:10.1172/JCI115179 (1991).
171 Assert, R. *et al.* Regulation of protein kinase C by short term hyperglycaemia in human platelets in vivo and in vitro. *Diabetologia* **44**, 188-195, doi:10.1007/s001250051598 (2001).
172 Carr, M. E. Diabetes mellitus: a hypercoagulable state. *J Diabetes Complications* **15**, 44-54 (2001).
173 Goldin, A., Beckman, J. A., Schmidt, A. M. & Creager, M. A. Advanced glycation end products: sparking the development of diabetic vascular injury. *Circulation* **114**, 597-605, doi:10.1161/CIRCULATIONAHA.106.621854 (2006).
174 Thornalley, P. J. The glyoxalase system: new developments towards functional characterization of a metabolic pathway fundamental to biological life. *Biochem J* **269**, 1-11 (1990).
175 Nishikawa, T. *et al.* Normalizing mitochondrial superoxide production blocks three pathways of hyperglycaemic damage. *Nature* **404**, 787-790, doi:10.1038/35008121 (2000).
176 Stitt, A. W. *et al.* Advanced glycation end products (AGEs) co-localize with AGE receptors in the retinal vasculature of diabetic and of AGE-infused rats. *Am J Pathol* **150**, 523-531 (1997).
177 Horie, K. *et al.* Immunohistochemical colocalization of glycoxidation products and lipid peroxidation products in diabetic renal glomerular lesions. Implication for glycoxidative stress in the pathogenesis of diabetic nephropathy. *J Clin Invest* **100**, 2995-3004, doi:10.1172/JCI119853 (1997).
178 Mozos, I. *et al.* Inflammatory Markers for Arterial Stiffness in Cardiovascular Diseases. *Front Immunol* **8**, 1058, doi:10.3389/fimmu.2017.01058 (2017).
179 Prasad, A., Bekker, P. & Tsimikas, S. Advanced glycation end products and diabetic cardiovascular disease. *Cardiol Rev* **20**, 177-183, doi:10.1097/CRD.0b013e318244e57c (2012).
180 Brownlee, M. Biochemistry and molecular cell biology of diabetic complications. *Nature* **414**, 813-820, doi:10.1038/414813a (2001).

181 2013, W. H. D. A global brief on Hypertension: silent killer, global public health crisis. *World Health Organization* (2013).
182 Tesfamariam, B. & Cohen, R. A. Inhibition of adrenergic vasoconstriction by endothelial cell shear stress. *Circ Res* **63**, 720-725 (1988).
183 Bevan, J. A. & Osher, J. V. A direct method for recording tension changes in the wall of small blood vessels in vitro. *Agents Actions* **2**, 257-260 (1972).
184 Mulvany, M. J. & Halpern, W. Mechanical properties of vascular smooth muscle cells in situ. *Nature* **260**, 617-619 (1976).
185 Duling, B. R., Gore, R. W., Dacey, R. G., Jr. & Damon, D. N. Methods for isolation, cannulation, and in vitro study of single microvessels. *Am J Physiol* **241**, H108-116, doi:10.1152/ajpheart.1981.241.1.H108 (1981).
186 Doring, H. J. The isolated perfused heart according to Langendorff technique--function--application. *Physiol Bohemoslov* **39**, 481-504 (1990).
187 Bell, R. M., Mocanu, M. M. & Yellon, D. M. Retrograde heart perfusion: the Langendorff technique of isolated heart perfusion. *J Mol Cell Cardiol* **50**, 940-950, doi:10.1016/j.yjmcc.2011.02.018 (2011).
188 Schechter, M. A. *et al.* An isolated working heart system for large animal models. *J Vis Exp*, doi:10.3791/51671 (2014).
189 Skrzypiec-Spring, M., Grotthus, B., Szelag, A. & Schulz, R. Isolated heart perfusion according to Langendorff---still viable in the new millennium. *J Pharmacol Toxicol Methods* **55**, 113-126, doi:10.1016/j.vascn.2006.05.006 (2007).
190 Zemelman, B. V., Lee, G. A., Ng, M. & Miesenbock, G. Selective photostimulation of genetically chARGed neurons. *Neuron* **33**, 15-22 (2002).
191 Dombeck, D. A., Harvey, C. D., Tian, L., Looger, L. L. & Tank, D. W. Functional imaging of hippocampal place cells at cellular resolution during virtual navigation. *Nat Neurosci* **13**, 1433-1440, doi:10.1038/nn.2648 (2010).
192 Mank, M. *et al.* A genetically encoded calcium indicator for chronic in vivo two-photon imaging. *Nat Methods* **5**, 805-811, doi:10.1038/nmeth.1243 (2008).
193 Bruegmann, T. *et al.* Optogenetic control of heart muscle in vitro and in vivo. *Nat Methods* **7**, 897-900, doi:10.1038/nmeth.1512 (2010).
194 Knollmann, B. C. Pacing lightly: optogenetics gets to the heart. *Nat Methods* **7**, 889-891, doi:10.1038/nmeth1110-889 (2010).
195 Jia, Z. *et al.* Stimulating cardiac muscle by light: cardiac optogenetics by cell delivery. *Circ Arrhythm Electrophysiol* **4**, 753-760, doi:10.1161/CIRCEP.111.964247 (2011).
196 Bingen, B. O. *et al.* Light-induced termination of spiral wave arrhythmias by optogenetic engineering of atrial cardiomyocytes. *Cardiovasc Res* **104**, 194-205, doi:10.1093/cvr/cvu179 (2014).
197 Bruegmann, T. *et al.* Optogenetic defibrillation terminates ventricular arrhythmia in mouse hearts and human simulations. *J Clin Invest* **126**, 3894-3904, doi:10.1172/JCI88950 (2016).
198 Nyns, E. C. A. *et al.* Optogenetic termination of ventricular arrhythmias in the whole heart: towards biological cardiac rhythm management. *Eur Heart J* **38**, 2132-2136, doi:10.1093/eurheartj/ehw574 (2017).
199 Crocini, C. *et al.* Optogenetics design of mechanistically-based stimulation patterns for cardiac defibrillation. *Sci Rep* **6**, 35628, doi:10.1038/srep35628 (2016).

200 Nussinovitch, U. & Gepstein, L. Optogenetics for in vivo cardiac pacing and resynchronization therapies. *Nat Biotechnol* **33**, 750-754, doi:10.1038/nbt.3268 (2015).
201 *Cardiovascular diseases (CVDs)*, <http://www.who.int/mediacentre/factsheets/fs317/en/> (2015).
202 Bourajjaj, M., Stehouwer, C. D., van Hinsbergh, V. W. & Schalkwijk, C. G. Role of methylglyoxal adducts in the development of vascular complications in diabetes mellitus. *Biochem Soc Trans* **31**, 1400-1402, doi:10.1042/ (2003).
203 Esterbauer, H., Cheeseman, K. H., Dianzani, M. U., Poli, G. & Slater, T. F. Separation and characterization of the aldehydic products of lipid peroxidation stimulated by ADP-Fe2+ in rat liver microsomes. *Biochem J* **208**, 129-140 (1982).
204 Ogawa, S. *et al.* Methylglyoxal is a predictor in type 2 diabetic patients of intima-media thickening and elevation of blood pressure. *Hypertension* **56**, 471-476, doi:10.1161/HYPERTENSIONAHA.110.156786 (2010).
205 Wang, X., Desai, K., Chang, T. & Wu, L. Vascular methylglyoxal metabolism and the development of hypertension. *J Hypertens* **23**, 1565-1573 (2005).
206 Yang, Y. *et al.* Prolonged exposure to methylglyoxal causes disruption of vascular KATP channel by mRNA instability. *Am J Physiol Cell Physiol* **303**, C1045-1054, doi:10.1152/ajpcell.00020.2012 (2012).
207 Havilio, M., Haddad, Y. & Smilansky, Z. Intensity-based statistical scorer for tandem mass spectrometry. *Anal Chem* **75**, 435-444 (2003).
208 Sadygov, R. G. & Yates, J. R., 3rd. A hypergeometric probability model for protein identification and validation using tandem mass spectral data and protein sequence databases. *Anal Chem* **75**, 3792-3798 (2003).
209 Peterson, S. M. *et al.* Common features of microRNA target prediction tools. *Front Genet* **5**, 23, doi:10.3389/fgene.2014.00023 (2014).
210 Shi, W. *et al.* Lipopolysaccharides up-regulate Kir6.1/SUR2B channel expression and enhance vascular KATP channel activity via NF-kappaB-dependent signaling. *J Biol Chem* **285**, 3021-3029, doi:10.1074/jbc.M109.058313 (2010).
211 Hagberg, B. Rett syndrome: long-term clinical follow-up experiences over four decades. *J Child Neurol* **20**, 722-727, doi:10.1177/08830738050200090401 (2005).
212 Neul, J. L. The relationship of Rett syndrome and MECP2 disorders to autism. *Dialogues Clin Neurosci* **14**, 253-262 (2012).
213 Weng, S. M., Bailey, M. E. & Cobb, S. R. Rett syndrome: from bed to bench. *Pediatr Neonatol* **52**, 309-316, doi:10.1016/j.pedneo.2011.08.002 (2011).
214 Ogier, M. & Katz, D. M. Breathing dysfunction in Rett syndrome: understanding epigenetic regulation of the respiratory network. *Respir Physiol Neurobiol* **164**, 55-63, doi:10.1016/j.resp.2008.04.005 (2008).
215 Rohdin, M. *et al.* Disturbances in cardiorespiratory function during day and night in Rett syndrome. *Pediatr Neurol* **37**, 338-344, doi:10.1016/j.pediatrneurol.2007.06.009 (2007).
216 Liyanage, V. R. & Rastegar, M. Rett syndrome and MeCP2. *Neuromolecular Med* **16**, 231-264, doi:10.1007/s12017-014-8295-9 (2014).
217 Samaco, R. C. & Neul, J. L. Complexities of Rett syndrome and MeCP2. *J Neurosci* **31**, 7951-7959, doi:10.1523/JNEUROSCI.0169-11.2011 (2011).
218 Joynt, K. E., Orav, E. J. & Jha, A. K. Physician volume, specialty, and outcomes of care for patients with heart failure. *Circ Heart Fail* **6**, 890-897, doi:10.1161/CIRCHEARTFAILURE.112.000064 (2013).

219 Lioy, D. T., Wu, W. W. & Bissonnette, J. M. Autonomic dysfunction with mutations in the gene that encodes methyl-CpG-binding protein 2: insights into Rett syndrome. *Auton Neurosci* **161**, 55-62, doi:10.1016/j.autneu.2011.01.006 (2011).
220 Silverman, J. L., Yang, M., Lord, C. & Crawley, J. N. Behavioural phenotyping assays for mouse models of autism. *Nat Rev Neurosci* **11**, 490-502, doi:10.1038/nrn2851 (2010).
221 Kaidanovich-Beilin, O., Lipina, T., Vukobradovic, I., Roder, J. & Woodgett, J. R. Assessment of social interaction behaviors. *J Vis Exp*, doi:10.3791/2473 (2011).
222 Moy, S. S. *et al.* Sociability and preference for social novelty in five inbred strains: an approach to assess autistic-like behavior in mice. *Genes Brain Behav* **3**, 287-302, doi:10.1111/j.1601-1848.2004.00076.x (2004).
223 Schanen, N. C. *et al.* Neonatal encephalopathy in two boys in families with recurrent Rett syndrome. *J Child Neurol* **13**, 229-231, doi:10.1177/088307389801300507 (1998).
224 Wan, M. *et al.* Rett syndrome and beyond: recurrent spontaneous and familial MECP2 mutations at CpG hotspots. *Am J Hum Genet* **65**, 1520-1529, doi:10.1086/302690 (1999).
225 Engineer, C. T. *et al.* Degraded neural and behavioral processing of speech sounds in a rat model of Rett syndrome. *Neurobiol Dis* **83**, 26-34, doi:10.1016/j.nbd.2015.08.019 (2015).
226 Liao, W., Gandal, M. J., Ehrlichman, R. S., Siegel, S. J. & Carlson, G. C. MeCP2+/- mouse model of RTT reproduces auditory phenotypes associated with Rett syndrome and replicate select EEG endophenotypes of autism spectrum disorder. *Neurobiol Dis* **46**, 88-92, doi:10.1016/j.nbd.2011.12.048 (2012).
227 Bader, G. G., Witt-Engerstrom, I. & Hagberg, B. Neurophysiological findings in the Rett syndrome, II: Visual and auditory brainstem, middle and late evoked responses. *Brain Dev* **11**, 110-114 (1989).
228 Hagberg, B., Aicardi, J., Dias, K. & Ramos, O. A progressive syndrome of autism, dementia, ataxia, and loss of purposeful hand use in girls: Rett's syndrome: report of 35 cases. *Ann Neurol* **14**, 471-479, doi:10.1002/ana.410140412 (1983).
229 Calfa, G., Percy, A. K. & Pozzo-Miller, L. Experimental models of Rett syndrome based on Mecp2 dysfunction. *Exp Biol Med (Maywood)* **236**, 3-19, doi:10.1258/ebm.2010.010261 (2011).
230 Stettner, G. M., Huppke, P., Gartner, J., Richter, D. W. & Dutschmann, M. Disturbances of breathing in Rett syndrome: results from patients and animal models. *Adv Exp Med Biol* **605**, 503-507, doi:10.1007/978-0-387-73693-8_88 (2008).
231 Santos, M., Silva-Fernandes, A., Oliveira, P., Sousa, N. & Maciel, P. Evidence for abnormal early development in a mouse model of Rett syndrome. *Genes Brain Behav* **6**, 277-286, doi:10.1111/j.1601-183X.2006.00258.x (2007).
232 Castro, J. *et al.* Functional recovery with recombinant human IGF1 treatment in a mouse model of Rett Syndrome. *Proc Natl Acad Sci U S A* **111**, 9941-9946, doi:10.1073/pnas.1311685111 (2014).
233 Samuels, E. R. & Szabadi, E. Functional neuroanatomy of the noradrenergic locus coeruleus: its roles in the regulation of arousal and autonomic function part I: principles of functional organisation. *Curr Neuropharmacol* **6**, 235-253, doi:10.2174/157015908785777229 (2008).
234 Samuels, E. R. & Szabadi, E. Functional neuroanatomy of the noradrenergic locus coeruleus: its roles in the regulation of arousal and autonomic function part II: physiological and pharmacological manipulations and pathological alterations of locus

coeruleus activity in humans. *Curr Neuropharmacol* **6**, 254-285, doi:10.2174/157015908785777193 (2008).

235 Jin, X., Zhong, W. & Jiang, C. Time-dependent modulation of GABA(A)-ergic synaptic transmission by allopregnanolone in locus coeruleus neurons of Mecp2-null mice. *Am J Physiol Cell Physiol* **305**, C1151-1160, doi:10.1152/ajpcell.00195.2013 (2013).

236 Pacheco, C. D., Elrick, M. J. & Lieberman, A. P. Tau deletion exacerbates the phenotype of Niemann-Pick type C mice and implicates autophagy in pathogenesis. *Hum Mol Genet* **18**, 956-965, doi:10.1093/hmg/ddn423 (2009).

237 Guy, J., Gan, J., Selfridge, J., Cobb, S. & Bird, A. Reversal of neurological defects in a mouse model of Rett syndrome. *Science* **315**, 1143-1147, doi:10.1126/science.1138389 (2007).

238 Kerr, B., Alvarez-Saavedra, M., Saez, M. A., Saona, A. & Young, J. I. Defective body-weight regulation, motor control and abnormal social interactions in Mecp2 hypomorphic mice. *Hum Mol Genet* **17**, 1707-1717, doi:10.1093/hmg/ddn061 (2008).

239 Wohr, M. & Scattoni, M. L. Behavioural methods used in rodent models of autism spectrum disorders: current standards and new developments. *Behav Brain Res* **251**, 5-17, doi:10.1016/j.bbr.2013.05.047 (2013).

240 Chahrour, M. & Zoghbi, H. Y. The story of Rett syndrome: from clinic to neurobiology. *Neuron* **56**, 422-437, doi:10.1016/j.neuron.2007.10.001 (2007).

241 Kerr, A. M., Armstrong, D. D., Prescott, R. J., Doyle, D. & Kearney, D. L. Rett syndrome: analysis of deaths in the British survey. *Eur Child Adolesc Psychiatry* **6 Suppl 1**, 71-74 (1997).

242 Marcus, C. L. *et al.* Polysomnographic characteristics of patients with Rett syndrome. *J Pediatr* **125**, 218-224 (1994).

243 Weese-Mayer, D. E. *et al.* Autonomic nervous system dysregulation: breathing and heart rate perturbation during wakefulness in young girls with Rett syndrome. *Pediatr Res* **60**, 443-449, doi:10.1203/01.pdr.0000238302.84552.d0 (2006).

244 Merrill, E. G. & Fedorko, L. Monosynaptic inhibition of phrenic motoneurons: a long descending projection from Botzinger neurons. *J Neurosci* **4**, 2350-2353 (1984).

245 Smith, J. C., Morrison, D. E., Ellenberger, H. H., Otto, M. R. & Feldman, J. L. Brainstem projections to the major respiratory neuron populations in the medulla of the cat. *J Comp Neurol* **281**, 69-96, doi:10.1002/cne.902810107 (1989).

246 Jiang, C. & Lipski, J. Extensive monosynaptic inhibition of ventral respiratory group neurons by augmenting neurons in the Botzinger complex in the cat. *Exp Brain Res* **81**, 639-648 (1990).

247 Ballantyne, D. & Richter, D. W. The non-uniform character of expiratory synaptic activity in expiratory bulbospinal neurones of the cat. *J Physiol* **370**, 433-456 (1986).

248 Bianchi, A. L., Grelot, L., Iscoe, S. & Remmers, J. E. Electrophysiological properties of rostral medullary respiratory neurones in the cat: an intracellular study. *J Physiol* **407**, 293-310 (1988).

249 Chen, C. Y. *et al.* Defective GABAergic neurotransmission in the nucleus tractus solitarius in Mecp2-null mice, a model of Rett syndrome. *Neurobiol Dis* **109**, 25-32, doi:10.1016/j.nbd.2017.09.006 (2018).

250 Creager, M. A., Luscher, T. F., Cosentino, F. & Beckman, J. A. Diabetes and vascular disease: pathophysiology, clinical consequences, and medical therapy: Part I. *Circulation* **108**, 1527-1532, doi:10.1161/01.CIR.0000091257.27563.32 (2003).

251 Cooper, K. O., Witz, G. & Witmer, C. M. Mutagenicity and toxicity studies of several alpha,beta-unsaturated aldehydes in the Salmonella typhimurium mutagenicity assay. *Environ Mutagen* **9**, 289-295 (1987).

252 Fang, J. L. & Vaca, C. E. Development of a 32P-postlabelling method for the analysis of adducts arising through the reaction of acetaldehyde with 2'-deoxyguanosine-3'-monophosphate and DNA. *Carcinogenesis* **16**, 2177-2185 (1995).

253 Marnett, L. J. *et al.* Naturally occurring carbonyl compounds are mutagens in Salmonella tester strain TA104. *Mutat Res* **148**, 25-34 (1985).

254 Sousa Silva, M., Gomes, R. A., Ferreira, A. E., Ponces Freire, A. & Cordeiro, C. The glyoxalase pathway: the first hundred years... and beyond. *Biochem J* **453**, 1-15, doi:10.1042/BJ20121743 (2013).

255 Thornalley, P. J. Glyoxalase I--structure, function and a critical role in the enzymatic defence against glycation. *Biochem Soc Trans* **31**, 1343-1348, doi:10.1042/ (2003).

256 Bansal, S. *et al.* A study on serum advanced glycation end products and its association with oxidative stress and paraoxonase activity in type 2 diabetic patients with vascular complications. *Clin Biochem* **46**, 109-114, doi:10.1016/j.clinbiochem.2012.10.019 (2013).

257 Chang, T. & Wu, L. Methylglyoxal, oxidative stress, and hypertension. *Can J Physiol Pharmacol* **84**, 1229-1238, doi:10.1139/y06-077 (2006).

258 Cooper, R. A. Metabolism of methylglyoxal in microorganisms. *Annu Rev Microbiol* **38**, 49-68, doi:10.1146/annurev.mi.38.100184.000405 (1984).

259 Vander Jagt, D. L., Robinson, B., Taylor, K. K. & Hunsaker, L. A. Reduction of trioses by NADPH-dependent aldo-keto reductases. Aldose reductase, methylglyoxal, and diabetic complications. *J Biol Chem* **267**, 4364-4369 (1992).

260 Vasdev, S., Ford, C. A., Longerich, L., Gadag, V. & Wadhawan, S. Role of aldehydes in fructose induced hypertension. *Mol Cell Biochem* **181**, 1-9 (1998).

261 Wang, H., Liu, J. & Wu, L. Methylglyoxal-induced mitochondrial dysfunction in vascular smooth muscle cells. *Biochem Pharmacol* **77**, 1709-1716, doi:10.1016/j.bcp.2009.02.024 (2009).

262 Yokoshiki, H., Sunagawa, M., Seki, T. & Sperelakis, N. ATP-sensitive K+ channels in pancreatic, cardiac, and vascular smooth muscle cells. *Am J Physiol* **274**, C25-37 (1998).

263 Brayden, J. E. Functional roles of KATP channels in vascular smooth muscle. *Clin Exp Pharmacol Physiol* **29**, 312-316 (2002).

264 Hibino, H. *et al.* Inwardly rectifying potassium channels: their structure, function, and physiological roles. *Physiol Rev* **90**, 291-366, doi:10.1152/physrev.00021.2009 (2010).

265 Chutkow, W. A. *et al.* Episodic coronary artery vasospasm and hypertension develop in the absence of Sur2 K(ATP) channels. *J Clin Invest* **110**, 203-208, doi:10.1172/JCI15672 (2002).

266 Croker, B. *et al.* ATP-sensitive potassium channels mediate survival during infection in mammals and insects. *Nat Genet* **39**, 1453-1460, doi:10.1038/ng.2007.25 (2007).

267 Kane, G. C. *et al.* Gene knockout of the KCNJ8-encoded Kir6.1 K(ATP) channel imparts fatal susceptibility to endotoxemia. *FASEB J* **20**, 2271-2280, doi:10.1096/fj.06-6349com (2006).

268 Miki, T. *et al.* Mouse model of Prinzmetal angina by disruption of the inward rectifier Kir6.1. *Nat Med* **8**, 466-472, doi:10.1038/nm0502-466 (2002).

269 Desai, K. M. *et al.* Oxidative stress and aging: is methylglyoxal the hidden enemy? *Can J Physiol Pharmacol* **88**, 273-284, doi:10.1139/Y10-001 (2010).
270 Miura, H. *et al.* Diabetes mellitus impairs vasodilation to hypoxia in human coronary arterioles: reduced activity of ATP-sensitive potassium channels. *Circ Res* **92**, 151-158 (2003).
271 Lapolla, A. *et al.* Glyoxal and methylglyoxal levels in diabetic patients: quantitative determination by a new GC/MS method. *Clin Chem Lab Med* **41**, 1166-1173, doi:10.1515/CCLM.2003.180 (2003).
272 Mukohda, M., Yamawaki, H., Okada, M. & Hara, Y. Methylglyoxal enhances sodium nitroprusside-induced relaxation in rat aorta. *J Pharmacol Sci* **112**, 176-183 (2010).
273 Buraczynska, M., Zukowski, P., Wacinski, P., Ksiazek, K. & Zaluska, W. Polymorphism in microRNA-196a2 contributes to the risk of cardiovascular disease in type 2 diabetes patients. *J Diabetes Complications* **28**, 617-620, doi:10.1016/j.jdiacomp.2014.05.006 (2014).
274 Dumortier, O. *et al.* Maternal protein restriction leads to pancreatic failure in offspring: role of misexpressed microRNA-375. *Diabetes* **63**, 3416-3427, doi:10.2337/db13-1431 (2014).
275 Osipova, J. *et al.* Diabetes-associated microRNAs in pediatric patients with type 1 diabetes mellitus: a cross-sectional cohort study. *J Clin Endocrinol Metab* **99**, E1661-1665, doi:10.1210/jc.2013-3868 (2014).
276 Wang, J. Y. *et al.* miR-21 overexpression enhances TGF-beta1-induced epithelial-to-mesenchymal transition by target smad7 and aggravates renal damage in diabetic nephropathy. *Mol Cell Endocrinol* **392**, 163-172, doi:10.1016/j.mce.2014.05.018 (2014).
277 Ramachandran, D. *et al.* Sirt1 and mir-9 expression is regulated during glucose-stimulated insulin secretion in pancreatic beta-islets. *FEBS J* **278**, 1167-1174, doi:10.1111/j.1742-4658.2011.08042.x (2011).
278 Hagiwara, S., McClelland, A. & Kantharidis, P. MicroRNA in diabetic nephropathy: renin angiotensin, aGE/RAGE, and oxidative stress pathway. *J Diabetes Res* **2013**, 173783, doi:10.1155/2013/173783 (2013).
279 Caporali, A. *et al.* Deregulation of microRNA-503 contributes to diabetes mellitus-induced impairment of endothelial function and reparative angiogenesis after limb ischemia. *Circulation* **123**, 282-291, doi:10.1161/CIRCULATIONAHA.110.952325 (2011).
280 Cheng, H. S. *et al.* MicroRNA-146 represses endothelial activation by inhibiting pro-inflammatory pathways. *EMBO Mol Med* **5**, 1017-1034, doi:10.1002/emmm.201202318 (2013).
281 Mortuza, R., Feng, B. & Chakrabarti, S. miR-195 regulates SIRT1-mediated changes in diabetic retinopathy. *Diabetologia* **57**, 1037-1046, doi:10.1007/s00125-014-3197-9 (2014).
282 Greco, S. *et al.* MicroRNA dysregulation in diabetic ischemic heart failure patients. *Diabetes* **61**, 1633-1641, doi:10.2337/db11-0952 (2012).
283 Lujambio, A. *et al.* A microRNA DNA methylation signature for human cancer metastasis. *Proc Natl Acad Sci U S A* **105**, 13556-13561, doi:10.1073/pnas.0803055105 (2008).
284 Lujambio, A. & Esteller, M. How epigenetics can explain human metastasis: a new role for microRNAs. *Cell Cycle* **8**, 377-382, doi:10.4161/cc.8.3.7526 (2009).

285 Palsamy, P. *et al.* Methylglyoxal induces endoplasmic reticulum stress and DNA demethylation in the Keap1 promoter of human lens epithelial cells and age-related cataracts. *Free Radic Biol Med* **72**, 134-148, doi:10.1016/j.freeradbiomed.2014.04.010 (2014).
286 Deisseroth, K. Optogenetics. *Nat Methods* **8**, 26-29, doi:10.1038/nmeth.f.324 (2011).
287 Lima, S. Q. & Miesenbock, G. Remote control of behavior through genetically targeted photostimulation of neurons. *Cell* **121**, 141-152, doi:10.1016/j.cell.2005.02.004 (2005).
288 Boyden, E. S., Zhang, F., Bamberg, E., Nagel, G. & Deisseroth, K. Millisecond-timescale, genetically targeted optical control of neural activity. *Nat Neurosci* **8**, 1263-1268, doi:10.1038/nn1525 (2005).
289 Zhang, F. *et al.* Multimodal fast optical interrogation of neural circuitry. *Nature* **446**, 633-639, doi:10.1038/nature05744 (2007).
290 Sohal, V. S., Zhang, F., Yizhar, O. & Deisseroth, K. Parvalbumin neurons and gamma rhythms enhance cortical circuit performance. *Nature* **459**, 698-702, doi:10.1038/nature07991 (2009).
291 Carter, M. E., Soden, M. E., Zweifel, L. S. & Palmiter, R. D. Genetic identification of a neural circuit that suppresses appetite. *Nature* **503**, 111-114, doi:10.1038/nature12596 (2013).
292 Gradinaru, V., Mogri, M., Thompson, K. R., Henderson, J. M. & Deisseroth, K. Optical deconstruction of parkinsonian neural circuitry. *Science* **324**, 354-359, doi:10.1126/science.1167093 (2009).
293 Gourine, A. V. *et al.* Astrocytes control breathing through pH-dependent release of ATP. *Science* **329**, 571-575, doi:10.1126/science.1190721 (2010).
294 Imayoshi, I. *et al.* Oscillatory control of factors determining multipotency and fate in mouse neural progenitors. *Science* **342**, 1203-1208, doi:10.1126/science.1242366 (2013).
295 Arrenberg, A. B., Stainier, D. Y., Baier, H. & Huisken, J. Optogenetic control of cardiac function. *Science* **330**, 971-974, doi:10.1126/science.1195929 (2010).
296 Gianakopoulos, P. J. *et al.* Mutations in MECP2 exon 1 in classical Rett patients disrupt MECP2_e1 transcription, but not transcription of MECP2_e2. *Am J Med Genet B Neuropsychiatr Genet* **159B**, 210-216, doi:10.1002/ajmg.b.32015 (2012).
297 Yu, L., Jin, X., Yang, Y., Cui, N. & Jiang, C. Rosiglitazone inhibits vascular KATP channels and coronary vasodilation produced by isoprenaline. *Br J Pharmacol* **164**, 2064-2072, doi:10.1111/j.1476-5381.2011.01539.x (2011).
298 Desai, K. H., Schauble, E., Luo, W., Kranias, E. & Bernstein, D. Phospholamban deficiency does not compromise exercise capacity. *Am J Physiol* **276**, H1172-1177 (1999).
299 Gao, F. *et al.* Both beta1- and beta2-adrenoceptors contribute to feedforward coronary resistance vessel dilation during exercise. *Am J Physiol Heart Circ Physiol* **298**, H921-929, doi:10.1152/ajpheart.00135.2009 (2010).
300 Sutherland, F. J., Shattock, M. J., Baker, K. E. & Hearse, D. J. Mouse isolated perfused heart: characteristics and cautions. *Clin Exp Pharmacol Physiol* **30**, 867-878 (2003).
301 Schrier, R. W., Lieberman, R. & Ufferman, R. C. Mechanism of antidiuretic effect of beta adrenergic stimulation. *J Clin Invest* **51**, 97-111, doi:10.1172/JCI106803 (1972).
302 Li, L., Miano, J. M., Cserjesi, P. & Olson, E. N. SM22 alpha, a marker of adult smooth muscle, is expressed in multiple myogenic lineages during embryogenesis. *Circ Res* **78**, 188-195 (1996).

303 Solway, J. *et al.* Structure and expression of a smooth muscle cell-specific gene, SM22 alpha. *J Biol Chem* **270**, 13460-13469 (1995).
304 Burstyn-Cohen, T., Heeb, M. J. & Lemke, G. Lack of protein S in mice causes embryonic lethal coagulopathy and vascular dysgenesis. *J Clin Invest* **119**, 2942-2953, doi:10.1172/JCI39325 (2009).
305 Holtwick, R. *et al.* Smooth muscle-selective deletion of guanylyl cyclase-A prevents the acute but not chronic effects of ANP on blood pressure. *Proc Natl Acad Sci U S A* **99**, 7142-7147, doi:10.1073/pnas.102650499 (2002).
306 Chen, Z. *et al.* DiGeorge syndrome critical region 8 (DGCR8) protein-mediated microRNA biogenesis is essential for vascular smooth muscle cell development in mice. *J Biol Chem* **287**, 19018-19028, doi:10.1074/jbc.M112.351791 (2012).
307 Albinsson, S. *et al.* MicroRNAs are necessary for vascular smooth muscle growth, differentiation, and function. *Arterioscler Thromb Vasc Biol* **30**, 1118-1126, doi:10.1161/ATVBAHA.109.200873 (2010).
308 Mesradi, M. *et al.* Experimental and analytical comparative study of optical coefficient of fresh and frozen rat tissues. *J Biomed Opt* **18**, 117010, doi:10.1117/1.JBO.18.11.117010 (2013).
309 Webb, R. C. Smooth muscle contraction and relaxation. *Adv Physiol Educ* **27**, 201-206, doi:10.1152/advances.2003.27.4.201 (2003).
310 Bradley, S. R. *et al.* Chemosensitive serotonergic neurons are closely associated with large medullary arteries. *Nat Neurosci* **5**, 401-402, doi:10.1038/nn848 (2002).
311 Walsh, J. K., Deacon, S., Dijk, D. J. & Lundahl, J. The selective extrasynaptic GABAA agonist, gaboxadol, improves traditional hypnotic efficacy measures and enhances slow wave activity in a model of transient insomnia. *Sleep* **30**, 593-602 (2007).
312 Olmos-Serrano, J. L., Corbin, J. G. & Burns, M. P. The GABA(A) receptor agonist THIP ameliorates specific behavioral deficits in the mouse model of fragile X syndrome. *Dev Neurosci* **33**, 395-403, doi:10.1159/000332884 (2011).
313 Olmos-Serrano, J. L. *et al.* Defective GABAergic neurotransmission and pharmacological rescue of neuronal hyperexcitability in the amygdala in a mouse model of fragile X syndrome. *J Neurosci* **30**, 9929-9938, doi:10.1523/JNEUROSCI.1714-10.2010 (2010).
314 Egawa, K. *et al.* Decreased tonic inhibition in cerebellar granule cells causes motor dysfunction in a mouse model of Angelman syndrome. *Sci Transl Med* **4**, 163ra157, doi:10.1126/scitranslmed.3004655 (2012).
315 Yamawaki, H., Saito, K., Okada, M. & Hara, Y. Methylglyoxal mediates vascular inflammation via JNK and p38 in human endothelial cells. *Am J Physiol Cell Physiol* **295**, C1510-1517, doi:10.1152/ajpcell.00252.2008 (2008).
316 Hien, T. T. *et al.* Elevated Glucose Levels Promote Contractile and Cytoskeletal Gene Expression in Vascular Smooth Muscle via Rho/Protein Kinase C and Actin Polymerization. *J Biol Chem* **291**, 3552-3568, doi:10.1074/jbc.M115.654384 (2016).
317 Xie, Z. *et al.* Up-regulation of CPI-17 phosphorylation in diabetic vasculature and high glucose cultured vascular smooth muscle cells. *Cardiovasc Res* **69**, 491-501, doi:10.1016/j.cardiores.2005.11.002 (2006).
318 Mirra, P. *et al.* The role of miR-190a in methylglyoxal-induced insulin resistance in endothelial cells. *Biochim Biophys Acta* **1863**, 440-449, doi:10.1016/j.bbadis.2016.11.018 (2017).

319 Li, Y. *et al.* MicroRNA-221 regulates high glucose-induced endothelial dysfunction. *Biochem Biophys Res Commun* **381**, 81-83, doi:10.1016/j.bbrc.2009.02.013 (2009).
320 Hien, T. T. *et al.* MicroRNA-dependent regulation of KLF4 by glucose in vascular smooth muscle. *J Cell Physiol*, doi:10.1002/jcp.26549 (2018).
321 Roncon, P. *et al.* MicroRNA profiles in hippocampal granule cells and plasma of rats with pilocarpine-induced epilepsy--comparison with human epileptic samples. *Sci Rep* **5**, 14143, doi:10.1038/srep14143 (2015).
322 Valadi, H. *et al.* Exosome-mediated transfer of mRNAs and microRNAs is a novel mechanism of genetic exchange between cells. *Nat Cell Biol* **9**, 654-659, doi:10.1038/ncb1596 (2007).
323 Kota, J. *et al.* Therapeutic microRNA delivery suppresses tumorigenesis in a murine liver cancer model. *Cell* **137**, 1005-1017, doi:10.1016/j.cell.2009.04.021 (2009).
324 Kim, M., Hong, J., Kim, J. & Shin, H. J. Fiber bundle-based integrated platform for wide-field fluorescence imaging and patterned optical stimulation for modulation of vasoconstriction in the deep brain of a living animal. *Biomed Opt Express* **8**, 2781-2795, doi:10.1364/BOE.8.002781 (2017).

APPENDIX: PUBLICATIONS

- **Wu Y**, Cui N, Xin H, Zhong W, Arrowood C, Johnson CM and Jiang. *Mecp2*-disruption in rats causes breathing disorders by reshaping medullary respiratory neuronal firing patterns: cellular defects and pharmacologic correction. *In preparation*.
- **Wu Y**, Zhong W, Cui N, Johnson CM, Xin H and Jiang C. Characterization of Rett Syndrome-like phenotypes in Mecp2-knockout rats. *Journal of Neurodevelopmental Disorder. 2016 June.*
- **Wu Y**, Li SS, Jin X, Cui N, Zhang S and Jiang C. Optogenetic approach for functional assays of the cardiovascular system by light activation of the vascular smooth muscle. *Vascul Pharmacol. 2015 April.*
- Li SS, **Wu Y**, Jin X, Jiang C. The SUR2B subunit of rat vascular KATP channel is targeted by miR-9a-3p induced by prolonged exposure to methylglyoxal. *Am J Physiol Cell Physiol. 2015 January.* (**Equal contribution**)
- Zhong W, Johnson CM, Cui N, Oginsky MF, **Wu Y**, Jiang C. Effects of early-life exposure to THIP on brainstem neuronal excitability in the Mecp2-null mouse model of Rett syndrome before and after drug withdrawal. *Physiol Rep. 2017 January*.
- Zhong W, Johnson CM, Cui N, Xing H, **Wu Y**, Jiang C. Effects of chronic exposure to low dose THIP on brainstem neuronal excitability in mouse models of Rett syndrome: Evidence from symptomatic females. *Neuropharmacology. 2017 January*.
- Jiang C, Cui N, Zhong W, Johnson CM, **WuY**. Breathing abnormalities in animal models of Rett syndrome a female neurogenetic disorder. *Respir Physiol Neurobiol. 2016 November*.
- Zhong W, Johnson CM, **Wu Y**, Cui N, Xing H, Zhang S, Jiang C. Effects of early-life exposure to THIP on phenotype development in a mouse model of Rett syndrome. *J Neurodev Disord. 2016 October.*
- Johnson CM, Zhong W, Cui N, **Wu Y**, Xing H, Zhang S, Jiang C. Defects in brainstem neurons associated with breathing and motor function in the Mecp2R168X/Y mouse model of Rett syndrome. *Am J Physiol Cell Physiol. 2016 December.*
- Zhang S, Johnson CM, Cui N, Xing H, Zhong W, **Wu Y**, Jiang C. An optogenetic mouse model of rett syndrome targeting on catecholaminergic neurons. *J Neurosci Res. 2016 October.*
- Jin X, Li S, Bondy B, Zhong W, Oginsky MF, **Wu Y**, Johnson CM, Zhang S, Cui N, Jiang C. Identification of a Group of GABAergic Neurons in the Dorsomedial Area of the Locus Coeruleus. *PLoS One. 2016 January.*
- Li SS, Cui N, Yang Y, Trower TC, Wei YM, **Wu Y**, Zhang S, Jin X, Jiang C. Impairment of the Vascular KATP Channel Imposes Fatal Susceptibility to Experimental Diabetes Due to Multi-Organ Injuries. *J Cell Physiol. 2015 December.*
- Zhang S, Cui N, **Wu Y**, Zhong W, Johnson CM, Jiang C. Brainstem Neuronal Networks for Breathing Control Involve a Disinhibitory Projection From the Dorsal Medulla. *Vascul Pharmacol. 2015 November.*

- Zhong W, Cui N, Jin X, Oginsky MF, **Wu Y**, Zhang S, Bondy B, Johnson CM, Jiang C. Methyl CpG binding protein-2 gene disruption augments tonic currents of γ-aminobutyric acid receptors in locus coeruleus neurons: Impact on neuronal excitability and breathing. *J Biol Chem. 2015 May.*
- Zhang S, Cui N, **Wu Y**, Zhong W, Johnson CM, Jiang C. Optogenetic intervention to the vascular endothelium. *Vascul Pharmacol. 2015 May.*
- Zhang S, Cui N, Li S, Guo L, **Wu Y**, Zhu D, Jiang C. Interception of the endotoxin-induced arterial hyporeactivity to vasoconstrictors. *Vascul Pharmacol. 2014 July.*
- Jin X, Yu L, **Wu Y**, Zhang S, Shi Z, Chen X, Yang Y, Zhang X, Jiang C. S-Glutathionylation underscores the modulation of the heteromeric Kir4.1-Kir5.1 channel in oxidative stress. *J Physiol. 2012 November*.
- Yu L, Jin X, Cui N, **Wu Y**, Shi Z, Zhu D, Jiang C. Rosiglitazone selectively inhibits KATP channels by acting on the Kir6 subunit. *Br J Pharmacol. 2012 September*.